AD 273 510

MASSACHUSETTS INSTITUTE OF TECHNOLOGY

LINCOLN LABORATORY

47G-3

THE DESIGN OF SEMICONDUCTOR-DIODE DETECTOR CIRCUITS

G. R. Curry

M. Axelbank

28 February 1962

The work reported in this document was performed at Lincoln Laboratory, a center for research operated by Massachusetts Institute of Technology; this work was supported by the U. S. Advanced Research Projects Agency under Air Force Contract AF 19(604)-7400 (ARPA Order 178).

LEXINGTON MASSACHUSETTS

THE DESIGN OF SEMICONDUCTOR-DIODE DETECTOR CIRCUITS

by

G. R. Curry
M. Axelbank

ABSTRACT

A theoretical and experimental investigation has been made of the design of detector circuits using semiconductor diodes. The detector circuits are intended for use with transistor circuits having impedance levels of a few thousand ohms and current levels of a few milliamperes at frequencies up to 100 Mcps. High-impedance detectors useful for measuring the level of a CW signal, and pulse detectors having rise-times of the order of 0.1 μsec are considered.

A survey of the literature on detector-circuit design and semiconductor-diode theory is given. Because of the complex nature of the semiconductor-diode, detector-circuit analyses using simple diode equivalent circuits do not yield accurate results at high signal frequencies. On the other hand, the results of theoretical diode studies are too complex to be used for practical detector-circuit design.

A detector-design procedure, based on semiconductor theory is presented that permits the calculation of detector-circuit performance on the basis of measurements of the parameters of the diode to be used. The effects of frequency, diode parameters, detector load and driving circuits, temperature, and output coupling are considered. Measurements are reported that show good agreement with calculated detector-circuit performance over moderate ranges of the parameters for high-impedance and pulse detectors using germanium and silicon diodes.

The application of the design theory to the practical design of detector circuits is given in Section V. Sample designs of both high-impedance and pulse detectors are carried out, and measurements on sample detectors are reported. Measurements for evaluating the performance of several diode types in high-impedance and pulse detector circuits are presented.

ii jd

TABLE OF CONTENTS

The Design of Semiconductor-Diode Detector Circuits

I. Introduction

1. Scope of the Study

The design of semiconductor-diode detectors intended for use with low-level transistor circuits in the 10-100 Mcps frequency range is investigated. The detectors operate with input currents of a few milliamperes and at impedance levels of a few thousand ohms. Variations in detector-circuit performance with temperature are considered at ambient temperatures from 10° C to 50° C.

A procedure, based on semiconductor-diode theory, is given for the design of the detector circuits. The design procedure makes possible the approximate calculation of the performance of a detector circuit after a few basic measurements have been made on the diode.

Two types of detectors are studied:

1. High-impedance detector — This detector produces small circuit loading for CW signals and has near-ideal efficiency. Because of its slow pulse response and the heavy loading that it presents to pulsed signals it can be used only with CW signals.
2. Pulse detector — This detector is designed for a specific rise-time. Detectors with rise-times as short as 0.1 microsecond have been built and tested. The detector input impedance is of the order of a few thousand ohms. Efficiency is less than for the high-impedance detector.

2. Basic Circuit and Definitions

Since the operation of a detector is affected by its signal source, and a detector driving circuit is loaded by the detector, it is necessary to design the detector and its driving circuit together. Figure 1 is a diagram of the basic circuit. The input signal from a transistor amplifier is assumed to be a sinusoidal current of angular frequency ω and peak amplitude I_{in}. The output resistance of the source transistor is included in the circuit load resistance R_A. The resonant circuit, L_A-C_A, is tuned (with the detector connected) to resonate at angular frequency ω. Due to the non-linear characteristic of the diode, the diode current i is greater in the positive direction than in the negative direction, causing the voltage v_L developed across the parallel combination of the load resistor R_L and the load capacitor C_L to have a positive DC component V_L. This voltage has the effect of back-biasing the diode, thereby reducing the current flow until an equilibrium condition is reached. The current efficiency e_i is defined as the ratio of the DC component I_o of the diode current to the peak value of the input current I_{in}:

$$e_i = \frac{I_o}{I_{in}} = \frac{V_L}{I_{in} R_L} .$$

Since the detector circuit presents a non-linear load to the sinusoidal current source, the detector input voltage v will not, in general, be sinusoidal. In many cases, however, the linear load presented by R_A and the shunting of harmonic currents by C_A cause the detector input voltage to be nearly sinusoidal in spite of the non-

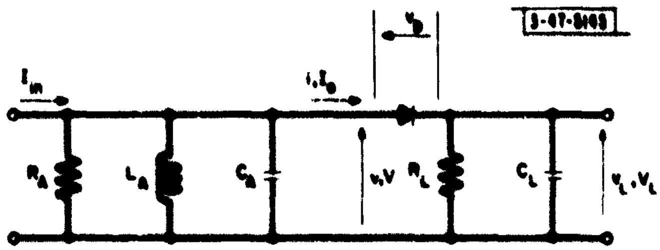

Fig. 1. Equivalent circuit for detector and driving circuit.

linear loading of the detector itself. Since circuit analyses are greatly simplified when v is sinusoidal, it is convenient to assume that this is the case. The departure of v from a sinusoid can later be evaluated and appropriate corrections can then be made.

When the detector input voltage is assumed sinusoidal with peak amplitude V, the detector voltage efficiency* e_v is defined as the ratio of the DC component V_L of the detector output voltage to the peak input voltage V:

$$e_v \equiv \frac{V_L}{V} .$$

The detector input resistance is defined as the ratio of the peak input voltage V to the peak value of the component of diode current I_1' having the same frequency and phase as the input voltage

$$R_{in} \equiv \frac{V}{I_1'} .$$

The detector input capacitance is defined as the ratio of the component of the diode current I_1'' having the same frequency as the input voltage and leading it by 90°, to the product of the angular frequency ω and the peak input voltage V

$$C_{in} \equiv \frac{I_1''}{\omega V}$$

---

*Current efficiency and voltage efficiency are not true efficiencies, but merely ratios of output to input signals

When v is assumed sinusoidal the current efficiency is given by

$$e_i = \frac{e_v}{R_L} \cdot \frac{R_A R_{in}}{R_A + R_{in}} \quad .$$

3. Procedure

A study of the detector literature has been made. An annotated bibliography appears at the end of this report. A survey of the detector literature showing the development of detector-circuit theory and applicable semiconductor-diode theory is presented in Section II

Because of the complex nature of the semiconductor diode, theoretical studies have not yielded results that are directly applicable to quantitative design of detector circuits employing semiconductor diodes. However, the theoretical studies have provided a basis for an approximate design procedure that is presented in Section III. This design theory permits the calculation of the voltage efficiency, input resistance, and input capacitance of a diode detector (assuming a sinusoidal input voltage) over restricted ranges of the following parameters:

1. Diode type.
2. Load resistance R_L.
3. Load capacitance C_L
4. Signal frequency
5. Input voltage V
6. Ambient temperature.

The effect on detector performance of AC and DC coupling of the detector output is discussed in Section III-7. An expression for the departure of the detector input voltage from a sinusoid is presented, and a qualitative discussion of the effect of this departure is given in Section III-5.

The results calculated using the detector-design procedure are compared with measurements for both high-impedance and pulse detectors in Section IV. Measurements are presented that show the effect of a non-sinusoidal detector input voltage on detector performance.

The application of the design theory to the practical design of detector circuits is discussed in Section V. The design of both high-impedance detectors and pulse detectors is illustrated by examples. Measurements of the performance of sample detectors are reported. Measurements that compare the performance of several diode types in both high-impedance and pulse detectors are presented.

II. Survey of Detector Literature

1. Approximate Analyses Limited to Low Frequencies

Early detector-circuit theory was developed for vacuum diodes at comparatively low frequencies. Reactive effects in the diode are neglected.[1-4]* The diode is usually assumed to present a constant resistance R_F to current in the forward direction and to allow no current flow in the reverse direction.[1-3] A typical voltage-current characteristic for such a diode is shown in Fig. 2.

When the detector load time constant $R_L C_L$ is much larger than the reciprocal of the angular signal frequency ω, the output voltage v_L is almost entirely DC. If the detector input voltage is assumed sinusoidal, the diode current pulse is a portion of a sinusoid as shown in Fig. 2. The voltage efficiency is then

$$e_v = \frac{V_L}{V} = \cos\theta \quad ,$$

where the angle θ** is given by an expression obtained by integrating the current pulse***:

$$\frac{\tan\theta - \theta}{\pi} = \frac{R_F}{R_L} \quad .$$

---

*Refer to numbered references in the bibliography

**The angle θ is equal to half the total angle during which conduction takes place.

***This expression is derived in Reference 3, p. 351, and in Reference 4, p. 641. A plot of e_v vs. R_L/R_F appears in Reference 3, p. 351.

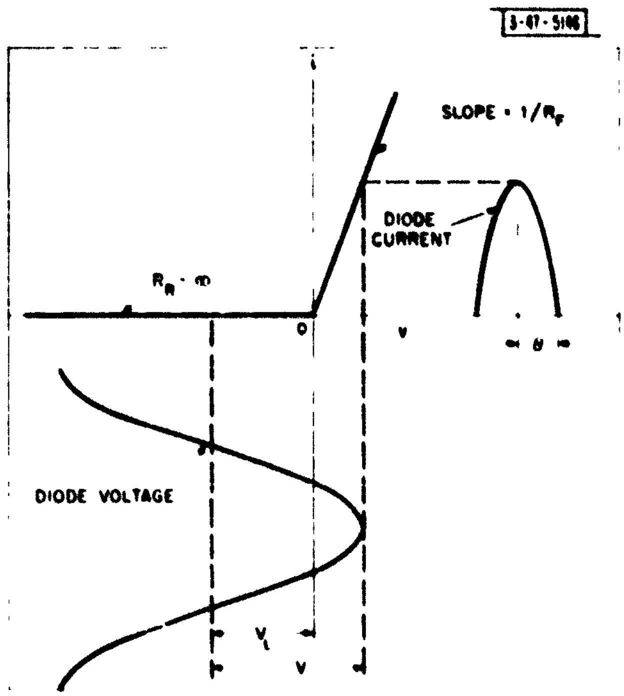

Fig. 2. A simple assumed diode static characteristic. Diode voltage and current are shown for a particular driving voltage and detector configuration.

The voltage efficiency approaches unity for small values of R_F/R_L, and decreases as R_F/R_L increases. The input resistance of the detector is obtained by a Fourier analysis of the current* pulse:

$$\frac{R_{in}}{R_L} = \frac{2 \tan \Theta - 2\Theta}{2\Theta - \sin 2\Theta} . \qquad (1)$$

The input resistance approaches $R_L/2$ for a voltage efficiency near unity, and increases for smaller voltage efficiency since less power is transferred from the input circuit to the load resistor. The voltage efficiency and input resistance are independent of input signal level as a consequence of the assumption of constant diode forward resistance. Since the load capacitor is assumed to be a short circuit at the signal frequency, the diode current is in phase with the input voltage and the input capacitance of the detector circuit is zero.

When the detector load time constant $R_L C_L$ is not large compared with $1/\omega$, the detector load capacitor C_L discharges appreciably between current pulses, and is recharged during the current pulses. In this case the detector output voltage v_L is not pure DC, and the above results are not valid. Marique[1] has shown that the voltage efficiency is a function of R_F/R_L and $\omega R_L C_L$, but the dependence is not given in closed form. Graphical calculations of the voltage efficiency are given for several values of the parameters.** The

*This expression is derived in Reference 3, p. 352-353, and in Reference 4, p. 641. A plot of R_{in}/R_L vs e_v appears in Reference 3, p. 352.

**The results of these calculation are given in Reference 1, p. 21. This work is also summarized in Reference 3, pp. 364-370, with the results of the calculations presented on p. 369.

voltage efficiency decreases when $\omega R_L C_L$ is reduced below a critical value that depends on R_F/R_L . As R_F/R_L is increased, the value of $\omega R_L C_L$ at which e_v begins to fall is reduced.

No exact solutions for the input resistance and input capacitance are given for the case when $R_L C_L$ is not large.* Power relationships give an estimate of the input resistance: The detector input power P_{in} is equal to the power loss in the diode P_D plus the DC and AC power dissipated in the load resistance, P_{L_o} and P_{L_1} respectively.

$$P_{in} = P_{L_o} + P_{L_1} + P_D \quad ,$$

$$\frac{P_{L_o}}{P_{in}} = 1 - \frac{P_{L_1} + P_D}{P_{in}} = \frac{2V_L{}^2 R_{in}}{V^2 R_L} \quad ,$$

$$\frac{R_{in}}{R_L} = \frac{1}{2e_v{}^2} \left(1 - \frac{P_{L_1} + P_D}{P_{in}}\right) .$$

Thus if the power loss in the diode P_D is approximately the same as for the large load time constant case giving the same efficiency, and if the AC power dissipation in the load resistance P_{L_1} is small compared with the input power P_{in} , then the detector input resistance is given approximately by Equation 1 with

$$\Theta = \cos^{-1} e_v .$$

---

*An approximate method for calculating e_v, R_{in}, and C_{in} in this case is given by Whalley, et al., in Reference 4, pp. 643-644. No estimate of the accuracy is given.

When P_{L1} or the increase in P_D is appreciable compared with P_{in}, the detector input resistance is smaller than given by Equation 1. When $R_L C_L$ is not large compared with $1/\omega$, the load capacitor C_L is not an effective bypass to the signal frequency, and a capacitive component of current flows in the detector circuit, resulting in a non-zero value for C_{in}.

When semiconductor diodes are used in detector circuits, the above theory is extended to take into account the back conduction of the diodes by assuming a constant resistance R_R to current flow in the reverse direction, while retaining the assumption of a constant forward resistance R_F.[4,5] Using the same methods as above, and assuming $R_L C_L$ much larger than $1/\omega$,

$$\frac{\tan\theta - \theta}{\pi} = \frac{R_F/R_L + R_F/R_R}{1 - R_F/R_R} \quad ,$$

$$e_v = \cos\theta \quad ,$$

$$\frac{R_{in}}{R_L} = \frac{1}{\left(1 + \frac{R_L}{R_R}\right)\left(\frac{2\theta - \sin 2\theta}{2\tan\theta - 2\theta}\right) + \frac{R_L}{R_R}} \quad .$$

Plots of e_v and R_{in}/R_L as functions of R_R/R_L with R_L/R_F as a parameter are shown in Figs. 3 and 4 respectively.* The voltage efficiency is nearly equal to that for infinite back resistance if R_R/R_L

*These curves are similar to those in Reference 4, p. 642, but show greater detail for low values of R_R/R_L

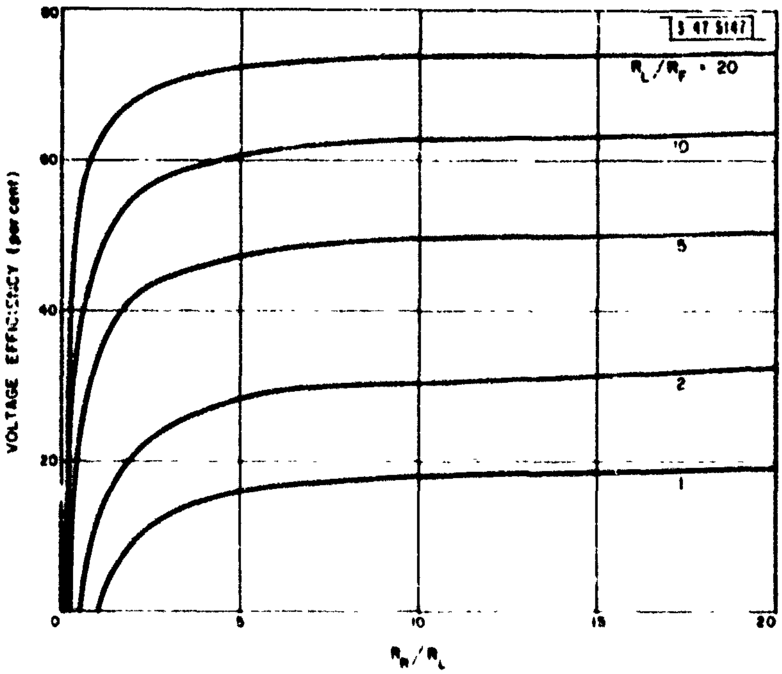

Fig. 3. Voltage efficiency as a function of R_R/R_L for several values of R_L/R_F.

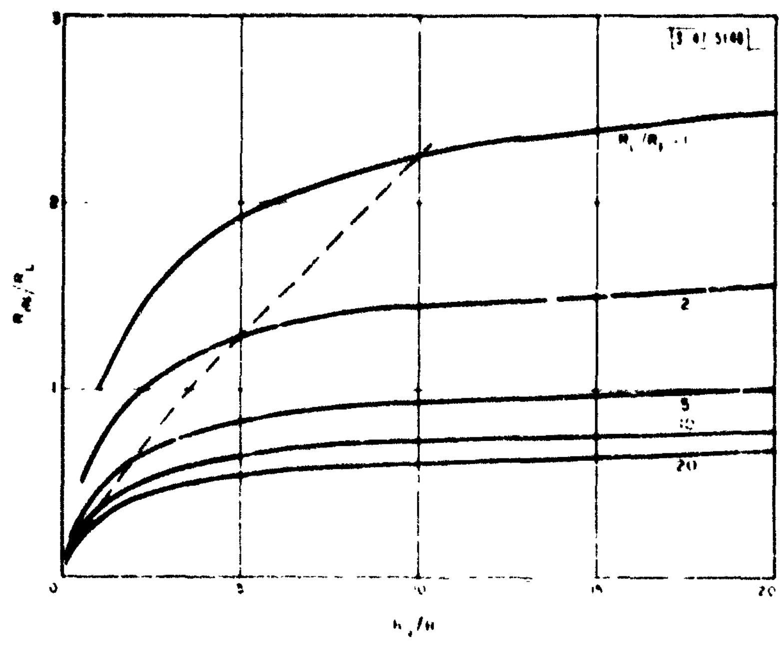

Fig. 4. Normalized input resistance as a function of R_R/R_L for several values R_L/R_F. (See text.)

is greater than five; for values of R_R/R_L less than two it is substantially lower. The input resistance is reduced from the value for infinite back resistance at larger values of R_R/R_L than those that affect the voltage efficiency. Values of R_{in}/R_L, corresponding with points to the right of the broken line in Fig. 4, can be calculated with less than 10 percent error by taking R_R in parallel with the input resistance calculated with an infinite back resistance. This includes most cases of interest.

A further attempt to approximate more closely a semiconductor-diode characteristic is to move the break point in the assumed broken-linear characteristic from zero to some small positive voltage V_B.[5] Figure 5 shows such an assumed characteristic along with a measured static characteristic of a semiconductor diode. (Note that different current scales are used for positive and negative current.) The equations for e_v and R_{in}, assuming $R_L C_L$ much larger than $1/\omega$, are as follows.

$$\left.\begin{aligned}
\frac{\tan\theta - \theta}{\pi} &= \frac{R_F/R_L\left(1 - \dfrac{V_B}{V\cos\theta}\right) + R_F/R_R}{1 - R_F/R_R}, \\[2ex]
e_v &= \cos\theta - \frac{V_B}{V}, \\[2ex]
\frac{R_{in}}{R_L} &= \frac{1}{\left(1 - \dfrac{V_B}{V\cos\theta} + \dfrac{R_L}{R_R}\right)\left(\dfrac{2\theta - \sin 2\theta}{2\tan\theta - 2\theta}\right) + \dfrac{R_L}{R_R}},
\end{aligned}\right\}\ \text{for } V \geq V_B .$$

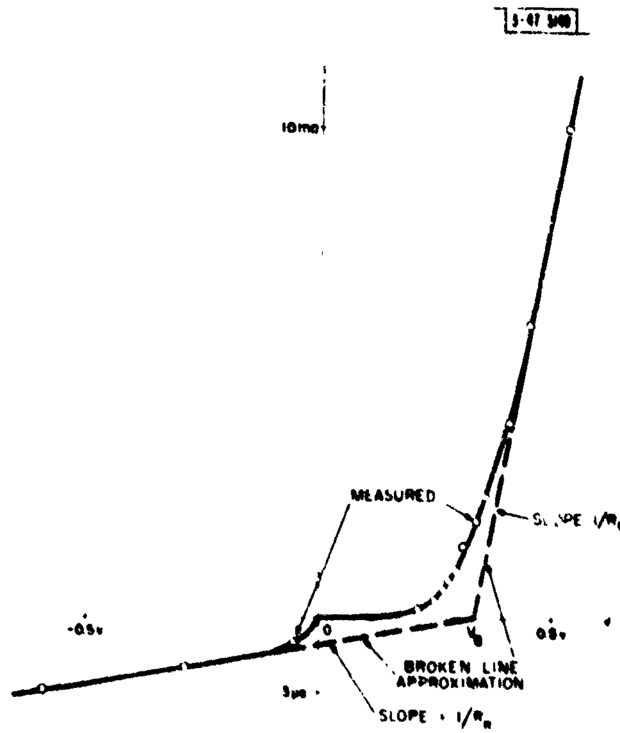

Fig. 5. Comparison of a typical measured diode static characteristic with a broken-line approximation. (Note change of current scales.)

$$\left.\begin{aligned} e_v &= 0 \ , \\ R_{in} &= R_R \ , \end{aligned}\right\} \quad \text{for } V \le V_B \ .$$

No rectification takes place for input voltages less than V_B. As V becomes larger than V_B, the voltage efficiency increases and the input resistance decreases, both approaching the values previously given for $V_B = 0$ as V becomes much larger than V_B.

Because of the errors in approximating a semiconductor-diode static characteristic with two straight lines, calculations of voltage efficiency and input resistance using the above results give values that are inaccurate even at low frequencies. However, the analyses do aid in understanding detector-circuit operation and often give useful qualitative information. Studies of more complex detector circuits[2] and of the response of detectors to modulated signals[2,33-35] often employ these approximations to simplify the analyses and obtain concise solutions.

2. High-Frequency Analyses Based on Equivalent Circuits

Reactive effects in semiconductor diodes can not be neglected in the design of detectors for the 10-100 Mcps frequency range. The capacitive effect of the barrier in a semiconductor diode has long been recognized.[5,7] More recently, semiconductor theory has shown how charge storage in a diode can result in an additional capacitive current across the junction,[8,9] and, at high forward currents, in an inductive effect in the semiconductor material around the junction.[25-27] While efforts are made to reduce the magnitude of these effects in fast-switching diodes, they still are significant in determining the performance of the detector circuit in the 10-100 Mcps frequency range.

A classical equivalent circuit for a semiconductor diode that takes the barrier capacitance into account is shown in Fig 6a.[5,7] The resistance due to the ohmic resistivity of the semiconductor material, called the spreading resistance, is represented by R_S. The barrier capacitance is represented by C_B, and the resistance of the barrier is represented by R_B. The assumed value of the barrier resistance R_B varies with the voltage across it; for positive voltages it takes on a low value, and for negative voltages a high value. Lapostolle[5] performed a transient analysis of a detector circuit using this equivalent circuit for the diode. He set R_S equal to an assumed diode forward resistance R_F, and let R_B take the value zero or $R_R - R_F$ for voltages across R_B in the forward and reverse directions respectively. At low frequencies, these assumptions correspond to the assumptions of constant forward and back resistances in the preceding analyses. The results of the transient analysis indicate that the effect of C_B is to reduce the detector voltage efficiency and input resistance at high frequency below those obtained when C_B is negligible. The input resistance is affected at a lower frequency than the voltage efficiency. Experimental verification is given at 3000 Mcps Apparently at this frequency the effect of charge storage is negligible compared with the effect of the barrier capacitance in the diode that was used. Other studies[6,8,9] show that charge storage can not be neglected in the 10-100 Mcps frequency range.

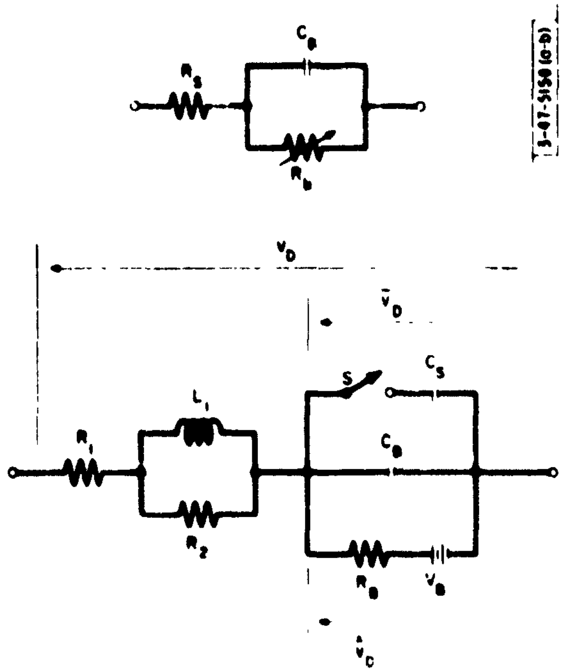

Fig. 6. Two equivalent circuits for diodes: a) Classical equivalent circuit. b) Equivalent circuit proposed by Heinlein.

A semiconductor-diode equivalent circuit that takes charge storage into account is given by Heinlein[6] and is shown in Fig. 6b. The capacitor C_B represents the barrier capacitance, and the capacitive charge-storage effect is represented by C_S in conjunction with the switch S. The charge-storage capacitance C_S is typically 50 times the barrier capacitance C_B, but its value varies with signal frequency and applied voltage. The switch S is closed when the voltage $\bar{v}_D$ across the junction is positive, allowing C_S to take on a positive charge, but the switch opens when $\bar{v}_D$ becomes negative, preventing C_S from taking on a negative charge. The barrier resistance R_B is assumed to take on a value of zero or infinity depending on whether the voltage $\hat{v}_D$ across it is positive or negative. The battery V_B prevents current flow through R_B until the junction voltage $\bar{v}_D$ is greater than V_B. The combination of R_1, R_2 and L_1 represents the bulk impedance of the semiconductor material. At low frequencies the bulk impedance is the resistance R_1, but at higher frequencies the impedance increases and becomes partially inductive. At very high frequencies, the impedance is again resistive but with a value $R_1 + R_2$.

The physical significance of the various portions of this equivalent circuit for a semiconductor diode is best understood in the light of semiconductor theory, a summary of which is given below. Heinlein[6] justifies the equivalent circuit on the basis of measurements made on actual diodes. Because of the complexity of the diode-equivalent circuit only a qualitative analysis of the operation of a detector circuit is given. The analysis shows a reduction of the detector-circuit input resistance with increasing frequency, due largely to the effect of the charge-storage capacitor C_S. A smaller reduction is noted in voltage efficiency, due principally to the effects of L_1 in the bulk impedance and the charge-storage capacitor C_S. Experimental data are given that verify qualitatively the results of the analysis.

3. Basic p-n Junction Theory

The complex nature of the semiconductor diode makes it difficult to represent the diode by a combination of conventional circuit elements with sufficient accuracy and simplicity to allow an accurate analysis of a detector circuit in the 10-100 Mcps frequency range. Another approach to the problem of designing detector circuits is to investigate the physical mechanisms of diode operation and develop formulae that can be used with circuit equations to calculate quantitative results.

The basic theory of p-n junction semiconductor diodes has been developed by Shockley.[8,9] Diagrams of two types of diodes are shown in Fig. 7. Figure 7a is a diagram of a planar p-n junction diode such as is analyzed by Shockley[8,9] and others.[10,22] Figure 7b shows a model commonly proposed[11,13,14,16] for point-contact and bonded diodes. The basic operation of both types of diodes is briefly reviewed in the following paragraphs.*

Impurities are present in the n-region such that at equilibrium the concentration of free electrons is much greater than the concentration of holes. Hence in the n-region electrons are called majority car

---

* This discussion follows that of Shockley Reference 8 pp. 456-462, and Reference 9 pp 309-318

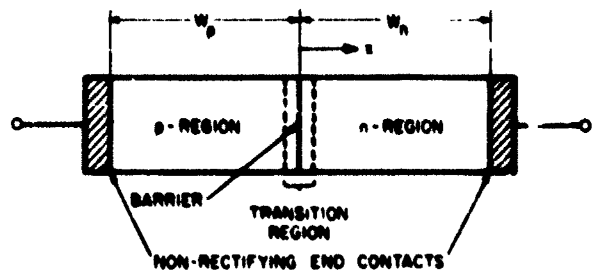

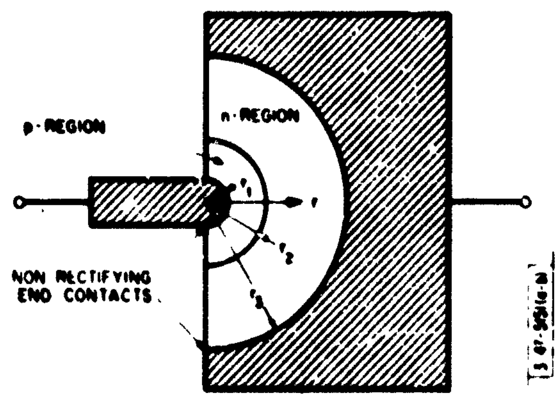

Fig. 7. Models for semiconductor diodes: a) Planar diode. b) Point contact or bonded diode.

rent carriers and holes are called minority current carriers. In the p-region the roles of the holes and electrons are reversed. When a positive potential difference is applied between the p- and n-regions, holes are injected across the barrier into the n-region, increasing the concentration of minority carriers in the n-region above the equilibrium concentration. Since the resistance in the p-region to the flow of holes is small, the flow of hole current across the junction is largely determined by the action of the holes in the n-region, where they are minority current carriers. Similarly, the flow of electrons across the junction is largely determined by the action of the electrons in the p-region. The total diode current is the sum of the hole and electron currents crossing the junction. The magnitudes of the hole and electron currents are not in general equal, but depend on the geometry of the diode and the concentrations of impurities in the p- and n-regions. The following discussion considers only hole current, but identical reasoning yields analogous results for electron current.

The hole-current density in the n-region $\vec{J}_p$ is given by*

$$\vec{J}_p = q \mu_p p \vec{E} - q D_p \vec{\nabla} p .$$

where

p - hole density,

$\vec{E}$ - electric field,

D_p - hole diffusion constant,

---

*Reference 9, p. 308, Equation 20

μ_p = hole mobility = qD_p/kT ,*

q = electron charge ,

k = Boltzmann's constant,

T = absolute temperature.

The first term represents the drift current and the second the diffusion current. The hole density in the n-region is given by the diffusion equation,**

$$\frac{\partial p}{\partial t} = - \frac{p - p_n}{\tau_p} - \frac{1}{q} \nabla \cdot \vec{J}_p \ ,$$

where

p_n = equilibrium hole density in the n-region,

τ_p = hole lifetime.

The second term represents the reduction in hole density due to the flow of hole current. The first term represents a reduction in hole density caused by the recombination of holes with free electrons in the n-region. The average distance a hole travels before recombining is called the hole diffusion length L_p , and is given by***

$$L_p = \sqrt{D_p \tau_p} \ .$$

*Reference 9, p 300, Equation 4.

**Reference 9, p. 313, Equation 13

***Reference 9, p. 314, Equation 18

Shockley solved the above equations under the following assumptions:

1. The junction is planar (as shown in Fig. 7a). This reduces the equations to a single dimension.

2. The junction is narrow compared with the diffusion length L_p. This permits neglect of recombination in the junction region.

3. The p- and n-regions are long compared with the diffusion length L_p. This provides a boundary condition for the diffusion equation,*

$$p = p_n , \quad \text{for} \quad x >> L_p . \tag{2}$$

4. The hole density is much lower than the equilibrium electron density. This, in conjunction with Assumption 2, provides the second boundary condition:**

$$p = p_n e^{\overline{V}_D q/kT} , \quad \text{for} \quad x = 0 ,$$

where $\overline{V}_D$ is the voltage across the junction.

---

*The use of this boundary condition is implied by Shockley.[8,9] It is clearly stated elsewhere.[13,22]

**Reference 9 p. 312. Equation 8

5. The diode current is sufficiently small so that the voltage drops across the diffusion regions may be neglected. With this assumption, the voltage across the junction $\overline{v}_D$ is equal to the voltage applied to the diode v_D. This assumption also allows the neglect of the drift current in the current equation.

6. The recombination time τ_p is constant.

The validity of these assumptions is discussed in Section II-4.

With the above assumptions, the current and diffusion equations become

$$J_{p_x} = -q D_p \frac{\partial p}{\partial x} ,$$

$$\frac{\partial p}{\partial t} = - \frac{p - p_n}{\tau_p} + D_p \frac{\partial^2 p}{\partial x^2} , \tag{3}$$

where J_{p_x} is the hole-current density in the x direction. The boundary conditions become:

$$p(0) = p_n e^{\overline{v}_D q/kT} , \tag{4}$$

$$p(\infty) = p_n .$$

Shockley[8,9] gives the solution to these equations for a diode voltage V_D of a small AC signal of angular frequency ω superimposed on a DC bias:

$$V_D = \overline{V}_o + V e^{j\omega t} \quad ,$$

where $V \ll kT/q$. The diffusion equation is solved and the result substituted into the current equation. The hole-current density at the junction is found by setting $x = 0$.

The DC hole-current density J_{p_o} is found to be

$$J_{p_o} = \frac{q p_n D_p}{L_p} \left(e^{\overline{V}_o q/kT} - 1\right) .$$

The DC hole current I_{p_o} is obtained by multiplying the DC hole-current density by the junction area A:

$$I_{p_o} = \frac{q A p_n D_p}{L_p} \left(e^{\overline{V}_o q/kT} - 1\right) .$$

A corresponding expression is obtained for the DC electron current I_{n_o}, and the total DC diode current I_o is

$$I_o = I_{p_o} + I_{n_o} = q A \left(\frac{p_n D_p}{L_p} + \frac{n_n D_n}{L_n} \right) \left(e^{\overline{V}_o q/kT} - 1\right) .$$

It is convenient to define

$$I_S = q A \left[\frac{p_n D_p}{L_p} + \frac{n_n D_n}{L_n} \right] \quad \text{(for wide planar diode).}$$

Then

$$I_o = I_S (e^{V_o q/kT} - 1) . \tag{5}$$

This is the conventional* exponential expression for the DC characteristic of a semiconductor diode. For large negative applied voltage V_o, the DC current approaches I_S. Hence I_S is called the reverse saturation current.

The AC hole-current density J_{p_1} and hole current I_{p_1} are given by

$$J_{p_1} = \frac{q p_n \mu_p}{L_p} (1 + j\omega T_p)^{\frac{1}{2}} e^{V_o q/kT} V ,$$

$$I_{p_1} = \frac{q A p_n \mu_p}{L_p} (1 + j\omega T_p)^{\frac{1}{2}} e^{V_o q/kT} V .$$

At a fixed frequency, the hole current varies exponentially with the DC bias voltage V_o, and linearly with the applied AC voltage V. The latter result is a consequence of the assumption that V is much smaller than kT/q, which is equivalent to assuming that the diode is linear over the range of V. The frequency dependence of the hole current is given by the term $(1 + j\omega T_p)^{1/2}$. It is convenient to define the effective hole-diffusion length L_{p_ω} for the diode being considered to include this frequency dependence:**

---

*Reference 7, p. 82.

**See Reference 10, p. 1185.

$$L_{p_\omega} = \frac{L_p}{(1 + j\omega\tau_p)^{1/2}}, \quad \text{(for wide planar diode).}$$

The AC hole current is then

$$I_{p_1} = \frac{qAp_n\mu_p}{L_{p_\omega}} e^{\overline{V}_o q/kT} \overline{V} \quad .$$

The real and imaginary parts of the hole current, normalised by dividi g by the low-frequency value of hole current, are plotted as functions of $\omega\tau_p$ in Fig. 8. The curves for $W_n/L_p = \infty$ apply to the diode having wide diffusion regions that has been considered. The real part of the hole current (in phase with the applied voltage) is nearly constant with frequency at angular frequencies well below $2/\tau_p$, and increases with frequency at a rate approaching 3 db per octave at angular frequencies well above $2/\tau_p$. The imaginary part of the hole current (leading the applied voltage by 90 degrees) increases with frequency at a 6 db-per-octave rate at angular frequencies well below $2/\tau_p$, and lessens its rate of increase to 3 db per octave at angular frequencies well above $2/\tau_p$. Thus at angular frequencies well below $2/\tau_p$ the diode hole current is analogous to the current through the parallel combination of a fixed resistance and a fixed capacitance. At angular frequencies well above $2/\tau_p$ the resistor and capacitor both decrease in value with increasing frequency at a rate of 3 db per octave.

The corresponding expression for the AC electron current I_{n_1} is

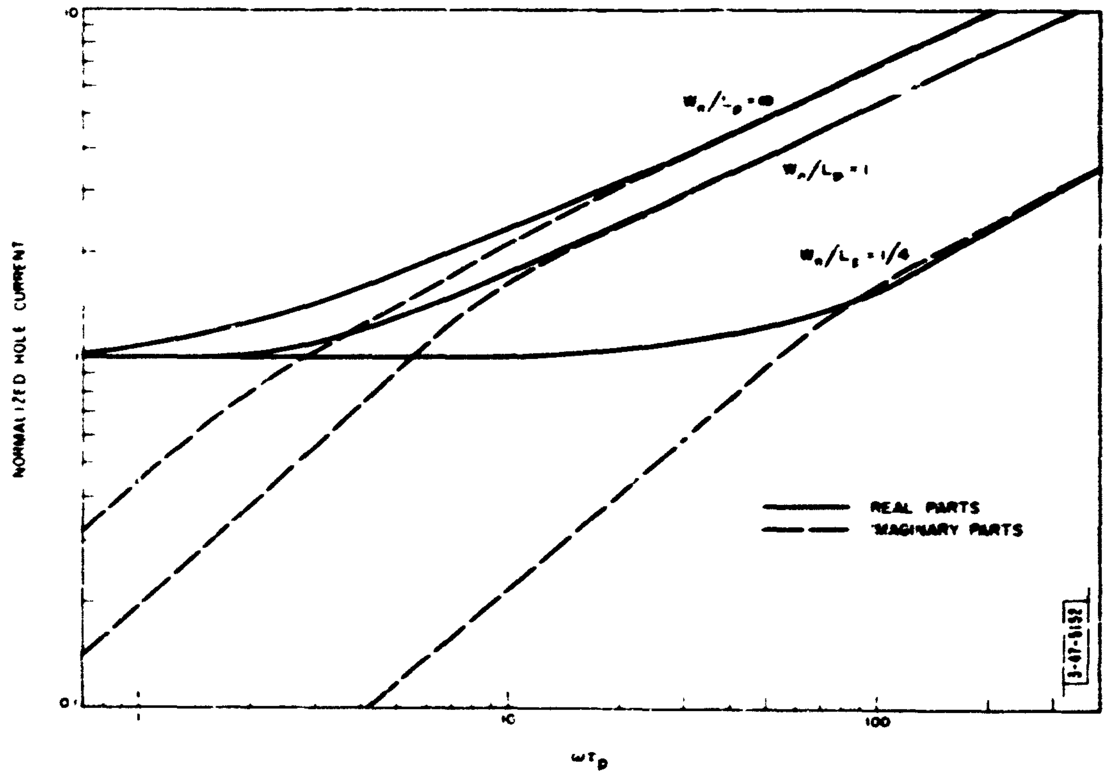

Fig. 8. Normalized hole current as a function of $\omega\tau_p$ for three values of W_n/L_p. The curves also give normalized electron current if corresponding parameters are substituted. (See text.)

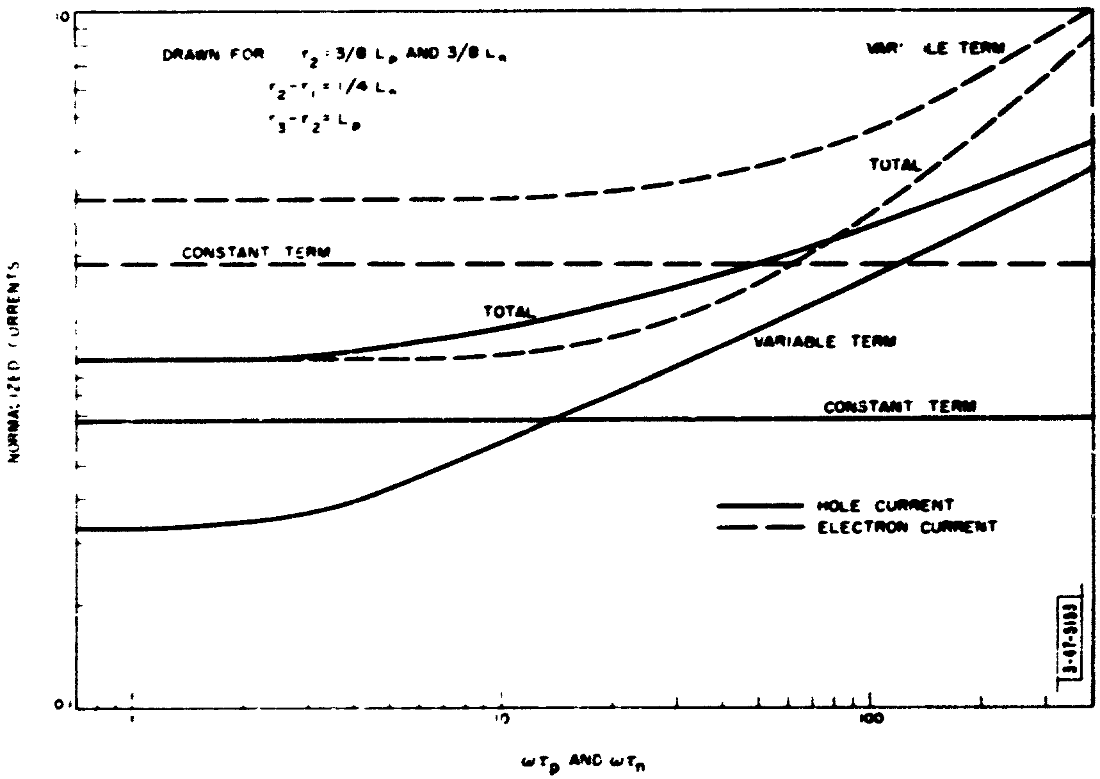

Fig. 9. An example showing the summation of hole and electron current terms in a hemispheric diode.

$$I_{n_1} = \frac{qA\, n_n \mu_n}{L_{n_\omega}} \; e^{V_o q/kT} \; V ,$$

where

$$L_{n_\omega} = \frac{L_n}{(1 + j\omega\tau_n)^{1/2}} , \quad \text{(for wide planar diode).}$$

The AC electron current behaves in the same way as the AC hole current, but since the constants in the expressions are different, the magnitudes of the two currents are in general different. The frequency dependence of the normalized electron current is given by Fig. 8 if the horizontal scale is calibrated in units of $\omega\tau_n$, which will in general be different from $\omega\tau_p$. The total AC diode current is

$$I_1 = I_{p_1} + I_{n_1} = qA\, e^{V_o q/kT} \left(\frac{p_n \mu_p}{L_{p_\omega}} + \frac{n_n \mu_n}{L_{n_\omega}} \right) V . \quad (6)$$

The total AC diode current varies with the applied DC bias and AC voltage in the same way as the hole and electron currents. The variation of I_1 with frequency is the appropriately weighted average of the variations of I_{p_1} and I_{n_1} with frequency

The above analysis may be modified to apply to a planar diode having diffusion regions that are not long compared with the diffusion lengths [10] In this case Assumption 3 is not valid, and the boundary condition given in Equation 2 is replaced by

$$p = p_n \quad \text{for} \quad x = W_n$$

$$I_{n_1} = \frac{qAn_n\mu_n}{L_{n_\omega}} e^{V_o q/kT} V ,$$

where

$$L_{n_\omega} = \frac{L_n}{(1 + j\omega T_n)^{1/2}} \quad , \text{ (for wide planar diode)}.$$

The AC electron current behaves in the same way as the AC hole current, but since the constants in the expressions are different, the magnitudes of the two currents are in general different. The frequency dependence of the normalized electron current is given by Fig. 8 if the horizontal scale is calibrated in units of ωT_n, which will in general be different from ωT_p. The total AC diode current is

$$I_1 = I_{p_1} + I_{n_1} = qAe^{V_o q/kT} \left(\frac{p_n\mu_p}{L_{p_\omega}} + \frac{n_n\mu_n}{L_{n_\omega}} \right) V . \quad (6)$$

The total AC diode current varies with the applied DC bias and AC voltage in the same way as the hole and electron currents. The variation of I_1 with frequency is the appropriately weighted average of the variations of I_{p_1} and I_{n_1} with frequency.

The above analysis may be modified to apply to a planar diode having diffusion regions that are not long compared with the diffusion lengths.[10] In this case Assumption 3 is not valid, and the boundary condition given in Equation 2 is replaced by

$$p = p_n \text{ for } x = W_n$$

The DC diode current I_o for the diode having narrow diffusion regions is again given by Equation 5, but the value of the reverse saturation current I_s is given by

$$I_s = qA \left[\frac{p_n D_p}{L_p \tanh W_n/L_p} + \frac{n_n D_n}{L_n \tanh W_p/L_n} \right] ,$$

(for narrow planar diode).

The AC diode current I_1 is given by Equation 6, but the effective diffusion le .gths L_{p_ω} and L_{n_ω} that determine the frequency dependence of the AC current are given by

$$\left.\begin{aligned} L_{p_\omega} &= \frac{L_p \tanh \left[W_n/L_p (1 + j\omega\tau_p)^{\frac{1}{2}} \right]}{(1 + j\omega\tau_p)^{1/2}} , \\ L_{n_\omega} &= \frac{L_n \tanh \left[W_p/L_n (1 + j\omega\tau_n)^{\frac{1}{2}} \right]}{(1 + j\omega\tau_n)^{1/2}} . \end{aligned}\right\} \text{(for narrow planar diode).}$$

The real and imaginary parts of the AC diode hole current I_{p_1}, normalized by dividing by the low-frequency value of I_{p_1}, are plotted as functions of $\omega\tau_p$ in Fig. 8. Curves are given for values of n-region width W_n of L_p and $L_p/4$, along with the curves for the wide n-region case. The curves show that, for the same value of τ_p, a diode having a narrow n-region maintains its low-frequency behavior to higher frequencies than a diode having a wide n-region. The change in the frequency dependence is marked only if the n-region width W_n is smaller than the hole-diffusion length L_p. The curves of Fig 8 also give the normalized electron current if the horizontal scale is calibrated in units of $\omega\tau_n$

The analysis of a diode having the hemispheric configuration* shown in Fig. 7b can be made by writing the diffusion equation and current equation in spherical coordinates and assuming only radial variation of hole density and hole-current density. If Assumptions 2, 4, 5, and 6 are applied, the diffusion equation and current equation take the form,

$$\frac{\partial p}{\partial t} = -\frac{p - p_n}{\tau_p} + D_p \left(\frac{\partial^2 p}{\partial r^2} + \frac{2}{r} \cdot \frac{\partial p}{\partial r} \right) ,$$

$$J_{p_r} = -q D_p \frac{\partial p}{\partial r} ,$$

where J_{p_r} is hole-current density in the radial direction. For the diode shown in Fig. 7b, the boundary conditions become

$$p(r_2) = p_n e^{V_D q/kt} ,$$

$$p(r_3) = p_n .$$

It is assumed here that the diode base material is n-type and that the small volume around the contact point is p-type. A corresponding analysis of p-type base diodes can be made following the same procedures.

The solution of these equations shows that the DC and AC diode currents I_o and I_1 are again given by equations 5 and 6 respectively. In this case, the reverse saturation current I_S is given by

*See for example References 13 and 14

$$I_S = qA\left[p_n D_p\left(\frac{1}{L_p \tanh\left(\frac{r_3 - r_2}{L_p}\right)} + \frac{1}{r_2}\right)\right.$$

$$\left. + \, n_n D_n\left(\frac{1}{L_n \tanh\left(\frac{r_2 - r_1}{L_n}\right)} - \frac{1}{r_2}\right)\right] ,$$

(for hemispheric diode),

and the effective diffusion lengths L_{p_ω} and L_{n_ω} are given by

$$\frac{1}{L_{p_\omega}} = \frac{(1 + j\omega\tau_p)^{1/2}}{L_p \tanh\left[\frac{r_3 - r_2}{L_p}(1 + j\omega\tau_p)^{1/2}\right]} + \frac{1}{r_2} ,$$

$$\frac{1}{L_{n_\omega}} = \frac{(1 + j\omega\tau_n)^{1/2}}{L_n \tanh\left[\frac{r_2 - r_1}{L_n}(1 + j\omega\tau_n)^{1/2}\right]} - \frac{1}{r_2} .$$

(for hemispheric diode).

The first terms in the above expressions are equal to the expressions for $1/L_{p_\omega}$ and $1/L_{n_\omega}$ for a narrow planar diode having corresponding p- and n-region widths:

$$W_n = r_3 - r_2 ,$$

$$W_p = r_2 - r_1$$

The real part of $1/L_{p_\omega}$ is larger than that for the narrow planar diode by $1/r_2$, and the real part of $1/L_{n_\omega}$ is smaller by the same amount. The variation of the real parts of the AC hole and electron currents with frequency is shown by an example in Fig. 9. The hole and electron currents are normalized by dividing by their low-frequency values, and are plotted as functions of ωT_p and ωT_n respectively. The addition of the constant term to the hole current extends its low-frequency behavior to higher frequencies, while the subtraction of the constant term from the electron current reduces the range of low-frequency behavior.*

The analyses given above show how the diode operation is affected by the changes in geometry:

1. The DC current and the low-frequency AC current are changed by a constant factor
2. The frequency dependence of the AC current is modified. The frequency range over which the diode resistance and capacitance are constant is extended by making the diffusion regions narrow, and by using the hemispheric geometry (providing the hole current predominates).

4. Limitations and Extensions of Basic p-n Junction Theory

It is necessary to examine the assumptions made in the analyses of diode operation in Section II-3 to determine the applicability of the results to circuit design problems. Assumptions 1 2, and 3 concern the geometry of the diode. When diodes having geometry different

*See Reference 13, pp 40-41

from that analyzed by Shockley are considered, an appropriate diode geometry is assumed and Assumptions 1 and 3 are modified accordingly. For each type of diode, the geometry assumed is generally thought to be valid,* at least to a first approximation. Substantial discrepancies between theoretical and experimental results are explained by other effects. Assumptions 4, 5, and 6 are found to be valid only at very low signal levels,** much lower than those normally found in detector circuits. Much work has been done to extend the analysis to obtain results valid at larger signal levels.[11-27]

For applied DC voltages of the order of 0.1 volt and larger, an appreciable part of the applied voltage is developed across the semiconductor diffusion regions, resulting in the junction voltage $\bar{v}_D$ being smaller than the applied voltage v_D. Classical theory*** took this into account by assuming a resistance R_S, called the spreading resistance, in series with the diode junction. Equation 5 then becomes

$$i = I_S \left[e^{\bar{v}_D q/kt} - 1 \right] = I_S \left[e^{\frac{(v_D - i R_S)q}{kT}} - 1 \right]$$

For large applied voltages, the toal diode resistance was assumed to approach R_S. Semiconductor theory shows that as the diode current increases, more charge carriers are present in the diffusion regions and the bulk resistivity of the semiconductor is thereby reduced[13,16,18]

*For example see Reference 8, p 456; and Reference 14, p 270.

**See References 13, 14, 15, 22, 23, and 24

***See Reference 7 p 83

The diode spreading resistance is not, then, a constant, but decreases with increasing forward current.

The semiconductor bulk resistivity is reduced only after the carriers flow into the diffusion regions. Therefore at high frequencies the diode current tends to lag behind the voltage across the diffusion regions, giving rise to an inductive component of the bulk impedance.[25-27] The effect of this inductive reactance is larger at higher forward currents and at higher frequencies.

An appreciable voltage across the diffusion region results in a drift component of current that can no longer be neglected in comparison with diffusion current. When the drift current term is retained in the current equation, the resulting diffusion equation is non-linear, making its solution extremely difficult.* Some of the papers[11,13,14,19] discussed below take into account the drift current and, by making appropriate simplifications, obtain solutions for the static diode characteristic.

When the concentration of minority carriers near the junction approaches the equilibrium concentration of majority carriers, the solution of the simplified diffusion equation (Equation 3) using the boundary condition given by Equation 4, is not valid.[14,22,23] This condition exists in practical diodes at levels far below those normally found in detector circuits.** Rittner[22] has modified the diffusion equation so that the simple boundary condition given in Equation 4 may

---

*Reference 22, p. 1163

**See Reference 14, p. 272, and Reference 22, p. 1164. Equations 28 to 32 in Reference 22 are applicable to diodes as well as transistors.

be applied at high levels. A general solution of the modified diffusion equation is not given. Misawa[23,24] has derived a modified boundary condition that can be used with the simplified diffusion equation given in Equation 3 at high levels. A general solution of the diffusion equation, using this boundary condition, is not given.

Hall[15] has shown that the recombination times τ_p and τ_n are not constant when the concentration of minority carriers approaches the concentration of majority carriers. The recombination times decrease with increasing forward current from their low-level values and approach constant values when the minority-carrier concentrations become greater than 100 times the majority-carrier concentrations. If τ_p and τ_n are known as functions of DC current, then the small signal ($\tilde{V} << kT/q$) AC current is still given by Equation 6. For larger AC signals, τ_p and τ_n vary with time, making the solution of the diffusion equation difficult.

Factors that affect the diode current generally affect the hole and electron currents crossing the p-n junction by different amounts. Thus, the portions of the total diode current carried across the junction by holes and by electron vary with signal level and signal frequency.

A complete solution for the diode current resulting from large applied AC and DC voltages is extremely difficult to obtain. Several analyses have yielded solutions for the static diode characteristic[11,13,18,19]. In each of these analyses specific diode parameters were assumed and appropriate simplifications and approximations were made. The characteristics were then calculated numerically. Three typical static characteristics obtained in these analyses are shown in Fig. 10 along

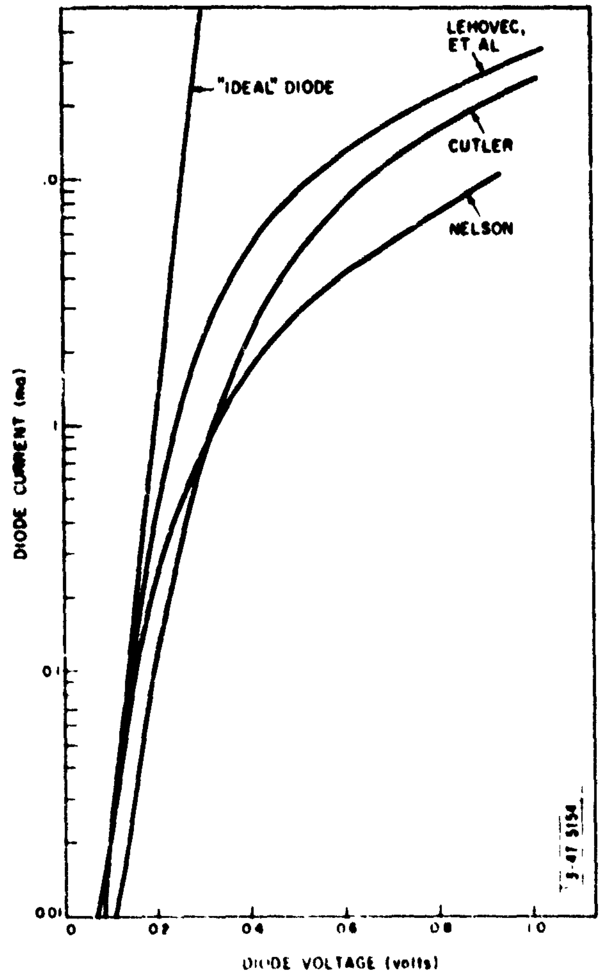

Fig. 10. Three calculated static characteristics for hemispheric diodes. An "ideal" exponential characteristic is shown for comparison.

with a curve representing an "ideal" diode having an exponential characteristic. Although the parameters assumed in the analyses differ somewhat, the shapes of the three curves are seen to be similar. In each case hemispheric geometry, appropriate for point-contact or bonded diodes, was assumed. Each of the characteristics departs from exponential at approximately 0.1 volt; the current rising less rapidly for larger voltages. Swanson[16] gives theoretical justification for a region following an $e^{v_D q/2kT}$ characteristic in the range just above 0.1 volt. At high levels the characteristic becomes approximately quadratic.* Comparisons of the calculated characteristics with measurements give good agreement.

Large AC signals are treated in the classical theory** by neglecting reactive effects and assuming that the diode current-voltage characteristic is exponential:

$$i = I_S \left(e^{v_D q/kT} - 1\right) .$$

For an applied voltage

$$v_D = V_o + V e^{j\omega t} \quad ,$$

the DC and AC diode current components are given by

---

*Reference 16, p. 320.

**Reference 7, p 155, and Reference 10.

$$I_o = I_S \left[e^{-V_o q/kt} \; I_o \left(\frac{Vq}{kT} \right) - 1 \right] ,$$

$$I_1 = 2 I_S \; e^{-V_o q/kT} \; I_1 \left(\frac{Vq}{kT} \right) ,$$

where I_o and I_1 are modified Bessel functions of orders zero and one respectively. Since reactive effects are important in the 10-100 Mcps frequency range, and the exponential characteristic is not valid for voltages greater than 0.1 volt, this treatment is not particularly useful for detector-circuit design.

Large-signal analyses that take into account departures of the diode characteristic from exponential and diode reactive effects lead to complex equations that are difficult to solve. In one analysis[12] a simplified diode model was assumed consisting of a resistance in series with a diode that follows the small-signal equations at large signal levels. Even in this case numerical methods were necessary to obtain a solution. While the possibility exists of solving the complex diode equations by using an analog or digital computer, the necessity of tabulating solutions for large ranges of many variables makes such a method of questionable value for circuit design.

5. Diode Reverse-Bias Characteristics

The limitations in the basic p-n junction theory discussed above apply when the diode forward current is large. Since large reverse currents do not occur (short of reverse breakdown), these limitations do not apply to the reverse characteristics of semiconductor diodes.

However, the application of a reverse voltage across the junction results in widening of the barrier region that modifies the diode characteristics. The results of the preceding analyses predict that for reverse-bias voltages greater than a few times kT/q, the diode DC current I_o approaches the value $-I_S$, and the incremental AC diode current I_1 approaches zero. The variation in the width of the barrier region with reverse voltage can result in a reverse current that is larger than I_S, and in larger incremental AC current than predicted by the basic p-n junction theory.

Shockley* has shown that the width W of the barrier region in an abrupt-junction planar diode with reverse bias is given by:

$$v_o - v_D = \frac{2\pi q p_p n_n}{\kappa (p_p + n_n)} W^2 ,$$

where κ is the dialectric constant of the semiconductor material and v_o is the contact potential between the p- and n-type semiconductor materials, which is normally 0.2 to 0.5 volt. Nelson** has calculated the barrier-region width in an abrupt-junction hemispheric diode. For small reverse biases the barrier region width W varies with reverse bias in approximately the same way as for the planar diode; for larger reverse biases the barrier-region width may be somewhat larger or smaller than for the planar diode, depending on the relative concentrations of holes and electrons in the diode diffusion regions.

---

*Reference 8, p. 450, Equation 2.53

**Reference 14, p. 272

The presence of layers of charges on each side of the barrier region of a reverse-biased diode results in a component of diode capacitance called the barrier capacitance C_B.[8] Since the capacitance resulting from the diode diffusion current approaches zero for reverse bias, the barrier capacitance accounts for practically the entire diode capacitance for reverse bias greater than 0.1 volt. The magnitude of the barrier capacitance C_B varies inversely with the barrier region width W. For abrupt-junction planar diodes[8],

$$C_B = \sqrt{\frac{K q p_p n_n}{8\pi (p_p + n_n)} \cdot \frac{1}{v_o - v_D}} .$$

A similar expression gives the approximate relationship for abrupt-junction hemispheric diodes for small reverse biases.*

The widening of the junction region may result in an increase of reverse current with reverse-bias voltage. It has been shown that, in diodes made of high-resistivity material, e.g., silicon, the generation of current carriers in the transition region results in a component of reverse current that varies with the barrier width.** In diodes having narrow diffusion regions, the widening of the barrier region results in an appreciable narrowing of the diffusion region. Nelson[13, 14] has shown that this narrowing of the diffusion regions results in an increase in the reverse diode current that is approximately proportional to the square root of the potential across the barrier $(v_o - v_D)$. In both cases the reverse diode characteristic is approximately given by

---

*Reference 14, p. 273; in Reference 13, pp. 50-51, Nelson shows that in a typical hemispheric-junction diode the inverse-square-root relationship is in error by only 25 percent for a reverse bias as large as 10 volts

**Reference 21, p. 1232

$$i = -I_S - D\sqrt{v_o - v_D} \quad ,$$

where D is a constant depending on the diode parameters.

III. Theory for Detector Design

1. Basis of Design Procedure

Because of the complex nature of the semiconductor diode, it is necessary to resort to approximations in describing its operation if the description is to be simple enough to be useful in designing practical detector circuits. In the procedure that is developed here, measurements are made of a few diode parameters, and expressions for the diode performance are given in terms of these parameters. It is assumed that these expressions approximate the actual diode behavior over the range of operating conditions found in the detector circuit. The expressions are then used to calculate the performance of detector circuit.

A procedure is first developed for calculating the performance of a detector circuit having a large load capacitor C_L and driven by a sinusoidal input voltage V . An approximate method is then given for evaluating the changes in detector performance resulting from a detector load capacitance that is not large. An approximate expression is derived for the flattening of the detector input voltage waveform when the detector is not driven from a voltage source, and the effects of this flattening on detector performance are discussed. Expressions for evaluating the effects of small changes in ambient temperature on detector performance are given. The effects on detector-circuit performance of the output coupling circuit are discussed. Finally, the theory for calculating the transient response of pulse detector circuits is given.

2. Low-Frequency Operation

In Section II-4 it was shown that the DC diode current departed markedly from the "ideal" characteristic

$$i = I_S \left[e^{v_D q/kT} - 1 \right] ,$$

for values of applied voltage v_D greater than 0.1 volt. However, values of the constants may be chosen so that an exponential expression gives a good approximation to a diode static characteristic over a restricted range of levels. Figures 11 and 12 show the measured forward and reverse characteristics respectively of a typical germanium diode, along with approximations to the characteristics. Curve A on both figures follows the expression

$$i = 0.001 \left(e^{v_D/0.0377} - 1 \right) ,$$

where i is the diode current in milliamperes and v_D is the diode voltage in volts. This expression gives a fair approximation to the forward diode characteristic for voltages less than 0.25 volt, but it is not a good approximation to the back characteristic due to the failure of the diode back current to saturate for large values of back voltage. A better approximation is obtained by adding a linear term to the diode current. Curve C in Figure 12 follows the expression

$$i = 0.001 \left(e^{v_D/0.0377} - 1 \right) + v_D/2270 ,$$

and gives a good approximation to the diode back characteristic. The linear term is so small that its effect on the forward characteristic is negligible.

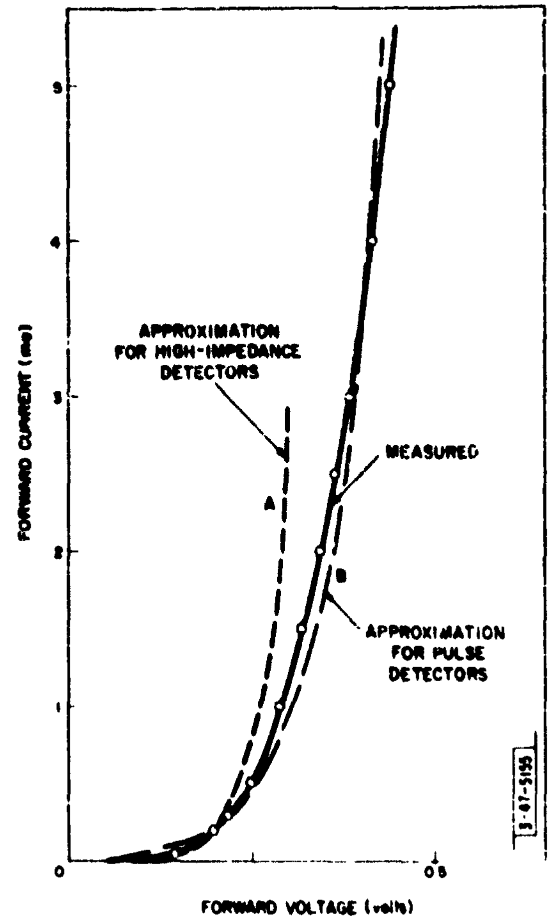

Fig. 11. A measured diode forward characteristic and two exponential approximations. (See text.)

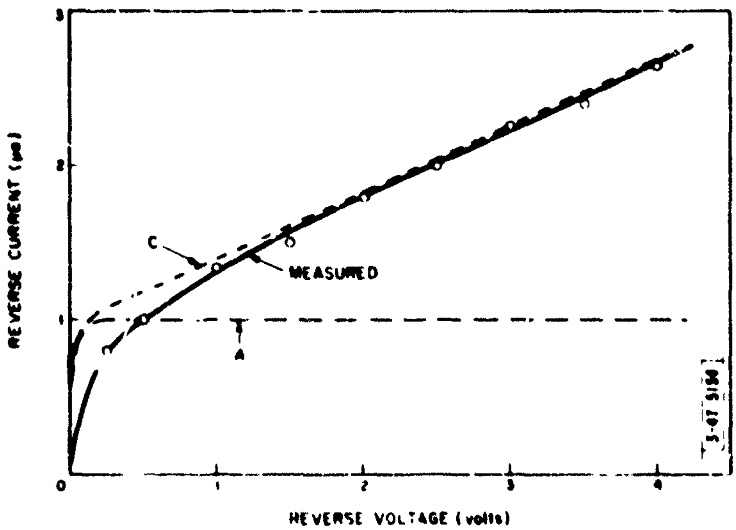

Fig. 12. A measured diode reverse characteristic and two approximations. (See text.)

An expression of this sort can be used to approximate the diode static characteristic for the design of high-impedance detectors, since the voltage range over which it is a good approximation to the diode characteristic includes the range of voltages applied to the diode. This can be shown by an example: With a peak detector input voltage V of 1.0 volt, the detector output voltage V_L cannot exceed 1.0 volt. Assuming a load resistance R_L of one megohm, the average diode current I_o is less than 1.0 μamp. Thus the diode must be biased in the reverse region most of the time. The peak diode forward current I_p may be estimated by using a linear approximation for the diode forward characteristic as described in Section II-1. For an assumed diode forward resistance R_F,

$$I_p = I_o \frac{R_L}{R_F} \frac{1 - e_v}{e_v} ,$$

where the voltage efficiency e_v is given in Section II-1. An assumed value of R_F of 10 ohms gives a peak diode current of 112 μamp, which is well within the range where the approximation is valid. A larger value of R_F would be more realistic, and would yield a smaller value of I_p

Similar reasoning shows that a diode in a pulse detector circuit having a load resistance R_L of a few thousand ohms may have forward currents of several ma for detector input voltages of the order of one volt. Curve B in Figure 11 follows the expression

$$i - 0.019\,(e^{v_D/0.0772} - 1),$$

and gives a good approximation to the diode characteristic in the 0.15 to 0.45 volt range. Such a curve can be used to approximate the diode forward characteristic for the design of low-level pulse detectors, since most of the forward current flows in the region where the approximation is good. The reverse-saturation current for this assumed characteristic is 19 μamp, which is not a good approximation to the diode back characteristic. In a typical pulse detector, however, the load resistor R_L discharges the load capacitor C_L with a current of the order of 0.25 ma. An inaccuracy in the assumed diode back characteristic of a few microamperes can be therefore neglected.

It is assumed that an expression of the form

$$i = I_R(e^{v_D/c} - 1) + v_D/R_R$$

can be used to approximate the static characteristic of a semiconductor diode for the design of detector circuits when appropriate values of I_R, c and R_R are selected. If a sinusoidal detector input voltage V and a large load capacitor C_L are assumed, the voltage across the diode is

$$v_D = V\cos\omega t - V_L$$

Using the approximate diode static characteristic, the diode current for low-frequency input signals is given by

$$i = I_R\left[\left(e^{\frac{V\cos\omega t - V_L}{c}} - 1\right)\right] + \frac{V\cos\omega t - V_L}{R_R} \quad \text{(low frequency)}$$

The DC and fundamental AC components of this current are found by Fourier analysis:

$$\left.\begin{aligned} I_o &= I_R\left[e^{-V_L/c}\, I_0(V/c) - 1\right] - V_L/R_R \,, \\ I_1 &= 2I_R\, e^{-V_L/c}\, I_1(V/c) + V/R_R \,, \end{aligned}\right\} \text{(low frequency)},$$

where I_0 and I_1 are modified Bessel functions of orders zero and one respectively. Using the relation

$$I_o = V_L/R_L \,,$$

an expression relating V and V_L is obtained:

$$\left[\frac{V_L(R_L + R_R)}{I_R R_L R_R} + 1\right] e^{V_L/c} = I_0(V/c) \,.$$

This expression can be evaluated graphically using tabulated[36] values of I_0, and the detector voltage efficiency calculated:

$$e_v = V_L/V$$

Values of I_0 for arguments from 0 to 28 are plotted in Figure 13. For arguments greater than 15, I_0 is given by the relation

$$I_0(x) \approx \frac{e^x}{\sqrt{2\pi x}} \,, \qquad (x > 15) \,,$$

with less than 1 percent error.*

The detector input resistance R_{in} may be calculated once the value of V_L resulting from a given V is known:

$$\left.\begin{aligned} R_{in} &= \frac{V}{I_1} = \frac{1}{\dfrac{2I_R}{V}\, e^{-V_L/c}\, \mathcal{I}_1(V/c) + \dfrac{1}{R_R}}\,, \\ &= \frac{1}{\dfrac{2I_R}{V}\left[\dfrac{V_L(R_L + R_R)}{I_R R_L R_R} + 1\right]\dfrac{\mathcal{I}_1(V/c)}{\mathcal{I}_0(V/c)} + \dfrac{1}{R_R}} \end{aligned}\right\}\text{(low frequency).}$$

The second expression is useful for computation since the exponential is not present. A plot of $\mathcal{I}_1/\mathcal{I}_0$ for arguments from 0 to 20 is given in Figure 14. For large values of the argument, $\mathcal{I}_1/\mathcal{I}_0$ approaches unity.

When a pulse detector circuit is analysed, an infinite value can usually be assumed for R_R. The preceding results show that when R_R is finite, it appears as a resistance in parallel with the detector load resistance R_L in the DC equation from which the voltage efficiency is obtained, and as a resistance shunting the detector input circuit in the AC equation from which R_{in} is calculated. These simple relationships are useful in determining when a finite value of R_R should be assumed.

The Fourier analysis of the diode current shows that the fundamental AC current component I_1 is in phase with the input voltage V, and hence that the detector input capacitance is zero. This is a

---

*See Reference 36, p. xxxiv, Equation 35a

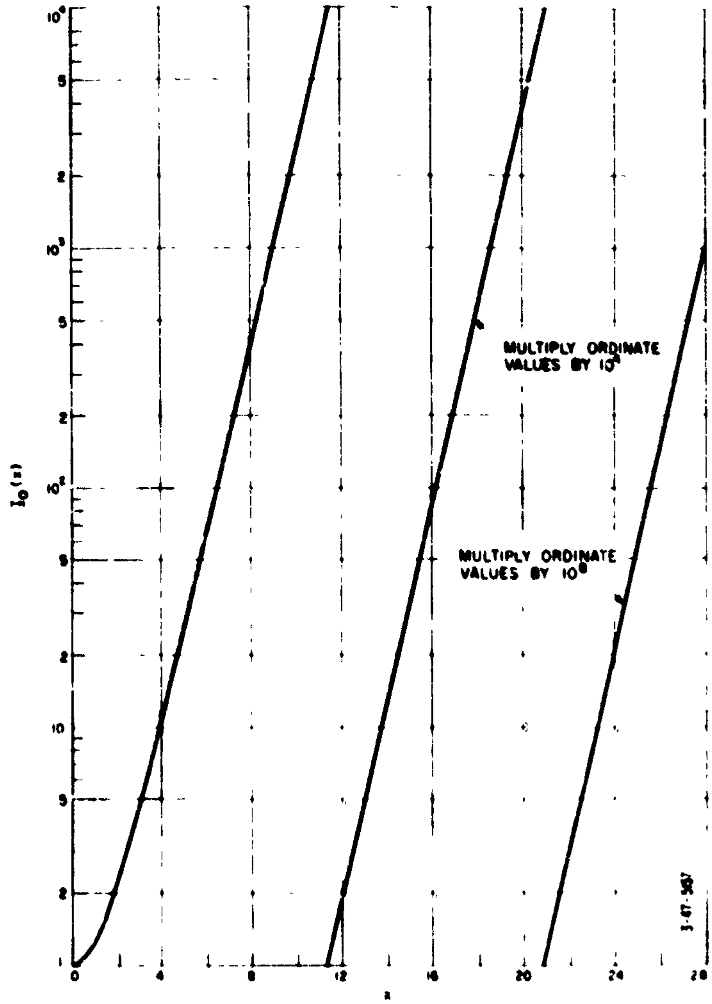

Fig. 13. The modified Bessel function of order zero for arguments from zero to 28.

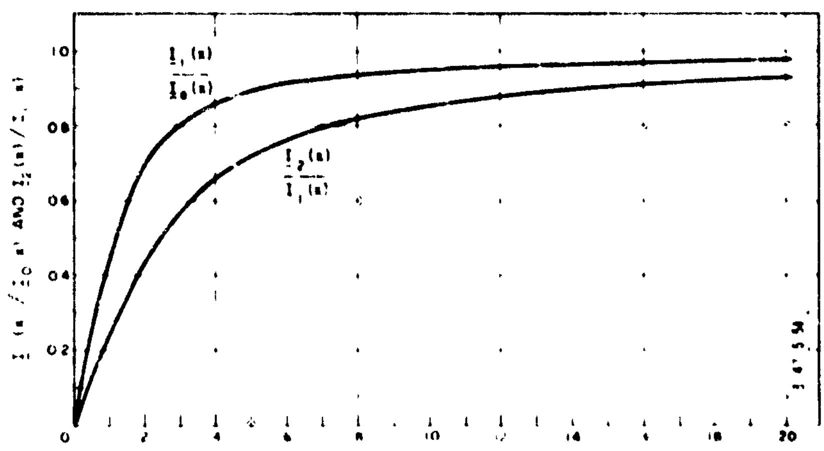

Fig. 14. Ratios of modified Bessel functions for arguments from zero to 20.

result of the assumption that at low frequencies the diode current follows the assumed static characteristic and that charge-storage effects are negligible. However, even at low frequencies where capacitance due to charge-storage is negligible, the barrier capacitance C_B is present. In practical cases the barrier capacitance C_B may be assumed to shunt the diode, and is much smaller than the load capacitance C_L. The barrier capacitance in effect shunts the detector input circuit, and hence:

$$C_{in} = C_B \quad , \text{ (low frequency)} .$$

The variation of the barrier capacitance C_B with reverse bias (here provided by the detector output voltage V_L) is best found experimentally. In many cases this variation is small over the range of operating voltages, and an average value of C_B may be used.

3. Extension to High Frequencies

In the 10-100 Mcps frequency range detector-circuit performance is affected by charge-storage and the results of the preceding discussion must be modified. In order to evaluate the effects of charge storage it is first assumed (contrary to fact) that the simplified diffusion equations, used by Shockley[8,9] for small signals, are applicable at the signal levels found in detector circuits. The solution of these equations for an applied voltage,

$$\bar{v}_D = V \cos \omega t - V_L \qquad (7)$$

is given in Appendix A. The DC and AC diode current components are given by

$$I_o = I_S \left[e^{-V_L q/kT} I_o\left(\frac{Vq}{kT}\right) - 1 \right] ,$$

$$I_1 = 2 I_S \, e^{-V_L q/kT} I_1\left(\frac{Vq}{kT}\right) \left[\frac{\dfrac{p_n \mu_p}{L_{p\omega}} + \dfrac{n_n \mu_n}{L_{p\omega}}}{\dfrac{p_n D_p}{L_{p\omega}(o)} + \dfrac{n_n D_n}{L_{n\omega}(o)}} \right] , \quad (8)$$

using the same symbols as in Section II-3. The DC current component I_o does not vary with frequency, and the AC current I_1 varies with frequency in the same way that the small-signal current was found to vary in Section II-3.

This result suggests approximating the DC and AC diode current components respectively by

$$I_o = I_R \left[e^{-V_L/c} I_o(V/c) - 1 \right] + V_L/R_R . \quad (9)$$

$$I_1 = 2 I_R \, e^{-V_L/c} I_1(V/c) \left[G(\omega) + j B(\omega) \right] + \frac{V}{R_R} + j V \omega C_B . \quad (10)$$

The approximate expression for the DC diode current does not vary with frequency, and is the same expression that is used to approximate the DC current at low signal frequencies. The approximate expression for the AC diode current is similar to that used at low frequencies, except that the first term in the expression the term resulting from the non-linear diode characteristic, is multiplied by the factor $\left[G(\omega) + j B(\omega) \right]$.

called the charge-storage factor. The last term represents the current through the barrier capacitance C_B. The charge-storage factor corresponds to the bracketed term in Equation 8, and gives the variation of the AC diode current with frequency. At low frequencies the charge-storage factor approaches unity, so that the approximate expression for the AC diode current is the same as that used at low frequencies. The charge-storage factor increases with frequency in similar fashion to the normalised hole currents plotted in Figs. 8 and 9. In practice the charge-storage factor is obtained experimentally.

The detector voltage efficiency e_v that is calculated using this approximation is the same as that calculated at low frequencies, since the expression for the DC current is the same. The detector input resistance R_{in} is calculated in the same way as at low frequencies, but using only the real part of the approximate AC diode current:

$$R_{in} = \frac{1}{\frac{2I_R}{V} e^{-V_L/c} I_1(V/c) G(\omega) + \frac{1}{R_R}}$$

$$= \frac{1}{\frac{2I_R}{V}\left[\frac{V_L(R_L + R_R)}{I_R R_L R_R} + 1\right] \frac{I_1(V/c)}{I_o(V/c)} G(\omega) + \frac{1}{R_R}} .$$

In cases where R_R is assumed infinite, the input resistance is equal to the value calculated at low frequencies divided by the real part of the charge-storage factor $G(\omega)$. The capacitance of the junction C_J is calculated using the imaginary part of the assumed AC diode current:

$$C_J = \frac{2 I_R \, e^{-V_L/c} \, I_1 (V/c) \, B(\omega)}{\omega V} + C_B \ .$$

When the peak forward diode current is small, as is the case for high-impedance detectors, the detector input capacitance is approximately equal to the diode junction capacitance C_J. However, when large forward current flows in the diode, the bulk impedance of the diffusion regions has an appreciable inductive component.[25-27] The effect of this inductance in series with the junction is to reduce the input capacitance C_{in} from the low-level value of C_J:

$$C_{in} \approx C_J - \frac{L_s}{R_{in}^2} \ , \quad \left\{ \begin{array}{l} \omega L_s \ll R_{in} \\ \omega C_J \ll 1/R_{in} \end{array} \right. \ .$$

The effective series inductance L_s depends on the diode parameters and operating conditions.

4. Effects of Detector Loads Having Short Time Constants

When detectors are designed to detect modulated signals, the time constant $R_L C_L$ of the detector load must be small enough to permit the detector output voltage to follow the modulation at the detector input.* In some cases the required detector load time constant is small enough to allow an appreciable AC signal to develop across the detector load. In such cases the voltage across the diode is

---

*The design of detectors having specified response times is discussed in Sections III-8.

different from that assumed in the preceding analysis, and the detector performance differs appreciably from that predicted. In general, reducing the time constant $R_L C_L$ results in a reduction in voltage efficiency e_v and increases in input resistance R_{in} and input capacitance C_{in}. An approximate method for evaluating these effects is given below.*

The detector output voltage is assumed to consist of a DC term V_L and an AC term containing only the fundamental frequency component V_o, lagging the detector input voltage V by an angle φ :

$$v_L = V_L + V_o \cos(\omega t - \varphi) .$$

The voltage v_D across the diode is then

$$v_D = V \cos \omega t - V_o \cos(\omega t - \varphi) - V_L ,$$

$$= V' \cos(\omega t + \beta) - V_L ,$$

where the AC diode voltage V' and its phase angle β relative to the detector input voltage V are related to V, V_o, and ϕ as shown in the vector diagram of Figure 15. The second form of the expression for the diode voltage v_D differs from that previously assumed (Equation 7) only in the amplitude and phase of the AC signal. Making the same approximations as in the above derivation, the DC and AC diode current components are given by Equations 9 and 10 with V' substituted for V and with the phase of the AC current taken with respect to V' :

*The approach here is similar to that used in Reference 4, but with a better approximation to the diode characteristic.

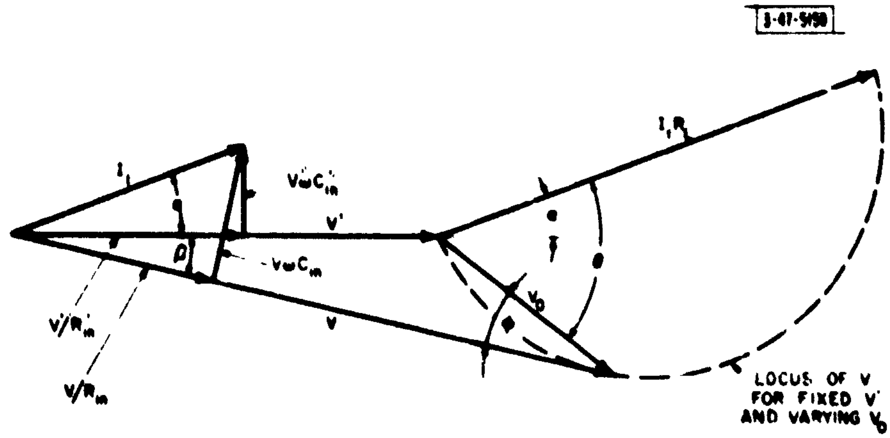

Fig. 15. Vector relationship in detectors having short load time constants. (See text.)

$$I_o = I_R \left[e^{-V_L/c} I_0(V'/c) - 1 \right] - V_L/R_R \; ,$$

$$I_1 = 2I_R \, e^{-V_L/c} I_1(V'/c) \left[G(\omega) + j B(\omega) \right] + \frac{V'}{R_R} + j V' \omega C_B \; .$$

Given a value of V', the corresponding values of V_L, I_o and I_1 are calculated in the same way as previously. Since the diode AC voltage V' is not in general equal to the detector input voltage V, the quantities

$$R'_{in} = \frac{V'}{\mathrm{Re}\left[I_1\right]} \; ,$$

$$C'_{in} = \frac{\mathrm{Im}\left[I_1\right]}{\omega V'} \; ,$$

are not the detector input resistance and input capacitance, but only quantities relating the AC diode current to the AC diode voltage. The vector representation of the AC diode current I_1 and its components is shown in Figure 15. The phase angle by which I_1 leads V' is called α :

$$\alpha = \tan^{-1} \frac{\mathrm{Im}\left[I_1\right]}{\mathrm{Re}\left[I_1\right]} = \tan^{-1} \omega R'_{in} C'_{in} \; .$$

The AC voltage V_o developed across the detector load circuit by the AC diode current I_1 is given by

$$V_o = I_1 R_L \quad \frac{1 - j\omega R_L C_L}{1 + (\omega R_L C_L)^2} \quad ,$$

where the phase of V_o is relative to I_1. The locus of V_o for varying C_L is a semicircle having the vector $I_1 R_L$ as its diameter, as shown in Fig. 15. The phase of V_o lags I_1 by an angle Θ.

$$\tan^{-1} \omega R_L C_L = \Theta = \alpha + \beta + \varphi \; .$$

The detector input voltage V is the vector sum of V' and V_o. The magnitude of the detector input voltage is given by

$$V = V' \left\{ \left[1 + \frac{R_L}{R'_{in}} \quad \frac{\cos(\Theta - \alpha)\cos\Theta}{\cos\alpha} \right]^2 + \left[\frac{R_L}{R'_{in}} \quad \frac{\sin(\Theta - \alpha)\cos\Theta}{\cos\alpha} \right]^2 \right\}^{\frac{1}{2}} \; ,$$

and the phase angle β by which V lags V' by

$$\beta = \tan^{-1} \left[\frac{\dfrac{R_L}{R'_{in}} \quad \dfrac{\sin(\Theta - \alpha)\cos\Theta}{\cos\alpha}}{1 + \dfrac{R_L}{R'_{in}} \quad \dfrac{\cos(\Theta - \alpha)\cos\Theta}{\cos\alpha}} \right] \; ,$$

where R'_{in} and α are the values corresponding to the assumed diode voltage V'. The detector circuit parameters for an input voltage V are readily calculated:

$$e_v = \frac{V_L}{V} \quad ,$$

$$R_{in} = \frac{V}{|I_1| \cos(\alpha + \beta)} \quad ,$$

$$C_{in} = \frac{|I_1| \sin(\alpha + \beta)}{\omega V} \quad .$$

The fact that the output voltage v_L in a detector having a small load-circuit time constant contains harmonics of the signal frequency as well as the DC and fundamental frequency AC components that were assumed, results in inaccuracies in the circuit parameters calculated using this method. In general, the reduction of voltage efficiency e_v and the increases of input resistance R_{in} and input capacitance C_{in} resulting from a reduced load time constant are greater than those calculated using the method described above. In many practical detector circuits, the reduction in e_v and increases in R_{in} and C_{in} are themselves small, and the errors in the calculated performance can be neglected.

5. The Effect of a Low-Q Driving Circuit

It has been assumed in the preceding analysis that the detector input voltage v (see Fig. 1) is sinusoidal. This is a good approximation when the Q of the tuned circuit loaded by the detector is high, since appreciable harmonic voltage components cannot exist across a high-Q tuned circuit. However, in many cases of practical interest, the Q of the tuned circuit is not large, and the non-linear loading of the detector circuit results in a non-sinusoidal voltage across the tuned circuit and the detector input. In the following discussion an expression for estimating the departure of the input voltage v from a sinusoid is developed, and the effect of this departure on the performance of the detector circuit is considered.

When the Q of the tuned circuit loaded by a detector is low, the current drawn by the detector during the positive peak of the detector input signal causes a flattening of the voltage waveform. The resulting detector input voltage v contains a fundamental component and harmonics.

A measure of the flattening of the voltage waveform is the ratio of the magnitude of the second harmonic voltage component V_2 to the fundamental voltage component V. The second harmonic voltage V_2 is developed by the second harmonic diode current I_2 which must flow through the tuned driving circuit since the input current I_{in} is assumed sinusoidal (see Fig. 1). The magnitude of the second harmonic voltage V_2 is given by

$$|V_2| = |I_2 Z_2| \quad ,$$

where Z_2 is the impedance of the tuned circuit at the second harmonic frequency. The second harmonic diode current I_2 can be approximated by the second harmonic current calculated in Appendix A for a sinusoidal input voltage V :

$$I_2 = 2I_S\, e^{-\frac{V_L q}{kT}}\, \underline{I}_2(Vq/kT) \left[\frac{\dfrac{D_p p_n}{L_{p_\omega}(2\omega)} + \dfrac{D_n n_n}{L_{n_\omega}(2\omega)}}{\dfrac{D_p p_n}{L_{p_\omega}(o)} + \dfrac{D_n n_n}{L_{n_\omega}(o)}} \right] .$$

Using the approximations of Section III-3,

$$I_2 = 2I_R\, e^{-V_L/c}\, \underline{I}_2(V/c)\, \left[G(2\omega) + jB(2\omega)\right] .$$

(Since only fundamental frequency diode voltage v_D is assumed, there are no terms in the expression for I_2 corresponding to the last two terms in Equation 10.) The impedance of the tuned circuit at twice the signal frequency is given by

$$|Z_2| = \frac{R_A}{\sqrt{1 + (\frac{3}{2}\,\omega R_A C_A)^2}} ,$$

where ω is the angular frequency of the <u>input</u> signal. The fundamental voltage component V is given by

$$V = R_{in}\, \mathrm{Re}\left[I_1\right] = R_{in}\, 2I_R\, e^{-V_L/c}\, \underline{I}_1(V/c)\, G(\omega) ;$$

the current V/R_R being neglected in comparison with the other term.

Combining these expressions, the ratio of second harmonic voltage to fundamental voltage is given by:

$$\left|\frac{V_2}{V}\right| = \frac{R_A}{R_{in}\sqrt{1 + (\frac{3}{2}\,\omega R_A C_A)^2}} \cdot \frac{I_2(V/c)}{I_1(V/c)} \cdot \frac{|G(2\omega) + jB(2\omega)|}{G(\omega)} .$$

In many cases, $(\frac{3}{2}\omega R_A C_A)^2$ is much larger than unity, and the expression can be simplified:

$$\left|\frac{V_2}{V}\right| = \frac{2}{3\omega R_{in} C_A} \cdot \frac{I_2(V/c)}{I_1(V/c)} \cdot \frac{|G(2\omega) + jB(2\omega)|}{G(\omega)} ,$$

$$\left\{(\tfrac{3}{2}\,\omega R_A C_A)^2 \gg 1\right\} .$$

The function $I_2(x)/I_1(x)$ is plotted as a function of x in Fig. 14. For large values of the argument the function approaches unity. The values of $|G(2\omega) + jB(2\omega)|$ and $G(\omega)$ can be found by measurement. The factor $|G(2\omega) + jB(2\omega)|/G(\omega)$ is expected to vary between unity at low frequencies where $G(\omega)$ is constant and $B(\omega)$ is small, and two at frequencies well above this region. The higher value is a good approximation for this factor for many diodes the 10-100 Mcps frequency range. Using these approximations,

$$\left|\frac{V_2}{V}\right| \approx \frac{4}{3\omega R_{in} C_A} , \quad \left\{\begin{array}{l} \frac{3}{2}\,\omega R_A C_A)^2 \gg 1 , \\ V/c \ \text{large} \\ \text{high frequency} \end{array}\right\}$$

This result shows that the flattening of the detector input waveform varies inversely with the detector input resistance R_{in} and the admittance of the capacitance C_A in the tuned circuit. Because of the approximations made in the derivation the resulting expression does not give an accurate evaluation of the actual ratio of second harmonic voltage to fundamental voltage when the second harmonic is appreciable. However, the expression is useful in estimating the amount of flattening of the detector input voltage waveform, and is used in calculating the performance of detectors driven from low-Q circuits as discussed below.

The detector voltage efficiency e_v and input resistance R_{in} are defined only for sinusoidal detector input voltages and therefore cannot be used when the input voltage waveform is flattened. The detector current efficiency e_i is therefore defined without reference to the voltage waveform and describes the overall performance of the detector and its driving circuit:

$$e_i \equiv \frac{I_o}{I_{in}} = \frac{I_o}{I'_1 + I_A} ,$$

where I'_1 is the resistive component of the AC detector input current I_1, and I_A is the fundamental-frequency component of the current through the driving-circuit resistance R_A. When the detector input voltage is sinusoidal, the current components are

$$I_o = \frac{V_L}{R_L} ,$$

$$I_A = \frac{V}{R_A} = \frac{V_L}{e_v R_A} ,$$

$$I'_1 = \frac{V}{R_{in}} = \frac{V_L}{e_v R_{in}} ,$$

and the current efficiency is

$$e_i = \frac{e_v}{R_L} \cdot \frac{R_{in} R_A}{R_{in} + R_A} \quad .$$

When the detector input voltage waveform is flattened, due to detector-circuit loading, the values of I_A and I'_1 that result in a given value of I_o are changed. The fundamental-frequency component of current I_A through the source resistance R_A is increased, since an input voltage waveform having a larger fundamental-frequency component is required to produce a given diode DC current I_o when the waveform is flattened than when the input voltage is sinusoidal. The value of I_A for a given value of I_o (and hence V_L) increases by a factor $1/a$, where $1/a \geq 1$ is a function of the input voltage waveform approaching unity for a sinusoid. The value of I_A is given by

$$I_A = \frac{V_L}{a\, e_v R_L} \quad .$$

However, the flattening of the voltage waveform results in a flattened diode-current pulse. The flattened current pulse has a smaller component of AC current I'_1 for a given value of DC current I_o. Thus the flattening of the current pulse tends to decrease the value of I'_1 by a factor $1/ab$, where $\frac{1}{ab} \simeq 1$ is a function of the input voltage waveform approaching unity for sinusoidal input voltages. The value of I'_1 is given by

$$I'_1 = \frac{V_L}{a\, b\, e_v R_{in}} \quad .$$

The current efficiency is then given by

$$e_i = \frac{a\, e_v}{R_L} \cdot \frac{b R_{in} R_A}{b R_{in} + R_A} ,$$

where e_v and R_{in} are the parameters calculated for a detector driven by a sinusoidal voltage having the same output voltage V_L as the detector for which the current efficiency is being calculated. The parameters a and b are functions of the flattening of the detector input voltage and hence of the quantity $|V_2/V|$ that was previously calculated. Values of these parameters, obtained from measurements of detector performance, are presented in Section IV-5.

6. Effects of Moderate Temperature Variations

Variations of detector performance with temperature may be calculated using diode parameters measured at various temperatures. However, when the range of temperature variation is not great, (e.g., normal room temperature variation,) the changes in detector performance can be estimated without the necessity for repeated calculations.

Schaffner and Shea[31] have shown that at low signal levels where the diode static characteristic is given by

$$i = I_S \left(e^{v_D q/kT} - 1\right) ,$$

the only significant change in this static characteristic with temperature is the variation of the saturation current I_S. (Since T in the exponential represents absolute temperature, changes due to moderate variations of

temperature around room temperature are small and can be neglected.)
The variation of I_S is given by

$$I_S = I'_S \, e^{\alpha \Delta T} \, , \tag{11}$$

where ΔT is the increase in temperature, I'_S is the saturation current at the original temperature, and α is a temperature coefficient equal to approximately 0.08 (degrees C)$^{-1}$ for both silicon and germanium. At higher signal levels, where the low-level diode characteristic is not valid, the diode voltage v_D required to produce a given diode current i is reduced by an amount proportional to the temperature increase:[31]

$$v_D = v'_D - \frac{\alpha \Delta T \, kT}{q} \, ,$$

where v'_D is the diode voltage at the original temperature.

If the assumed diode characteristic at the original temperature is

$$i = I'_R \left[e^{v'_D / c} - 1 \right] \, ,$$

then for an increase in temperature of ΔT the characteristic becomes

$$i = I'_R \left[e^{\frac{v_D}{c} + \frac{\alpha \Delta T \, kT}{cq}} - 1 \right]$$

When the low-level diode characteristic is not valid, the second term in the brackets can be neglected and the characteristic can be approximated by

$$\left.\begin{aligned} i &= I'_R \, e^{\frac{\alpha \Delta T kT}{cq}} \, e^{v_D/c} , \\ &= I_R \, e^{v_D/c} , \end{aligned}\right\} \quad v_T/c >> 1 ,$$

where

$$I_R = I'_R \, e^{\frac{\alpha \Delta T kT}{cq}} .$$

When the assumed diode characteristic is chosen for use at low signal levels,

$$\left.\begin{aligned} I'_R &\approx I'_S , \\ c &\approx \frac{kT}{q} , \end{aligned}\right\} \quad \text{(low-level approximations)} ,$$

and reference to Equation 11 shows that the equation for I_R applies to the low-level approximate characteristic as well as the high-level approximations. Thus the principal effect of temperature variations on the diode characteristic is a change in the assumed reverse-saturation current. The change in I_R for small temperature changes is given by the derivative of I_R with respect to T:

$$\frac{dI_R}{dT} = \lim_{\Delta T \to 0} \frac{I'_R \left(e^{\frac{\alpha \Delta T kT}{cq}} - 1\right)}{\Delta T} = I_R \frac{\alpha kT}{cq} .$$

The effect of small changes of I_R on the operation of the detector circuit is found by calculating the derivatives of the detector-circuit parameters with respect to I_R. These calculations are shown in Appendix B. The normalised derivative of the voltage efficiency e_v is

$$\frac{1}{e_v} \cdot \frac{de_v}{dI_R} = \frac{c}{I_R(V_L + c + R_L I_R)} ,$$

where the reverse resistance R_R is included in the detector load resistance R_L. The normalised derivative of e_v with respect to temperature is then

$$\frac{1}{e_v} \cdot \frac{de_v}{dT} = \frac{1}{e_v} \cdot \frac{de_v}{dI_R} \cdot \frac{dI_R}{dT} ,$$

$$= \frac{\alpha kT}{q(V_L + c + R_L I_R)} .$$

For many pulse detectors, $V_L >> c + R_L I_R$, and the above expression becomes

$$\frac{1}{e_v} \cdot \frac{de_v}{dT} = \frac{\alpha kT}{qV_L} , \quad (V_L >> c + R_L I_R) .$$

For a value of α of 0.08 (degrees C)$^{-1}$ and for $kT/q = 0.025$ volt the fractional increase in the voltage efficiency e_v per degree C of temperature rise is $0.002/V_L$.

The detector input resistance R_{in} may be considered as a parallel combination of a resistance R_D resulting from the diffusion current, and the reverse resistance R_R. The variation of R_D with small changes of I_R is shown in Appendix B to be

$$\frac{1}{R_D} \frac{dR_D}{dI_R} = - \frac{c + R_L I_R}{I_R(V_L + c + R_L I_R)} .$$

The normalized derivative of R_{in} with respect to T is then

$$\frac{1}{R_{in}} \frac{dR_{in}}{dT} = \frac{R_R + R_D}{R_R R_D} \cdot \frac{R_R^2 R_D}{(R_R + R_D)^2} \frac{1}{R_D} \frac{dR_D}{dI_R} \frac{dI_R}{dT} ,$$

$$= - \frac{R_R}{R_R + R_D} \cdot \frac{\alpha kT(c + R_L I_R)}{cq(V_L + c + R_L I_R)} .$$

For the case when $c >> R_L I_R$ and $R_R >> R_D$, the input resistance is reduced by the same factor as the voltage efficiency is increased. When these conditions are not met, the change of input resistance may be greater or less than this value.

The derivative of the diffusion capacitance C_D with respect to T is found in a way similar to that used for R_{in}:

$$\frac{1}{C_D} \frac{dC_D}{dI_R} = \frac{c + R_L I_R}{I_R(V_L + c + R_L I_R)} ,$$

$$\frac{1}{C_D} \frac{dC_D}{dT} = \frac{\alpha kT(c + R_L I_R)}{cq(V_L + c + R_L I_R)} .$$

When $c >> R_L I_R$, the diffusion capacitance increases by the same factor as the voltage efficiency.

When the detector input resistance R_{in} is much smaller than the driving circuit resistance R_A, the current efficiency is approximately given by

$$e_i \approx \frac{e_v R_{in}}{R_L} \qquad (R_A >> R_{in}) .$$

The normalised derivative of the current efficiency with respect to temperature is then

$$\frac{1}{e_i}\frac{de_i}{dT} = \frac{1}{R_{in}}\frac{dR_{in}}{dT} + \frac{1}{e_v}\frac{de_v}{dT}\ , \quad (R_A >> R_{in})\ .$$

When the diffusion resistance R_D is much less than the diode reverse resistance R_R,

$$\frac{1}{e_i}\frac{de_i}{dT} = -\frac{\alpha kT\, R_L I_R}{cq(V_L + c + R_L I_R)}\ , \qquad \begin{pmatrix} R_A >> R_{in} \\ R_R >> R_D \end{pmatrix}.$$

At high signal levels the variation of current efficiency with temperature is small.

7. The Effects of Output Circuit Loading on Detector Performance

The circuit to which the detector output is connected may affect the detector performance. The output of a high-impedance detector is normally connected directly to a high-resistance DC indicating device. Since the input resistance of the device is in parallel with the detector load resistor, the value of the parallel combination may be used as R_L in calculating the detector performance. The output of a pulse detector is normally connected to a video circuit, either directly or through a coupling capacitor. The effects of these output connections on detector performance are discussed below.

Figure 16a shows a detector circuit capacitively coupled to load represented by a resistance R_o. It is assumed that the coupling capacitor C_o is large enough so that no video signal is developed across

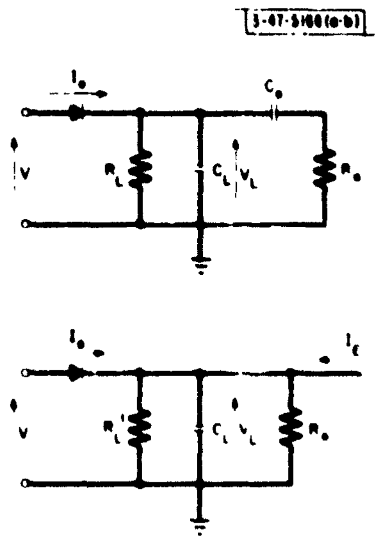

Fig. 16. Equivalent circuits for two detector output connections: a) AC coupling. b) Direct coupling to the base of a transistor.

it, and that any capacitance associated with the loading circuit is included in the detector load capacitance C_L. The coupling capacitor C_o charges up to a DC voltage equal to the average value of the detector output voltage V_{L_o}. When the detector input voltage V is not modulated, there is no change in the detector output voltage and no current flows in C_o and R_o. When the modulation changes V from its average value, the detector output voltage is changed by an amount ΔV_L. Since the voltage across the coupling capacitor C_o cannot change with the modulation, a portion of the diode current flows through C_o and R_o. The diode video current I_o (which varies with the signal modulation) is given by

$$I_o = \frac{V_{L_o} + \Delta V_L}{R_L} + \frac{\Delta V_L}{R_o} .$$

The detector voltage efficiency e_v and input resistance R_{in} may be calculated, using this value of I_o, by the method described in Section III-2. The effect of the output loading circuit is negligible when the second term above is much smaller than the first term, or equivalently,

$$\frac{R_o}{R_L} >> \frac{\Delta V_L}{V_{L_o} + \Delta V_L} .$$

When ΔV_L is negative and approaches V_{L_o} in magnitude, this condition is difficult to meet. When the two terms are equal in magnitude and ΔV_L is negative, the DC diode current I_o is zero. Since only very small negative DC diode currents can flow, the output voltage waveform is clipped at a value of ΔV_L given by:*

*This is equivalent to the negative peak clipping discussed by Temman in Ref. 37, pp. 554-557.

$$-\frac{\Delta V_L}{V_{L_o}} = \frac{R_o}{R_o + R_L} .$$

When the detector ouput is directly coupled to the base of a transistor the loading circuit may be represented by a current I_E shunted by a resistance R_o, as shown in Fig. 16b. The detector load resistance R_L may be taken as the parallel combination of R'_L and R_o. The diode DC current I_o is given by

$$I_o = \frac{V_L}{R_L} - I_E .$$

Setting this equal to the expression derived from the diode characteristic,

$$I_E = \frac{V_L}{R_L} + I_R - I_R \, e^{-V_L/c} \, I_o(V/c) .$$

(The diode reverse resistance R_R is assumed to be combined with R_L.) Calculating the derivative of V_L with respect to I_E,

$$dI_E = \left[\frac{1}{R_L} - \frac{I_R}{c} \, e^{-V_L/c} \, I_o(V/c)\right] dV_L ,$$

$$\frac{dV_L}{dI_E} = \frac{1}{\frac{1}{R_L} - \frac{I_R}{c} \, e^{-V_L/c} \, I_o(V/c)} .$$

For values of I_E near zero, this may be written:

$$\frac{dV_L}{dI_E} = \frac{c}{I_R + \dfrac{c + V_L}{R_L}} \; .$$

The relative change in V_L for small values of I_E can be calculated from

$$\frac{dV_L}{V_L} = \frac{c/V_L}{I_R + \dfrac{c + V_L}{R_L}} \, dI_E \; .$$

For large values of V_L such that $V_L >> c$ and $V_L >> I_R R_L$, this may be simplified:

$$\frac{dV_L}{V_L} = \frac{R_L c}{V_L{}^2} \, dI_E \; , \quad \left\{ \begin{array}{l} V_L >> c \\ V_L >> I_R R_L \end{array} \right. \; .$$

The change in the detector input resistance R_{in} is calculated as follows:

$$R_{in} = \frac{V e^{V_L/c}}{2 I_R I_1 (V/c) G(\omega)} \; ,$$

$$\frac{dR_{in}}{R_{in}} = \frac{dV_L}{c}$$

$$= \frac{dI_E}{I_R + \dfrac{c + V_L}{R_L}} \; .$$

(The diode reverse resistance R_R is omitted here, and can be added in parallel with R_{in}.) For large values of V_L this may be approximated by

$$\frac{dR_{in}}{R_{in}} = \frac{R_L}{V_L}\, dI_E \; , \quad \begin{cases} V_L \gg c \\ V_L \gg I_R R_L \end{cases}$$

At very low input voltages, a positive value of bias current I_E develops a voltage approximately equal to $I_E R_L$ across the load resistance and back biases the diode. The voltage efficiency approaches infinity as the detector input voltage approaches zero. The detector input resistance is equal to the incremental resistance of the diode with a back bias of $I_E R_L$ volts. At very low input voltages and negative values of bias current I_E, the bias current divides between the detector load resistance and the diode itself. The detector output voltage V_L and the voltage efficiency are zero for a value of detector input voltage approximately equal to $-I_E R_L$. The detector input resistance equals the incremental resistance of the diode with a forward bias resulting from the portion of I_E that flows in the diode.

8. The Response Time of Pulse Detectors

The speed of response of a pulse detector is given by its rise-time τ_r and fall-time τ_f. The rise-time τ_r is defined as the time the detector output takes to change from 10 to 90 percent of the voltage between its initial and final levels when an abrupt increase of input signal level occurs. Fall-time is similarly defined for a decrease in input signal level. Since the detector response time depends on the driving circuit as well as the detector itself, the two circuits are designed together and the rise-time and fall-times considered are those of the combined circuit.

Callandar[32] has analyzed a detector driven by a single-tuned circuit as shown in Fig. 1.* In order to obtain simple results the following assumptions are made:

1. The detector output voltage V_L follows the envelope of the voltage V across the tuned circuit.
2. The quantity $h = R_L/2R_{in}$ is constant.
3. The input signal frequency is at the resonant frequency of the tuned circuit.

Under these assumptions, the overall rise- and fall-times for the circuit are equal, and given by

$$
\begin{aligned}
\tau_r = \tau_f &= 2.2 \; \frac{2R_{in}R_A}{R_{in} + R_A} \; (C_A + hC_L) \, . \\
&= 2.2 \; \frac{R_L R_A}{\frac{R_L}{2h} + R_A} \; (C_L + C_A/h) \, .
\end{aligned}
\tag{12}
$$

This time is the same as the video rise-time of an R-C circuit with $R = 2R_{in}R_A/(R_{in} + R_A)$, and $C = C_A + hC_L$. When R_A is large and the circuit loading is due largely to the detector,

$$\tau_r = \tau_f = 2.2\, R_L\, (C_L + C_A/h) \, . \quad (R_A \gg R_{in})$$

---

*Detectors driven by more complex circuits are discussed in Ref. 33, 34, and 35.

The validity of the first assumption is assured if

$$2.2\, R_L C_L \le \tau_r \ , \tag{13}$$

or equivalently,

$$R_L C_L \le 2 C_A R_A \ ,$$

or,

$$h\, R_{in}\, C_L \le C_A R_A \ .$$

If this condition is not met, the fall-time is limited by the response time of the detector load circuit:

$$\tau_f = 2.2\, R_L C_L \ . \tag{14}$$

In other words, the detector rise-time τ_r is given by Equation 12 whether the condition given in Equation 13 is satisfied or not. The fall-time τ_f is given by Equation 12 or 14, whichever is the larger.

The second assumption is not entirely justified since R_{in} does vary with signal level for a constant R_L. However, h may be considered constant for small-changes of signal level, and the result is a reasonable approximation for larger changes if a suitable value of h is chosen. The third assumption is valid in many practical cases. It does not appear that the results are affected appreciably when the signal frequency is within the 3db bandwidth of the tuned circuit.*

Callandar gives experimental verification of these results for vacuum-diode detectors.

---

*The effects of detector driving circuits not tuned to the signal frequency are discussed in Ref. 35.

IV. Measurements and Comparison with Theory

1. Procedures and Measuring Techniques

Measurements have been made to establish the range of validity of the detector-design theory presented in Section III. The diode types used for the detector measurements are the S570G gold bonded germanium diode, manufactured by Transitron Electronic Corporation, and the FD100 diffused silicon planar diode, manufactured by Fairchild Semiconductor Corporation. They were selected as representative high-performance, commercially-available, germanium and silicon diodes for detector circuits in the 10-100 Mcps frequency range.

The diode parameters that are used in the design theory were measured for the two diode types. Using these measured values, the theoretical performance of both high-impedance and pulse detectors was calculated for a variety of circuit parameters and operating conditions. Corresponding detector circuits were built and their performance measured. The results of the measurements are compared with the calculated performance later in this section. Measurements of pulse response are reported and discussed separately in Section V-3.

Since detector-circuit voltage efficiency e_v, input resistance R_{in}, and input capacitance C_{in} depend on the input voltage V, (and also on the waveform of the input voltage), it is necessary to measure the detector performance with the desired input voltage applied to the detector input. Three techniques were used in measuring detector-circuit performance:

1. Q Meter. Measurements were made at signal frequencies from 20 to 100 Mcps with a Boonton Model 190-A Q Meter, and at fre-

quencies below 20 Mcps with a Boonton Model 160-A Q Meter. The measuring procedure is as follows: The Q Meter oscillator is set to the desired frequency. A coil is connected to the "L" terminals and is resonated by adjusting the internal capacitor. The Q Meter capacitor reading and measured Q are recorded as C_1 and Q_1. The detector circuit shown in Fig. 17a is then connected to the "C" terminals of the Q Meter and the internal capacitance is again adjusted for resonance. The desired input voltage V is obtained by adjusting the Q Multiplier control on the Q Meter. The input voltage V is measured using either a Hewlett-Packard 410B VTVM or a previously calibrated high-impedance detector. Since a change in V may affect the detector input capacitance C_{in}, the Q Meter internal capacitor and the Q Multiplier are readjusted until the desired input voltage is obtained at resonance. The Q Meter capacitor reading and the measured Q are recorded as C_2 and Q_2. The DC detector output voltage V_L is read using a high impedance DC voltmeter. The R-C filter following the detector removes any AC signals from the detector output. The detector voltage efficiency is:

$$e_v = \frac{V_L}{V} .$$

The equivalent parallel resistance R_p and capacitance C_p of the circuit are given by

$$R_p = \frac{Q_1 Q_2}{2\pi f C_1 (Q_1 - Q_2)} .$$

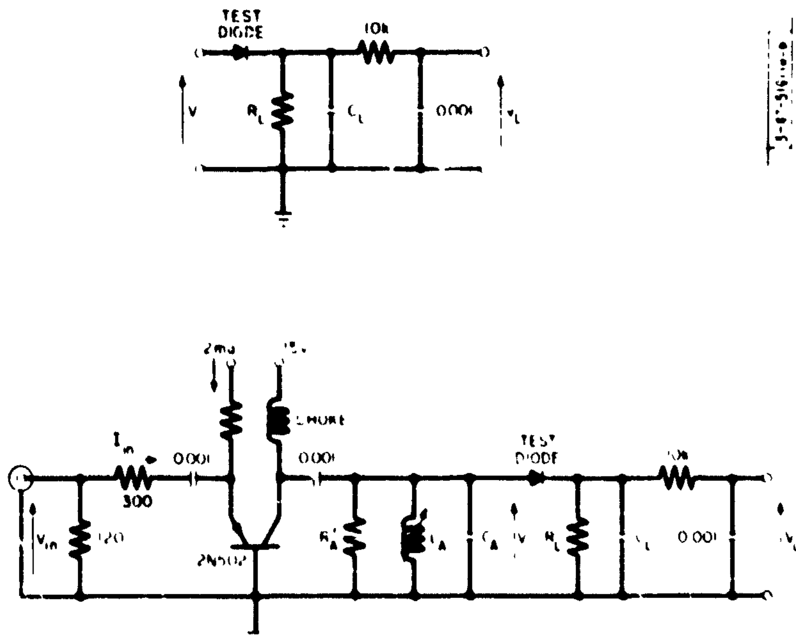

Fig. 17. Circuits used for detector measurements: a) Q meter and admittance bridge measurements b) Transistor circuit measurements.

$$C_p = C_1 - C_2 \quad .$$

The loading due to the input voltage measuring instrument and stray capacitance are measured on the Q Meter with the detector diode disconnected. The input resistance R_{in} and input capacitance C_{in} of the detector are then calculated.

The range of input voltages over which the performance of a detector may be measured on either of the Q Meters is limited, and varies with the detector input resistance and the signal frequency. However, Q Meter measurements are often convenient for comparing similar circuits, or for evaluating small changes in circuit performance, e.g., with changing temperature. Since the detector is driven from a tuned circuit, the analysis in Section III-5 may be used to determine if the input voltage waveform is flattened. In most cases the waveform is nearly sinusoidal. This may be verified when a high-impedance detector is used to measure the detector input voltage by reversing the diode and noting if the indicated voltage changes.

It is estimated that the values of R_{in} obtained from the Q-Meter measurements are accurate to better than $\pm$ 10 percent, the values of C_{in} are accurate to $\pm$0.2 μμf, and the values of e_v are accurate to $\pm$5 percent.

2. Admittance Bridge. Measurements were made at signal frequencies from 1 to 100 Mcps with a Wayne-Kerr B801 Admittance Bridge. The measuring procedure is as follows: The oscillator driving the bridge is set to the desired signal frequency and the bridge is balanced. The detector circuit shown in Fig. 17a is connected to the

"unknown" terminals of the bridge. The oscillator output level is adjusted to produce the desired detector input voltage V, and the bridge is again balanced. The detector output voltage V_L is measured, and the circuit conductance G_p and capacitance C_p are read from the bridge. The detector input resistance R_{in} and input capacitance C_{in} are obtained by calculations after measuring the loading of the input voltage measuring instrument and stray capacitance. The detector voltage efficiency e_v is calculated as above.

Since the source impedance of the admittance bridge is not a tuned circuit, the bridge impedance at the second-harmonic frequency is appreciable compared with the input resistance of most pulse detectors. Following the discussion of Section III-5, the admittance bridge can not therefore by used to measure these pulse detectors without flattening of the detector input voltage waveform. The admittance bridge is useful for measuring high-impedance detector performance, and in making small-signal measurements of diode admittance. The accuracy of values of R_{in} and C_{in} obtained from these measurements is usually limited by the discrimination of the admittance bridge. At frequencies below 50 Mcps the discrimination is 0.02 m mho, above 50 Mcps the discrimination falls to 0.1 m mho. Thus the accuracy obtained decreases as the value of R_{in} increases. The accuracy of values of C_{in} is estimated to be ±0.2 μμf.

3. Transistor Circuit Measurements were made at signal frequencies from 1 to 100 Mcps using the circuit shown in Fig. 17b. The detector is driven by a grounded base transistor amplifier with a single-tuned collector circuit. Measurements showed the transistor current gain to be very close to unity over the frequency range of

interest. Therefore, the input current to the tuned circuit and detector is approximately equal to the transistor emitter current. The input current I_{in} is calculated from a measurement of the input voltage V_{in} to the transistor circuit. A resistor approximately ten times the transistor emitter resistance is connected in series with the emitter to prevent the uncertainty in the value of emitter resistance from affecting the accuracy of calculated values of I_{in}. A shunt resistor at the input of the circuit provides proper termination for a 91 ohm coaxial cable from the signal generator. The transistor is biased with 2 ma DC to permit measurements with peak input current I_{in} as large as 1 ma without risk of non-linearity in the transistor. The collector voltage is supplied through a choke having a high impedance at the measurement frequency. The value of the tuned-circuit capacitance C_A is chosen to give the desired detector input voltage waveform. A large value of C_A is used when a sinusoidal detector input voltage is desired, and a smaller value is used when a flattened waveform is desired. The tuned-circuit inductance L_A is adjusted for resonance at the desired signal frequency. The effective resistance R_A shunting the tuned circuit (not including the loading due to the detector) is the actual resistance R'_A added to the circuit in parallel with the loading due to the choke and coil losses and the transistor collector resistance. The value of R_A is obtained by substituting a resistor of known value for the detector circuit, and measuring the voltage V developed across the parallel combination of the known resistance and R_A for a known input current I_{in}.

The detector voltage efficiency e_v, input resistance R_{in}, and input capacitance C_{in} are measured using no added shunt resistance and a value of C_A large enough to ensure a sinusoidal detector input voltage. (This can be verified in the same way as for the Q Meter measurements.) The detector input voltage V is measured with a calibrated high-impedance detector. The high-impedance detector is used in obtaining the value of R_A, so no additional correction is made for its input resistance. The detector voltage efficiency is

$$e_v = \frac{V_L}{V} ,$$

and the input resistance is found from the expression

$$\frac{V}{I_{in}} = \frac{R_A R_{in}}{R_A + R_{in}}$$

The approximate detector input capacitance C_{in} is obtained by noting the change Δf in the resonant frequency f of the tuned circuit when a resistor having a known shunt capacitance C_o is substituted for the detector circuit.

$$C_{in} = C_o + \frac{2 C_A \Delta f}{f}$$

Current efficiency is measured for any desired values of R_A and C_A.

$$e_i = \frac{V_L}{R_L I_{in}}$$

Accurate values of detector input resistance R_{in} can be obtained only when the shunt circuit resistance R_A is of the same order of magnitude or larger. Since maximum attainable values of R_A are of the order 10 K ohms, high-impedance detectors are not measured using the transistor circuit. The accuracy of values of R_{in} obtained for pulse detectors is estimated to be ± 10 percent. Because of the large value of tuned-circuit capacitance C_A required to produce a sinusoidal detector input voltage at low frequency, the detector input capacitance C_{in} can be measured only at frequencies above 30 Mcps. The accuracy of these values of C_{in} is estimated to be ± 0.2 μμf. Measured values of voltage efficiency e_v and current efficiency e_i are accurate to about ± 5 percent.

2. Measurement of Diode Parameters

Measurements were made of the static characteristics, charge-storage effects, and barrier capacitance of an S570G germanium diode and an FD100 silicon diode. The parameters used for calculating detector-circuit performance on the basis of the detector-design theory presented in Section III are obtained from these measurements in Sections IV-3 and IV-4.

The static characteristics of the diodes were measured with DC instruments. The forward characteristics are shown in Fig. 18. The use of a logarithmic scale for current makes possible the detailed display of the high- and low-current portions of the characteristics on a single graph. The approach of the curves to straight lines at low currents indicates that the static characteristics are approximately exponential in this region. The reverse diode characteristics are

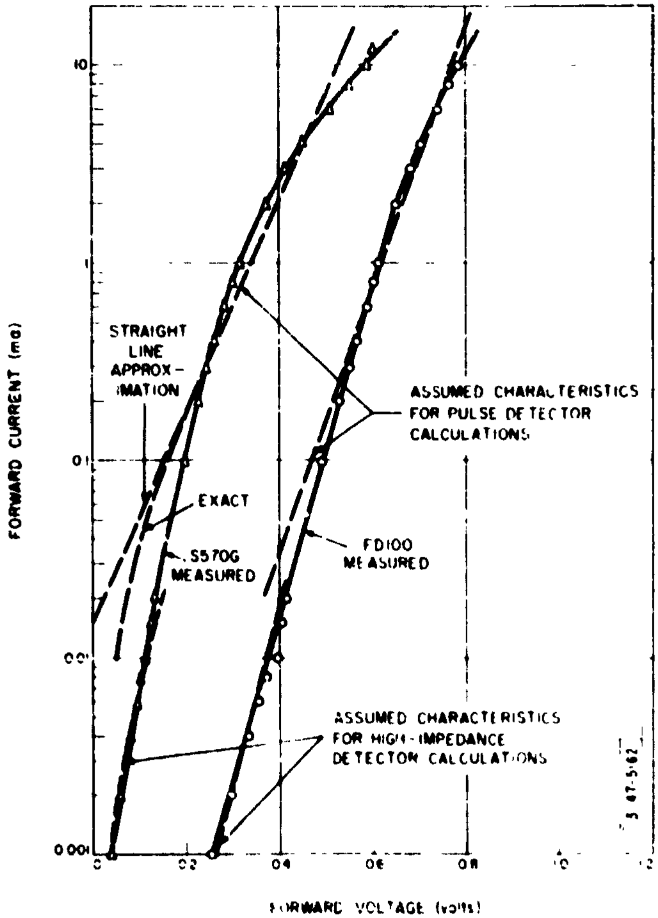

Fig. 18. Measured forward diode characteristics and assumed characteristics used for circuit calculations.

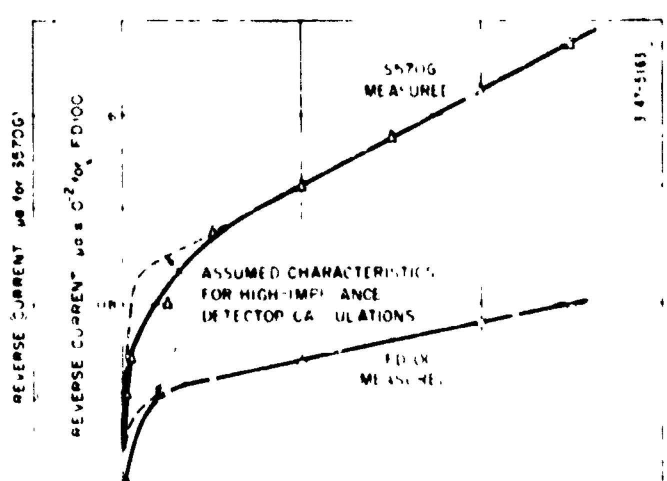

Fig. 19. Measured reverse diode characteristics and assumed characteristics used for high-impedance detector calculations.

plotted in Fig. 19. (Note that different current scales are used for the germanium and the silicon diodes.)

The real part of the frequency dependent charge-storage factor $G(\omega)$ defined in Section III-3 is obtained from measurements of detector input resistance as a function of signal frequency. The detector input voltage is held constant, resulting in a constant detector output voltage when the approximation of Equation 9 in Section III-3 is valid. The validity of this assumption is verified by measuring the detector voltage efficiency as a function of frequency. The value of $G(\omega)$ is then the ratio of the low frequency input resistance to the input resistance at the desired frequency:

$$G(\omega) = \frac{R_{in} \text{ (low frequency)}}{R_{in}(\omega)}$$

The detector voltage efficiency was measured as a function of frequency for all load resistances and input voltages for which the detector input resistance was measured. The measured voltage efficiency of the pulse-detector circuits is plotted as a function of frequency in Fig. 20. The voltage efficiency decreases less than 5 percent with increasing frequency from 1 to 100 Mcps, except at low input voltage where the decrease is as large as 12 percent for the FD100 diode. The measured voltage efficiency of the high-impedance detectors, (not shown), was constant with frequency to within the measurement accuracy.

It is convenient to assume that $G(\omega)$ is independent of signal level and detector load resistance. In order to determine the range of validity of this assumption, measurements were made on both

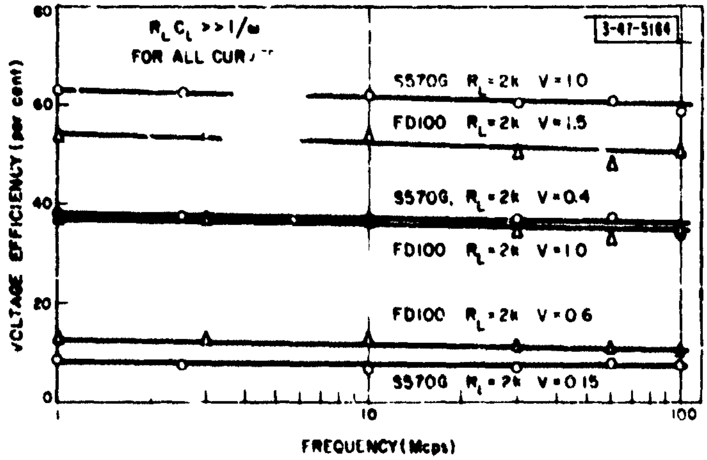

Fig. 20. Measured voltage efficiency as a function of frequency for several circuit conditions.

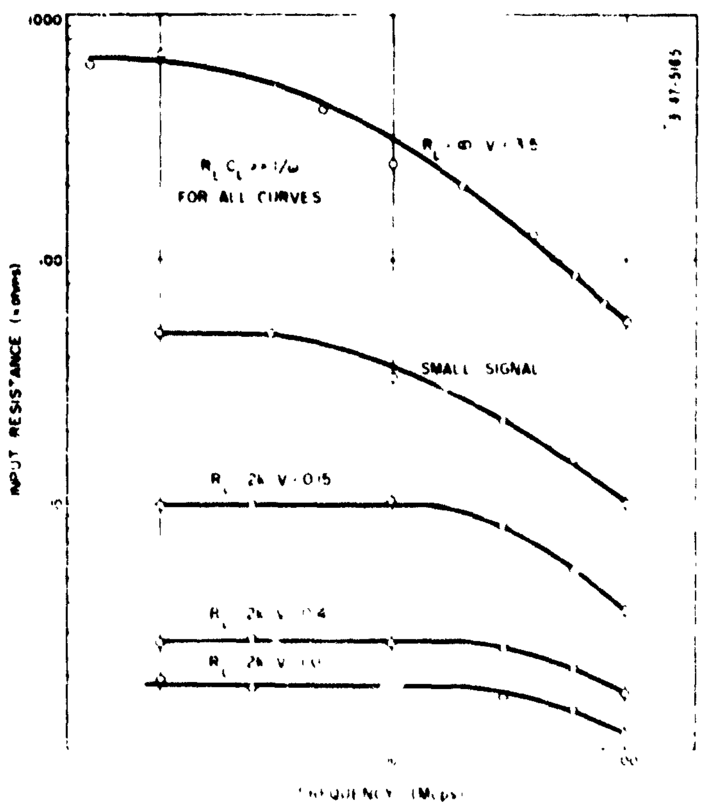

Fig. 21. Measured input resistance as a function of frequency for detectors using an S570G diode.

high-impedance and pulse detectors. Measurements of the input resistance of several S570G germanium diode detectors were made at frequencies from 0.5 to 100 Mcps. A pulse detector with a load resistance of 2 K ohms and a large load capacitance (0.001 μf) was measured with input voltages of 0.15, 0.4, and 1.0 volts peak, using the transistor circuit described in Section IV-1. A high-impedance detector with an infinite load resistance and a 0.001 μf load capacitance was measured with an input voltage of 3.5 volts peak, using the Q Meters. At very low input voltages, the detector voltage efficiency approaches zero, and the input resistance approaches the small-signal resistance of the diode (with no bias). This small-signal diode resistance was measured using the admittance bridge.

The input resistance values obtained from the S570G diode measurements are plotted as functions of frequency in Fig. 21. A logarithmic scale of input resistance allows visual comparison of the values of $G(\omega)$ that can be obtained from each curve. Curves separated by a constant vertical distance yield identical values of $G(\omega)$. Each curve reaches its low-frequency value $(G(\omega) = 1)$ at a frequency higher than 0.5 Mcps.

The curves of input resistance for the pulse detectors are nearly parallel, indicating that a single $G(\omega)$ function can be used for pulse-detector performance calculations over a substantial range of signal levels. The input resistance of the high impedance detector decreases more rapidly with frequency, and larger values of $G(\omega)$ are therefore used for high-impedance detector calculations than for pulse-detector calculations.

The input-resistance measurements made using the FD100 diode are shown in Fig. 22. The pulse-detector measurements were made with input voltages of 0.6, 1.0, and 1.5 volts. The curves are nearly parallel for this diode also. The small-signal resistance, measured using the admittance bridge, is shown by a broken line. The measurement error of the admittance bridge for the high resistances presented by this diode may be considerable, and the curve is presented only to indicate its approximate position. The high-impedance detector was measured with an input voltage of 3.5 volts, using the Q Meters. The decrease of input resistance with frequency for this detector is very pronounced. The low-frequency value of the input resistance is beyond the range of the Q Meter measurements.

The diode barrier capacitance C_B is obtained from measurements of the diode capacitance with reverse bias. Since the diffusion capacitance and bulk inductive effect are negligible with reverse bias the measured capacitance is equal to the barrier capacitance. The barrier capacitances of the S570G and FD100 were measured with the admittance bridge at 30 Mcps with back biases varying from 0.1 to 3.0 volts. Values of barrier capacitance of approximately 0.6 μμf for the S570G diode and 0.8 μμf for the FD100 were obtained in this voltage range. The variation of the barrier capacitance with reverse voltage in this range is too small to be determined with any accuracy.

The imaginary part of the charge storage factor $B(\omega)$ defined in Section III-3 could not be obtained from the measurements. For the reasons discussed in Section IV-1 the input capacitance of the pulse detectors was measured using the transistor circuit only at fre

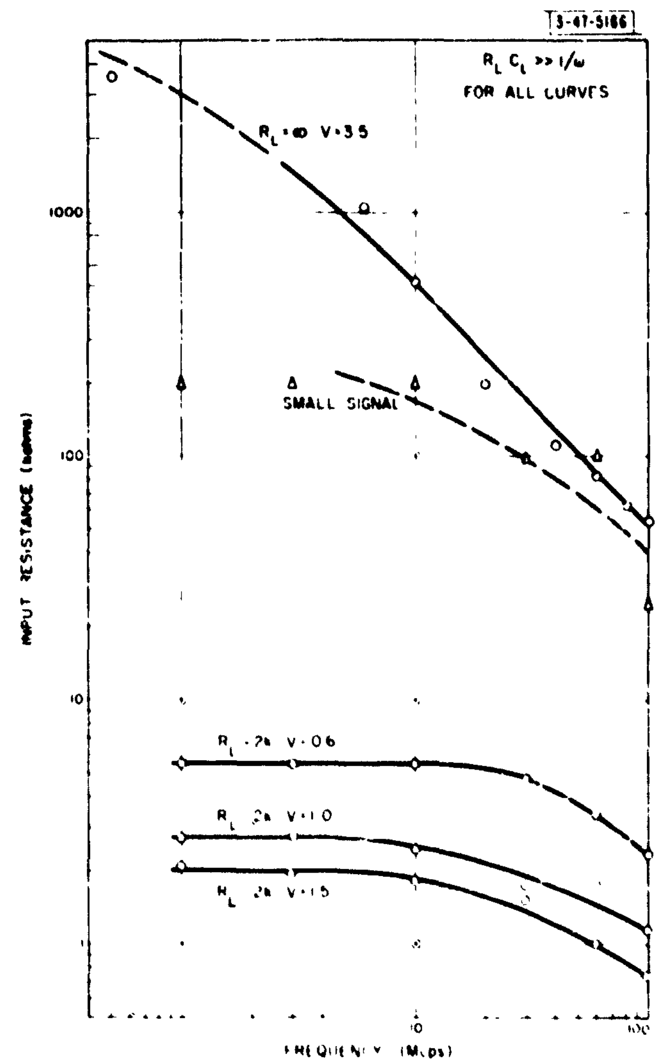

Fig. 22. Measured input resistance as a function of frequency for detectors using an FD100 diode.

quencies of 30 Mcps and higher. These measurements are presented in Section IV-4. Due to the inductive effect of the diode bulk impedance discussed in Section III-3 the capacitance of the diode junction C_J, and therefore the capacitance resulting from the diffusion current, can not be determined from these measurements.

The input capacitances of the high-impedance detectors were measured using the Q Meters, and are plotted in Figs. 23 and 24 as functions of frequency for the S570G and FD100 diodes respectively. The input capacitance of each detector is a few tenths of a micro-microfarad larger than the measured diode barrier capacitance. This increase of the input capacitance over the barrier capacitance is attributed to the capacitive component of the diffusion current crossing the junction. This capacitance decreases with increasing frequency, in agreement with the theory of Section III-3. The effect of the diode bulk impedance is not significant in high impedance detectors. Since the changes of capacitance are of the same magnitude as the accuracy of the capacitance measurements, no attempt was made to evaluate $B(\omega)$ for the high-impedance detectors. The small-signal diode capacitances, measured with the admittance bridge, are also plotted in Figs. 23 and 24. Comparison of the small-signal diode capacitance with the high-impedance detector input capacitance measured with an input voltage of 3.5 volts gives good agreement. This indicates that the change of the input capacitance of the high impedance detectors with signal level is small. (See Section IV-3.)

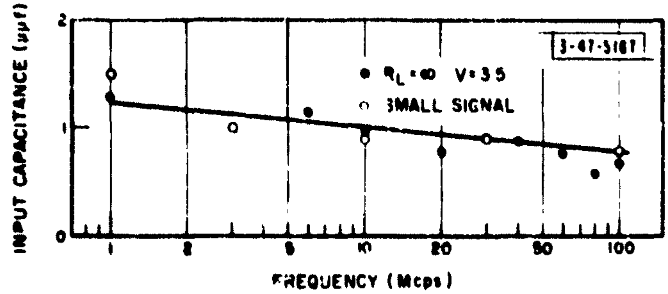

Fig. 23. Measured input capacitance as a function of frequency for a high-impedance detector using an S570G diode.

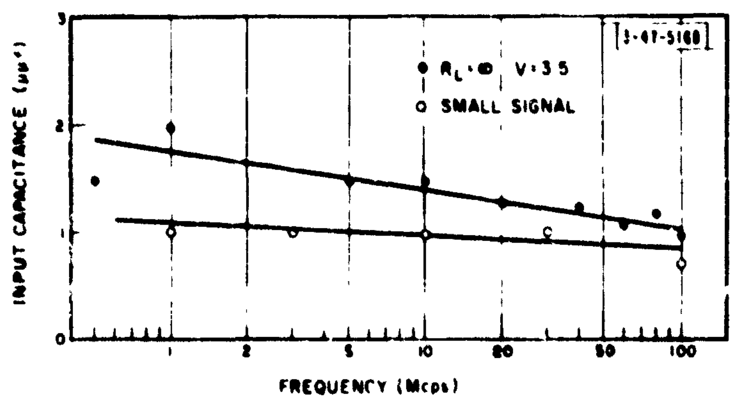

Fig. 24. Measured input capacitance as a function of frequency for a high-impedance detector using an FD100 diode.

3. High-Impedance Detectors

Calculations have been made of the performance of high-impedance detector circuits using the S570G and FD100 diodes and having input voltages of the order of 1 volt peak. The values of the diode parameters used for the calculations are obtained from the measurements reported in the preceding section as follows: The values of diode reverse-saturation current I_R and reverse resistance R_R are obtained from the plots of the measured diode reverse characteristics in Fig. 19. The diode reverse resistance is the slope of a straight line that approximates the diode reverse characteristic for reverse voltages larger than approximately 1 volt. The reverse saturation current is the intercept on the current axis of this linear approximation. The exponential constants c are chosen so that the assumed diode characteristics, having the form given in Section III-2,

$$i = I_R (e^{v_D/c} - 1) + \frac{v_D}{R_R}$$

are good approximations to the measured forward characteristics plotted in Fig. 18, in the low-current range. Values of c were calculated that allow the assumed and measured characteristics to coincide for values of forward current of 5 μamp. The assumed static characteristics are plotted as dashed lines in Figs. 18 and 19. The values of the corresponding static parameters are given in Table 1.

The real part of the charge-storage factor $G(\omega)$ for the S570G diode is obtained from the input resistance of the high-impedance detector, measured with an input voltage of 3.5 volts peak, plotted in

Fig. 21. Since the low-frequency value of input resistance of the FD100 diode could not be measured, the 30 Mcps value of $G(\omega)$ is chosen to give agreement between the measured and calculated input resistance at 1.1 volts. The 100 Mcps value of $G(\omega)$ is obtained by multiplying the 30 Mcps value by the ratio of the measured input resistances at 30 and 100 Mcps. (See Fig. 22.) The values used in the calculations at 30 and 100 Mcps are given in Table 1.

Table 1

Diode Parameters for High-Impedance Detector Calculations

Diode	R_R (in meg ohms)	I_R (in μamp)	[illegible] (in volts)	$G(\omega)$ 30 Mcps	$G(\omega)$ 100 Mcps
S570G	5	0.9	0.0478	4.46	11.7
FD100	1250	0.004	0.0477	1330	4480

Using the method described in Sections III-2 and III-3, and the diode parameters given in Table 1, the voltage efficiency and input resistance were calculated as functions of input voltage from 0.1 to 5.0 volts peak for high-impedance detectors with S570G and FD100 diodes, infinite load resistance and large load capacitance (0.001 μf) at frequencies of 30 Mcps and 100 Mcps. The results of the calculations are shown as broken lines in Figs. 25 through 28. The voltage efficiency, input resistance and input capacitance of detector circuits having the parameters used in the calculations were measured and the results are plotted in Figs. 25 through 30. The Q Meter was used for measure-

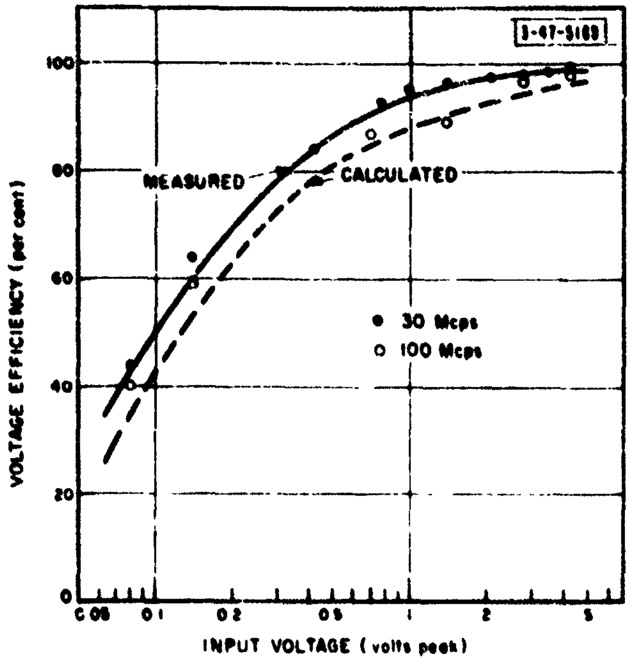

Fig. 25. Measured and calculated voltage efficiency as a function of input voltage for a high-impedance detector using an S570G diode.

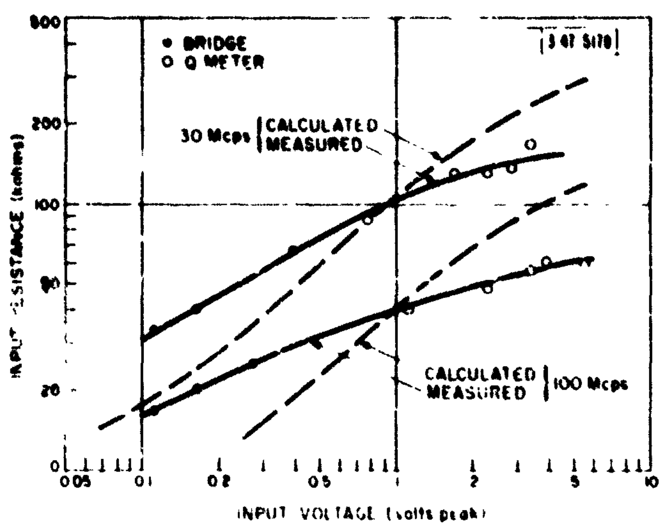

Fig. 26. Measured and calculated input resistance as a function of input voltage for a high-impedance detector using an S570G diode.

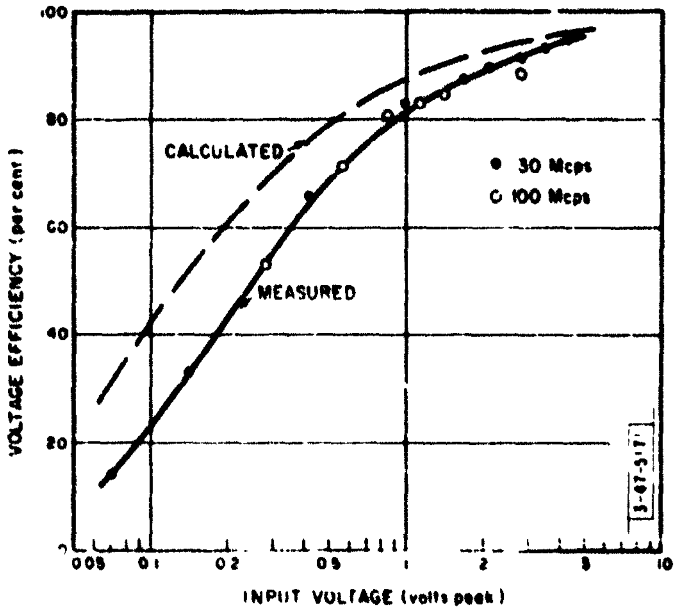

Fig. 27. Measured and calculated voltage efficiency as a function of input voltage for a high-impedance detector using an FD100 diode.

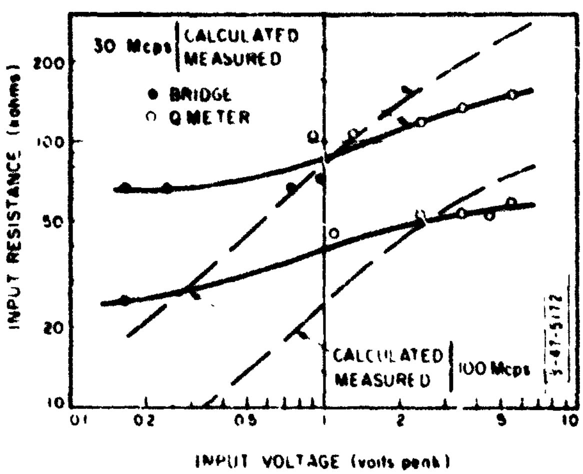

Fig. 28. Measured and calculated input resistance as a function of input voltage for a high-impedance detector using an FD100 diode.

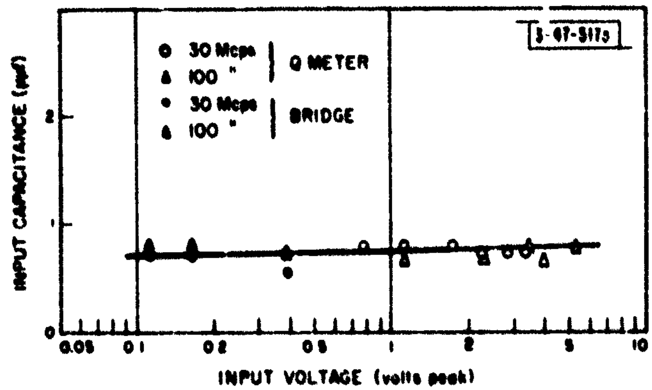

Fig. 29. Measured input capacitance as a function of input voltage for a high-impedance detector using an S570G diode.

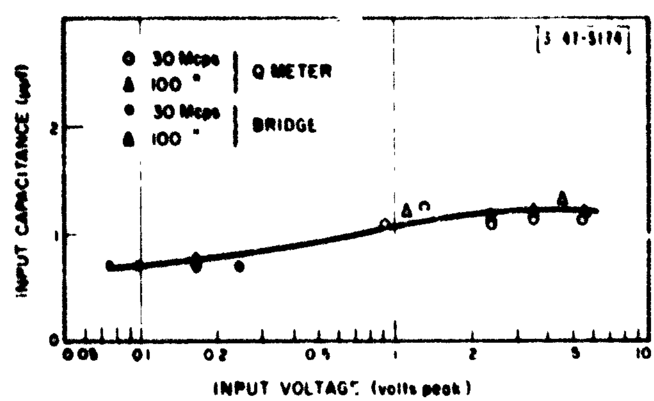

Fig. 30. Measured input capacitance as a function of input voltage for a high-impedance detector using an FD100 diode.

ments at input voltages from 0.75 to 5 volts. The admittance bridge was us· · or measurements at input voltages below this range.

The measured and calculated values of voltage efficiency agree to within 10 percent for input voltages from 0.2 to 4.0 volts for the S570G diode and from 0.7 to 4.0 volts for the FD100 diode. The disagreement between the measured and calculated values at lower signal levels is attributed to experimental error and to the failure of the assumed diode static characteristics to closely approximate the actual characteristics over a wide range of signal levels. Note that the voltage efficiency points measured at both 30 Mcps and 100 Mcps fall along a single curve for each diode.

The variation with input voltage of the measured input resistance is considerably less than the calculated variation. This is attributable at least in part to the variation of the real part of the charge-storage factor $G(\omega)$ with signal level in high-impedance detectors. Fig. 21 shows that the values of $G(\omega)$ for the S570G diode at 3.5 volts are approximately twice the values of $G(\omega)$ for small signals. The approximate curves in Fig. 22 indicate a larger variation for the FD100 diode. The discrepancy between the measured and calculated values of input resistance at 30 and 100 Mcps is less than ±50 percent for input voltage from 0.4 to 2.5 for the S570G diode and from 1.0 to 4.0 for the FD100 diode. Larger discrepancies occur outside these voltage ranges.

The variation of input capacitance with input voltage is shown in Figs. 29 and 30 for the high-impedance detectors using the S570G and FD100 diodes respectively. For each detector the input capacitance is nearly the same at 30 and 100 Mcps. The input capacitance of the detectors increases slightly with a change of input voltage from 0.1 to 5 volts peak. The major portion of the input capacitance is due to the diode barrier capacitance which remains nearly constant with frequency and input voltage in the range of these measurements. The slight increase of the input capacitance at high input voltage is attributed to the diode diffusion capacitance which increases at higher input signal levels as discussed in Section III-3.

4. Pulse Detectors

Calculations have been made of the performance of pulse-detector circuits using the S570G and FD100 diodes with peak input currents of the order of 2 ma peak. The resulting diode current pulses have an average value I_o of the order of 0.5 ma and peak values perhaps ten times the average value. The assumed static characteristics used for the calculations of pulse detector performance are chosen to approximate the measured characteristics over the range of diode forward currents from 0.1 to 10 ma. It is assumed that this current range includes the portion of the static characteristic where most of the diode current flow takes place. Since the reverse diode current is small compared with the average diode current, the assumed reverse characteristic need not closely approximate the measured characteristic, providing the assumed reverse current is also small compared with the average diode current. An infinite value of diode reverse resistance R_R is assumed, and the diode characteristic is of the form

$$i = I_R (e^{v_D/c} - 1)$$

For values of v_D/c much larger than unity, the second term in the brackets may be neglected. Taking the logarithm of each side of the expression then yields

$$\log_e i = (\log_e I_R) + v_D/c \quad ,$$

$$\log_{10} i = (\log_{10} I_R) + v_D/2.3\,c \quad .$$

The assumed characteristic is determined by drawing a straight line on a semi-logarithmic plot that approximates the measured characteristic over the desired range. The intercept of this line on the current axis gives the value of I_R, and the slope of the line equals $1/2.3\,c$. (The slope is the change in current in decades divided by the corresponding change in voltage.) The exact value of current given by the assumed characteristic differs from that given by the linear plot only at small values of voltage.

The assumed static characteristics for the S570G and FD100 diodes used in the pulse detector calculations are shown as broken lines in Fig. 18. For the S570G diode both the linear approximation and the exact plot are shown. The resulting values for the diode static parameters are given in Table 2.

The assumed values for the real part of the charge-storage factor $G(\omega)$ are obtained from the measurements of pulse-detector input resistance as a function of frequency that are shown in Figs. 21 and 22. The curve for a detector input voltage of 1.0 volt was used for the S570G diode, and the curve for an input voltage of 1.5 volts was used for the FD100. The values of G(ω) used in the calculations at 30 Mcps and 100 Mcps are shown in Table 2.

Table 2

Diode Parameters for Pulse-Detector Calculations

Diode	I_R (in ma)	c (in volts)	G(ω) 30 Mcps	G(ω) 100 Mcps
S570G	0 015	0 0805	1 10	1.55
FD100	0.00007	0.0652	1.45	2.60

Using the method described in Sections III-2 and III-3 and the parameters given in Table 2, the voltage efficiency and input resistance were calculated as functions of input voltage for detectors with S570G and FD100 diodes, 2 K ohms load resistance and a large (0 001 μf) load capacitance at frequencies of 30 Mcps and 100 Mcps The results of these calculations are shown as broken lines in Figs. 31, 32, 34, 35, 37, 38, 40 and 41. The voltage efficiency, input resistance and input capacitance of detectors with the same circuit parameters were measured using the transistor circuit method described in Section IV-1 The results are plotted in Figs. 31 through 42.

Comparison of the calculated and measured values of voltage efficiency shows that the agreement is better than ± 10 percent over an input voltage range from 0 25 to 1.8 volts for the S570G germanium diode and over an input voltage range from 0.65 to 1.5 for the FD100 silicon diode The calculated voltage efficiency at both 30 and 100 Mcps

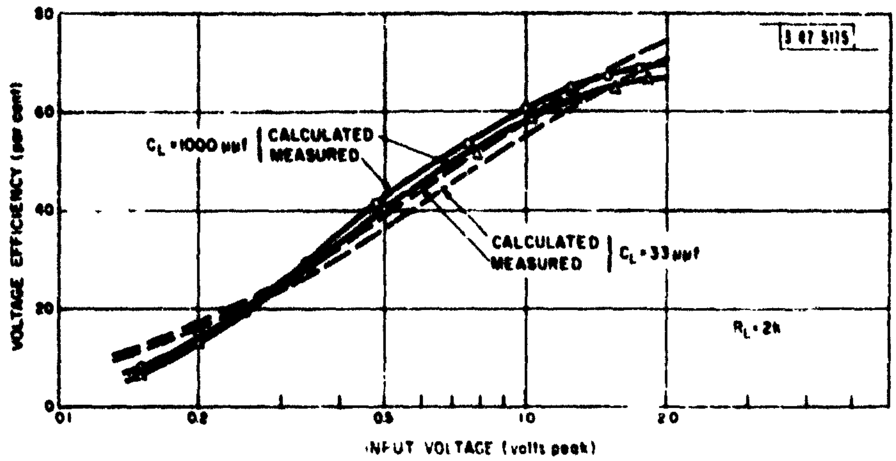

Fig. 31. Measured and calculated voltage efficiency as a function of input voltage at 30 Mcps for pulse detectors using an S570G diode.

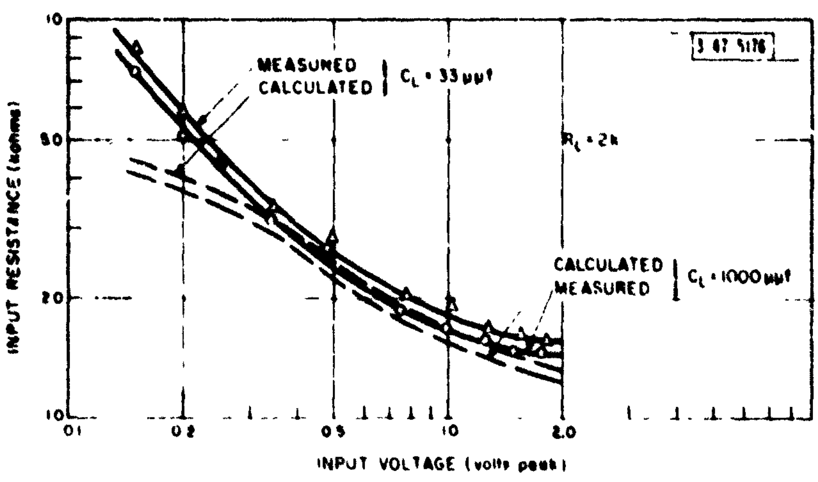

Fig. 32. Measured and calculated input resistance as a function of input voltage at 30 Mcps for pulse detectors using an S570G diode.

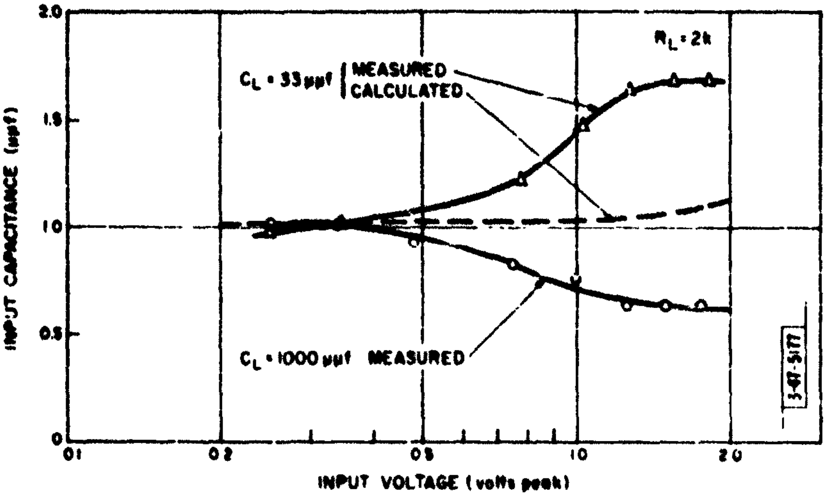

Fig. 33. Measured input capacitance as a function of input voltage at 30 Mcps for pulse detectors using an S570G diode. A calculated curve is shown for the detector having a short load time constant. (See text)

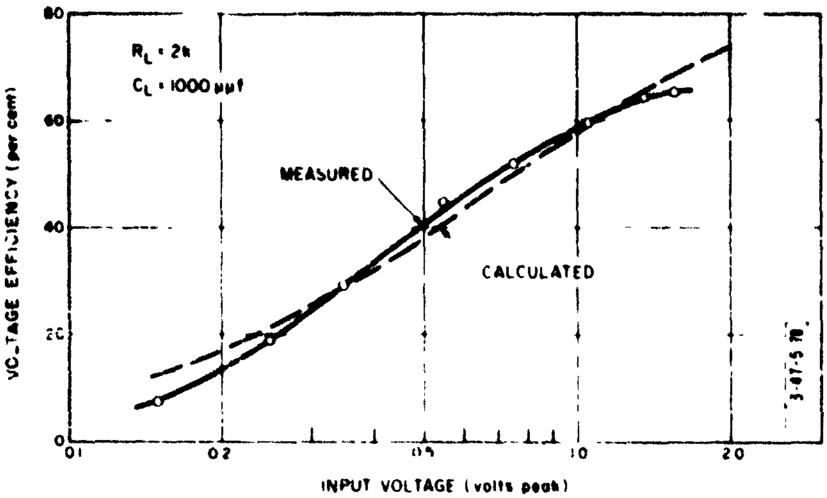

Fig. 34. Measured and calculated voltage efficiency as a function of input voltage at 100 Mcps for a pulse detector using an S570G diode.

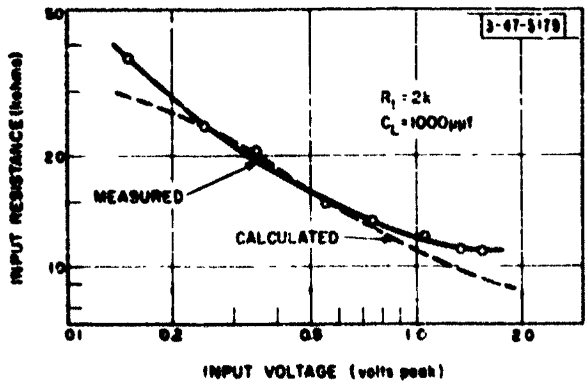

Fig. 35. Measured and calculated input resistance as a function of input voltage at 100 Mcps for a pulse detector using an S570G diode.

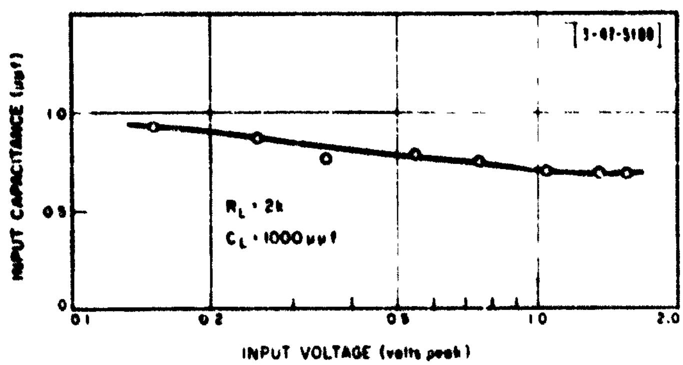

Fig. 36. Measured input capacitance as a function of input voltage at 100 Mcps for a pulse detector using an S570G diode.

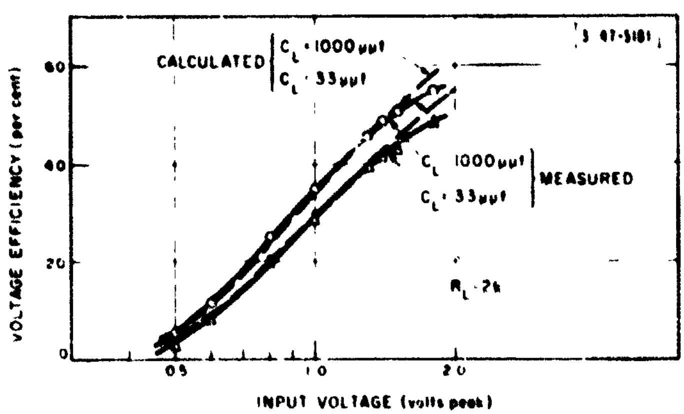

Fig. 37. Measured and calculated voltage efficiency as a function of input voltage at 30 Mcps for pulse detectors using an FD100 diode.

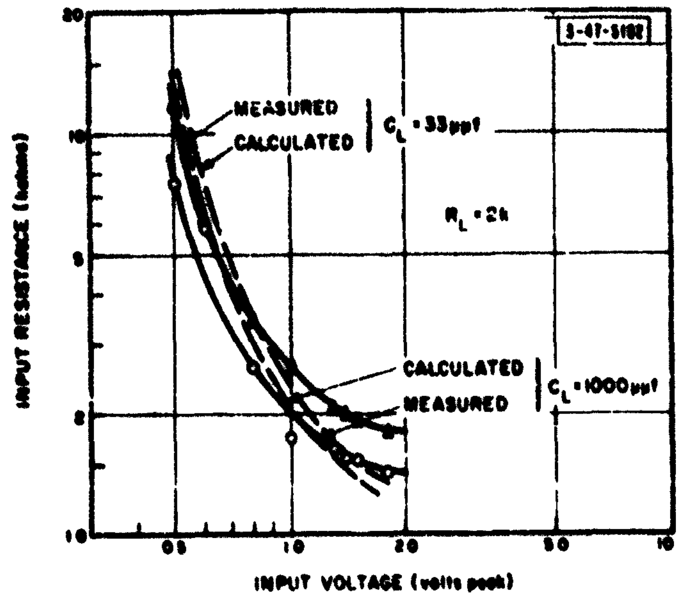

Fig. 38. Measured and calculated input resistance as a function of input voltage at 30 Mcps for pulse detectors using an FD100 diode.

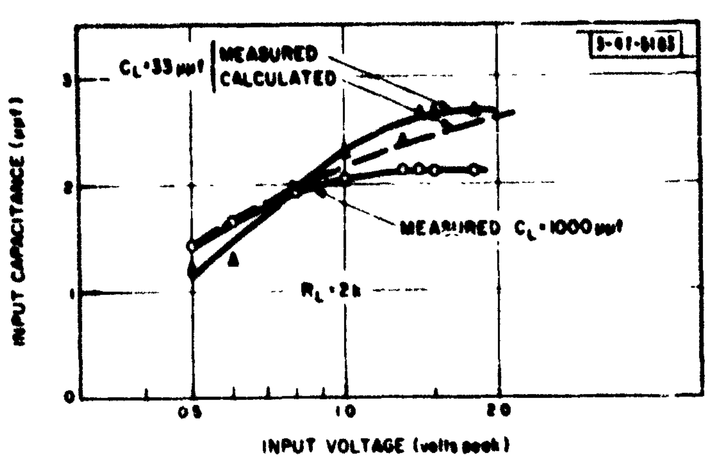

Fig. 39. Measured input capacitance as a function of input voltage at 30 Mcps for pulse detectors using an FD100 diode. A calculated curve is shown for the detector having a short load time constant. (See text.)

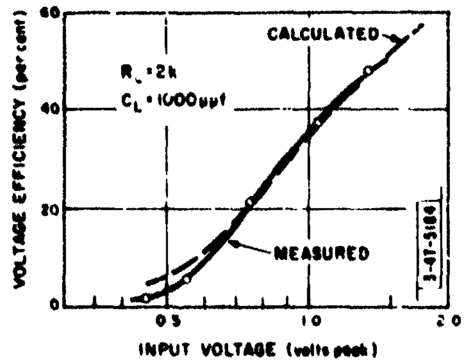

Fig. 40. Measured and calculated voltage efficiency as a function of input voltage at 100 Mcps for a pulse detector using an FD100 diode.

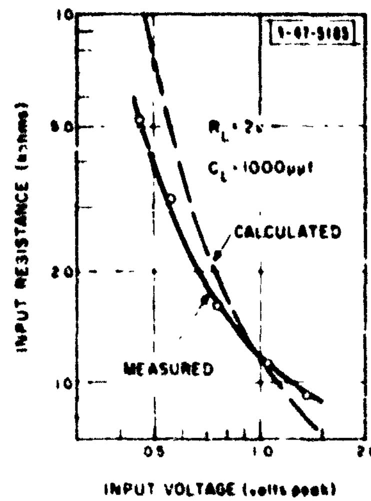

Fig. 41. Measured and calculated input resistance as a function of input voltage at 100 Mcps for a pulse detector using an FD100 diode.

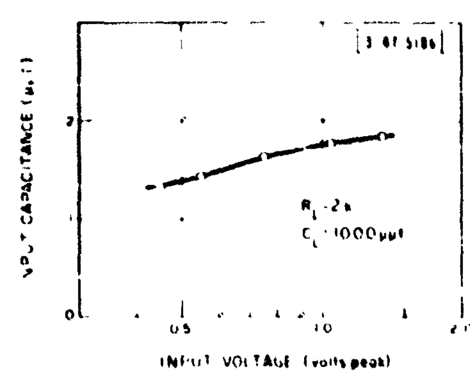

Fig. 42. Measured input capacitance as a function of input voltage at 100 Mcps for a pulse detector using an FD100 diode.

is 50 percent higher than the measured value at an input voltage of 0.15 volt for the S570G and 0.5 volt for the FD100. For both diodes, the calculated voltage efficiency is higher than the measured value at high and low input voltages, and lower than the measured value at intermediate values of input voltage. This is attributed to the fact that the assumed static characteristic indicates a forward current larger than the measured forward current at high and low current levels and smaller than the measured forward current at intermediate current levels.

The calculated and measured values of detector input resistance agree to within ± 15 percent over a range of input voltages from 0.3 to 1.5 volts for the S570G diode, and a range of input voltages from 0.8 to 1.2 volts for the FD100 diode. At lower input voltages the calculated input resistance is substantially lower than the measured value for the S570G diode, and higher for the FD100 diode. The discrepancy is 50 percent at 0.15 volt for the S570G diode at 30 Mcps, and 90 percent at 0.5 volt for the FD100 diode at 100 Mcps. The differences between the measured and calculated values of input resistance are attributed largely to the approximations made in the assumed static characteristics, although an increase in the charge-storage factor at low signal levels may be partially responsible for the large discrepancies at low input voltages.

The detector theory of Section III 3 shows that the capacitance of the diode junction increases with signal level. However, at high current levels such as are found in pulse detectors the inductive component of the bulk impedance results in a detector input capacitance smaller than the diode junction capacitance. The input capacitance of the (well-bypassed) detector with an S570G diode decreases somewhat with increasing level. This may be attributed to the effect of the inductive component of the bulk impedance being sufficiently pronounced at high levels to counteract the increase of the diode junction capacitance. The input capacitance of the detector with an FD100 diode shows a moderate increase with increasing input voltage, indicating that the effect of the bulk inductance is less significant in the FD100 than in the S570G.

The voltage efficiency, input resistance and input capacitance of detectors with S570G and FD100 diodes, 2 K ohms load resistance and a 33 $\mu\mu f$ load capacitance were calculated as functions of input voltage at 30 Mcps using the method described in Section III-4. The previously calculated values of voltage efficiency and input resistance for the detectors with 0.001 μf load capacitance were used in the calculations; however, the <u>measured</u> values of input capacitance for these detectors were used since the input capacitance of these detectors was not calculated. The results of the calculations are shown in Figs. 31, 32, 33, 37, 38 and 39. The corresponding quantities were measured in the transistor circuit and are plotted on the same figures for comparison.

The measured and calculated values of voltage efficiency and input resistance for the detectors with 33 $\mu\mu f$ load capacitance agree to within the same accuracy as for the detectors with large load capacitance. The calculated values of input capacitance are larger than those measured with large load capacitance, the increase being greater at higher signal levels. The measured values of input capacitance also show this increase. The measured input capacitance of the S570G diode detector increases approximately twice as much as the calculated value, the maximum error being 0.6 μμf. The agreement between the calculated and measured values of input capacitance for the FD100 diode detector is better than ±0.3 μμf

The voltage efficiency and input resistance of an S570G diode detector with 0.001 μf load capacitance and an input voltage of 1.0 volt were calculated for load resistances varying from 1 to 100 K ohms using the diode parameters given in Table 2 at a frequency of 30 Mcps. The results are plotted in Figs. 43 and 44 as functions of load resistance. The voltage efficiency, input resistance and input capacitance of corresponding detectors were measured in the transistor circuit. The results are plotted in Figs. 43 through 45. The calculated and measured values of voltage efficiency agree to within ±10 percent. The calculated and measured values of input resistance agree to within ±15 percent. The largest discrepancies for both voltage efficiency and input resistance occur for the largest values of detector load resistance. The input capacitance decreases somewhat with increasing load resistance. Since less diode current flows with a larger load resistance, the capacitance resulting from the diffusion current (and therefore the input capacitance), is smaller. (See Section III-3.)

5. Low-Q Driving Circuits

In Section III-5 it is shown that the current efficiency of a detector with a low-Q driving circuit is given by

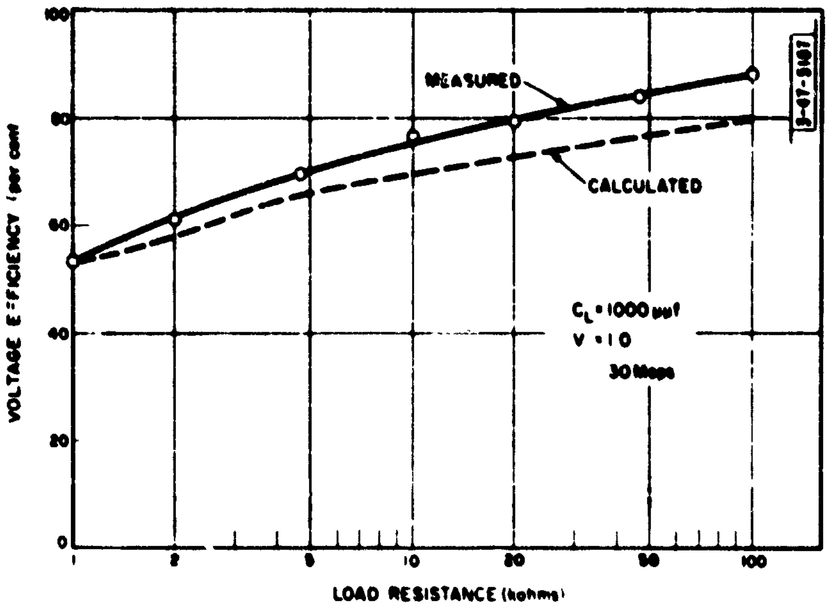

Fig. 43. Measured and calculated voltage efficiency as a function of load resistance for detectors using an SS70G diode and large load time constants.

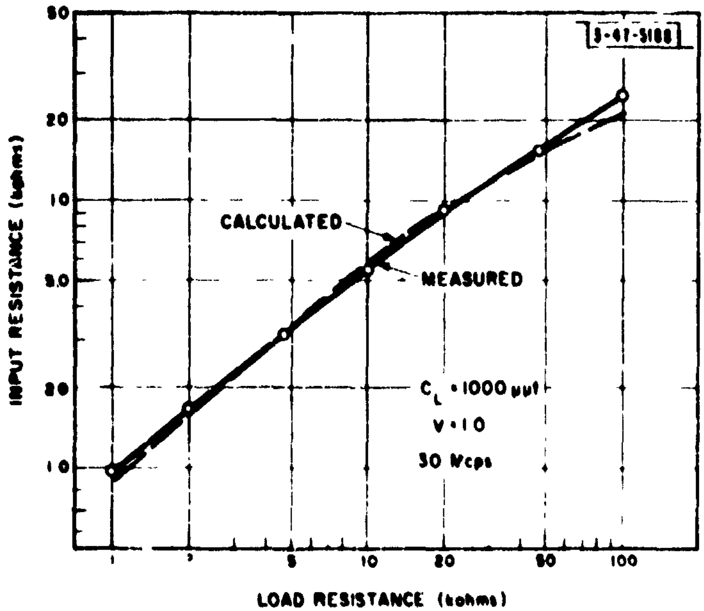

Fig. 44. Measured and calculated input resistance as a function of load resistance for detectors using an S570G diode and having large load time constants.

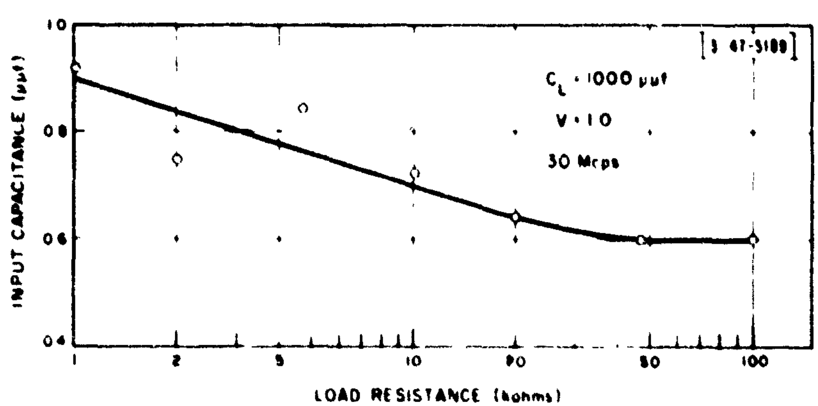

Fig. 45. Measured input capacitance as a function of load resistance for detectors using an S570G diode and large load time constants.

$$e_i = \frac{a e_v}{R_L} \cdot \frac{b R_{in} R_A}{b R_{in} + R_A} .$$

where e_v and R_{in} are the voltage efficiency and input resistance of the detector when it is driven by a sinusoidal voltage and has the same output voltage V_L. The parameters $\underline{a}$ and b are functions of the flattening of the detector input voltage waveform. Measurements were made to evaluate these parameters under variety of conditions as follows:

At each of several frequencies, signal levels and driving-circuit capacitances C_A, the current efficiency e_i was measured in the transistor circuit for two values of driving-circuit resistance R_A. One measurement was made with no shunt resistance added, giving a value of R_A of the order of 10 K ohms. The second measurement was made with a 2 K ohm resistor added across the tuned circuit. At each frequency and signal level, the values of e_v and R_{in} were calculated from measurements made using a (large) value of C_A such that the detector input voltage was approximately sinusoidal. The two sets of values of e_i and R_A were substituted in the above expression and values of e_v and R_{in} were calculated assuming values of unity for $\underline{a}$ and b. The resulting values of e_v and R_{in} were used, along with the measurements of e_i and R_A made with smaller values of C_A, to calculate $\underline{a}$ and b.

The detector used for the measurements consisted of an S570G diode, a 2 K ohm load resistor and a 0.001 µf load capacitor. Signal frequencies of 10, 30, and 60 Mcps were used, with signal levels giving detector output voltages V_L of 0.1 and 0.6 volts. Values of driving circuit capacitance C_A ranging from the minimum obtainable value of 6 μμf to a value so large that the detector input voltage was effectively sinusoidal were used.

In Section III-5 it is shown that, under conditions usually satisfied in practice, the flattening of the detector input voltage waveform is approximately inversely proportional to $\omega R_{in} C_A$, where ω is the angular signal frequency. The values of the parameters $\underline{a}$ and b that were obtained from measurements of current efficiency are plotted as functions of $\omega R_{in} C_A$ in Figs. 46 and 47. All points fell within ± 15 percent of the curves that are shown. Although the current efficiency measurements should be accurate to better than ± 5 percent, measurement errors increase in the calculation of $\underline{a}$ and b to a point where the accuracy of the calculated values of $\underline{a}$ and b is estimated to be ± 15 percent.

The results of these measurements indicate that the theory for waveform distortion given in Section III-5 is valid over the range of the measurements. The values of $\underline{a}$ and b given in Figs. 46 and 47 may be used for calculating detector current efficiency

6 <u>Temperature Variations</u>

Measurements were made of the voltage efficiency, input resistance, and input capacitance of detector circuits as functions of temperature. The temperature was varied from 10° to 50° C, a range considerably greater than normal room-temperature variations. High-impedance detectors having infinite load resistance and large (0.001 μf) load capacitance and pulse detectors having 2 K ohm load resistance

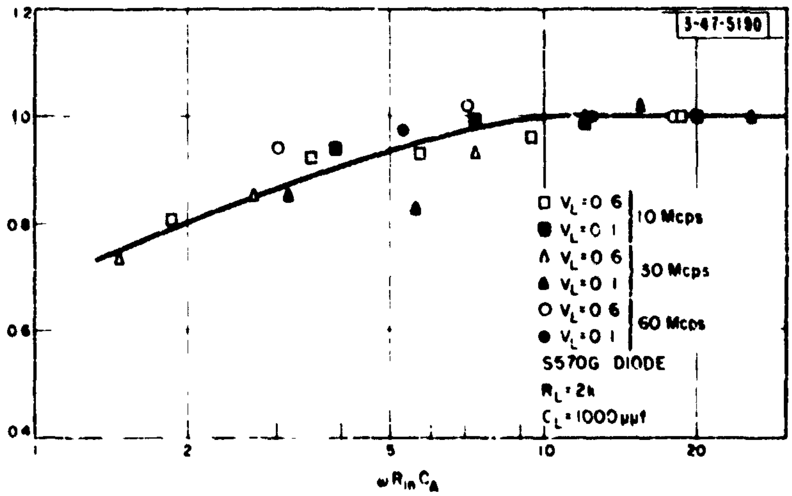

Fig. 46. Values of the current efficiency parameter a, obtained from measurements, plotted versus $\omega R_{in} C_A$.

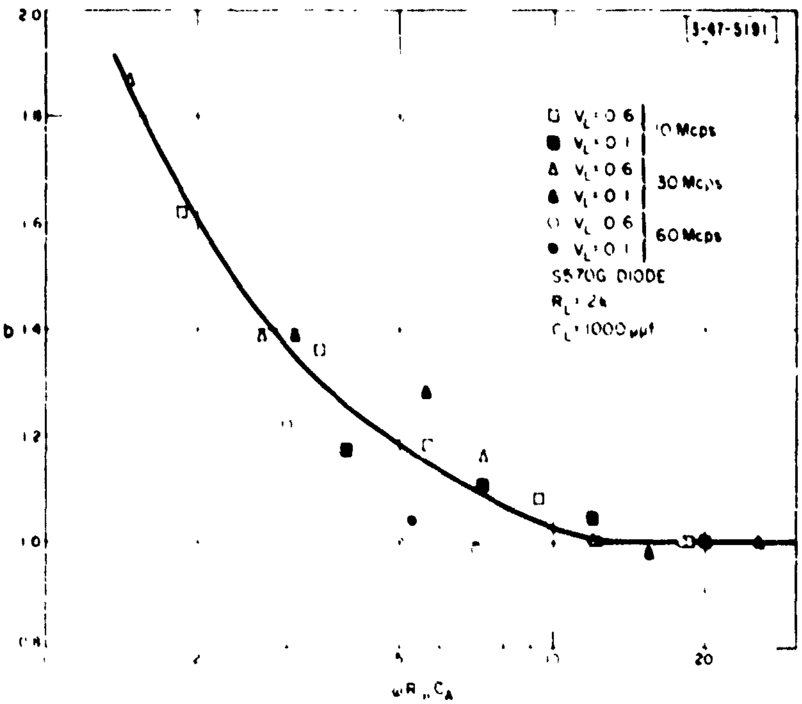

Fig. 47. Values of the current efficiency parameter b, obtained from measurements, plotted versus $\omega R_{in} C_A$.

and large (0.001 μf) load capacitance were measured using S570G and FD100 diodes. The measurements were made at 30 Mcps on the Q Meter. For each detector the input voltage was held constant, as the temperature was varied, at a level at which accurate Q Meter measurements can be made. An input voltage of 3.2 volts peak was used for the high-impedance detectors. The input voltages for the pulse detectors were 0.35 and 0.65 volts peak for the detectors using the S570G and FD100 diodes respectively.

The measured values of voltage efficiency, input resistance and input capacitance are plotted as functions of temperature in Figs. 48 through 51. The measured variation of the voltage efficiency for the high-impedance detectors is less than 2 percent, and is therefore not plotted. The curves of voltage efficiency and input resistance shown in Figs. 48 through 50 were calculated using the differential expressions, derived in Section III-6, for variations of temperature around 20° C. The calculated variation of voltage efficiency with temperature is linear,

$$\frac{de_v}{dT} = \frac{e_v \alpha kT}{q(V_L + \epsilon + R_L I_R)}$$

since e_v is proportional to V_L and the expression in the parentheses is also approximately proportional to V_L. The calculated input resistance varies exponentially with temperature:

$$\frac{dR_{in}}{dT} = \frac{R_R}{R_R + R_D} \cdot \frac{\alpha kT(\epsilon + R_L I_R)}{q(V_L + \epsilon + R_L I_R)} R_{in}$$

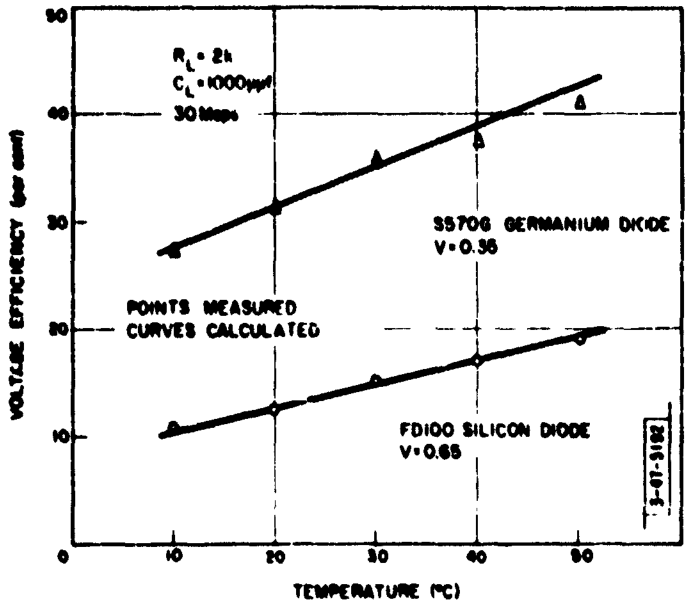

Fig. 48. Measured and calculated voltage efficiency as a function of temperature for pulse detectors using S570G and FD100 diodes.

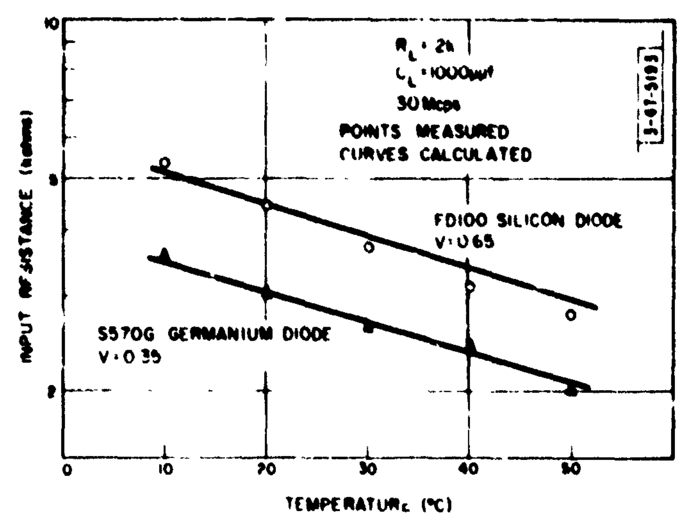

Fig. 49. Measured and calculated input resistance as a function of temperature for pulse detectors using S570G and FD100 diodes.

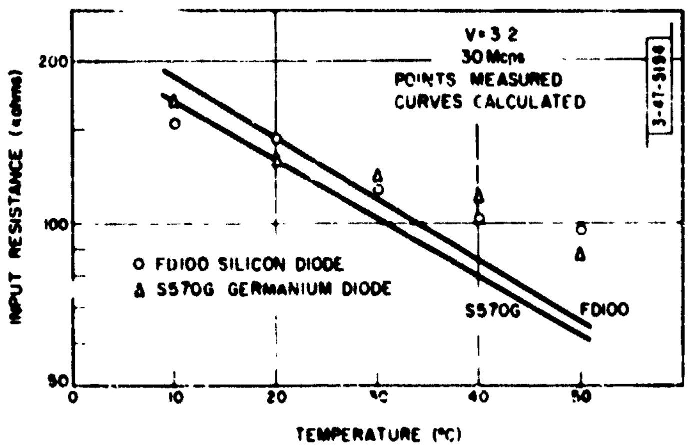

Fig. 50. Measured and calculated input resistance as a function of temperature for high-impedance detectors using S570G and FD100 diodes.

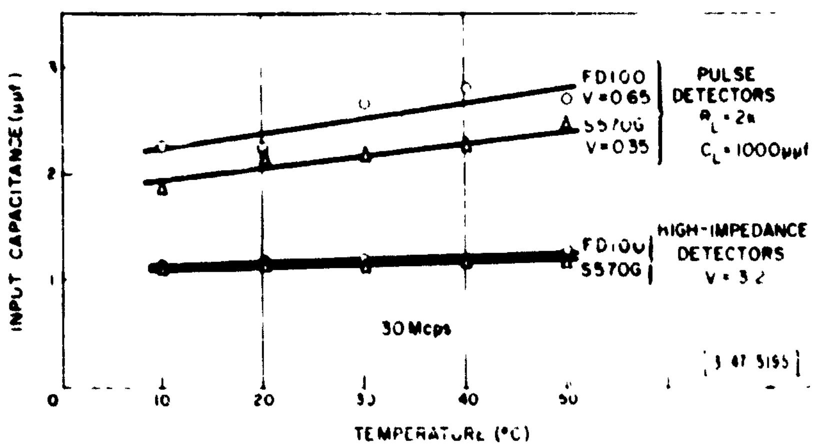

Fig. 51. Measured input capacitance as a function of temperature for high-impedance and pulse detectors using S570G and FD100 diodes.

$$R_{in} = e^{-\left[\frac{R_R}{R_R + R_D} \; \frac{\alpha k T (c + R_L I_R)}{c q (V_L + c + R_L I_R)}\right] T} .$$

The calculated value of R_{in} therefore plots linearally with temperature on semi-logarithmic graph paper. The assumed diode parameters given in Tables 1 and 2 were used in the calculations. The value of temperature coefficient of 0.08 (degrees C)$^{-1}$ suggested by Schaffner and Shea[31] is used for both the germanium and the silicon diode.

The measured and calculated values of voltage efficiency and input resistance for the pulse detector circuits agree to within ±5 percent. The calculated decrease of input resistance with temperature is considerably greater than the measured value for the high-impedance detectors. This discrepancy is attributed to the fact that the input resistance of high impedance detectors is dependent on the charge-storage factor which is not constant with signal level. The calculated and measured variation of the voltage efficiency of the high impedance detectors with temperature from 10 to 50° C is less than 2 percent.

The input capacitance of the detector circuits plotted in Fig. 51 increases with temperature at a rate of approximately 0.01 μμf per degree C for pulse detectors, and 0.0025 μμf per degree C for the high-impedance detectors. The discussion in Section III-6 indicates that the diode diffusion capacitance increases with temperature. Since the barrier capacitance and the bulk impedance also affect the input capacitance of the detectors (see Section III-3) no attempt is made to calculate the changes of input capacitance with temperature.

7. Bias Currents in Pulse-Detector Output Circuits

Measurements were made of the detector voltage efficiency and input resistance as functions of input voltage with a bias current I_E flowing into the detector load circuit The measurements were made at a frequency of 30 Mcps, using the transistor circuit. The detector consisted of an S570G diode, a 2 K ohm load resistance, and a 0.001 μf load capacitance. Bias-currents values of plus and minus 0.05 ma were used.

The measured voltage efficiency and input resistance are plotted in Figs. 52 and 53 respectively for the two bias-current values, along with the voltage efficiency and input resistance measured with no bias current The values of voltage efficiency and input resistance calculated using the methods of Section III-7 are shown by broken lines The agreement between the measured and calculated values is good except at low input voltage where the bias current causes large changes in the voltage efficiency and input resistance and the assumptions made in the derivation are therfore not valid.

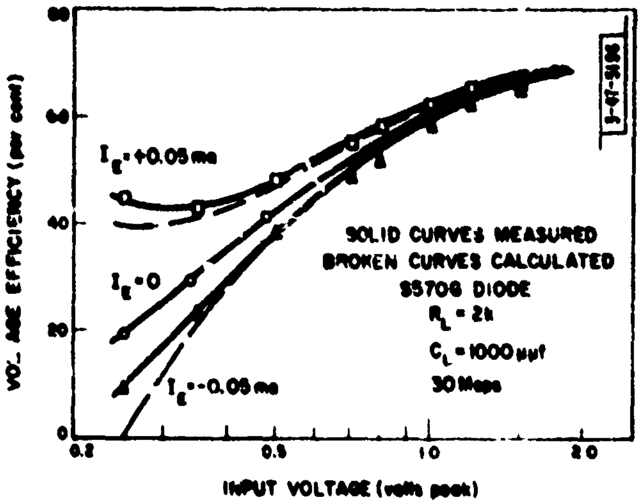

Fig. 52. Measured and calculated voltage efficiency as a function of input voltage for a pulse detector with positive and negative bias currents. A curve measured with no bias current is shown for comparison.

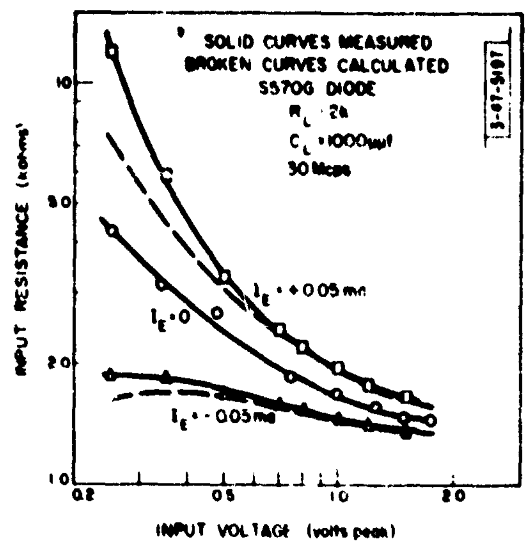

Fig. 53. Measured and calculated input resistance as a function of input voltage for a pulse detector with positive and negative bias currents. A curve measured with no bias current is shown for comparison.

V. Detector-Circuit Design

1. Review

The principal factors that affect detector-circuit operation are discussed in the preceding sections. The detector circuit is shown in Fig. 1. Basic terms and symbols are defined in Section I-2. A survey of the detector-circuit design literature is presented in Sections II-1 and II-2. A survey of semiconductor theory that is applicable to diodes and diode detectors is given in Sections II-3, II-4 and II-5. Neither the detector-circuit design literature nor semiconductor theory yield results that are directly applicable to quantitative design of semiconductor-diode detectors.

A detector-design theory, based on semiconductor theory, is presented in Section III. It permits the calculation of detector-circuit performance on the basis of measurements of the parameters of the diode. The basic theory of Sections III-2 and III-3 permits the calculation of voltage efficiency and input resistance of detectors driven by sinusoidal voltage sources and having load time constants $R_L C_L$ large compared with the reciprocal of the angular signal frequency $1/\omega$. The detector input capacitance is discussed, but no method is given for its calculation in most cases of interest.

A method is given in Section III-4 for calculating voltage efficiency, input resistance and input capacitance for detectors having short load time constants, using the corresponding values of these quantities for a detector with a large load capacitor. The distortion of the detector input voltage waveform resulting when the detector is driven by a low-Q turned circuit, and the effects of this distortion on detector-circuit operation are discussed in Section III-5. A method is given in Section III-6 for calculating the changes in detector-circuit performance resulting from moderate changes in ambient temperature. The effects of AC and DC output coupling on detector-circuit performance are discussed in Section III-7. A method for calculating the rise- and fall-times of pulse detectors driven by a tuned circuit is given in Section III-8.

Measurements of detector-circuit performance are presented in Section IV. The measurements are compared with calculated detector-circuit performance to establish the range of validity of the detector-design theory. The methods used to measure diode parameters and detector-circuit performance are described in Section IV-1. The measurements from which the diode parameters were obtained are presented in Section IV-2. The methods used for calculating the performance of high-impedance and pulse detectors, on the basis of the measured diode parameters, are described in Sections IV-3 and IV-4 respectively. Measurements of the performance of pulse detectors driven from low-Q tuned circuits are reported in Section IV-5. Curves are given that permit the performance of such circuits to be estimated.

In the following sections the application of the theory that has been given is illustrated by the design of sample detector circuits. The practical considerations in the design of high-impedance detectors are discussed in Section V-2. Measurements are presented on two sample high-impedance detectors. The practical considerations in the design of pulse detectors are discussed in Section V-3. Four sample pulse detectors are designed, and measurements of their performance are given. Measurements that compare the performance of several diode types in both high-impedance and pulse detector circuits are presented in Section V-4. The selection of the diode types used in the sample detectors is discussed.

2. High-Impedance Detectors

High-impedance detectors are designed to have high voltage efficiency and high input resistance over a wide range of input signal levels. In addition, it is often desirable that the input resistance either remain constant with varying signal level and temperature, or be large enough to produce a negligible change in loading over the anticipated ranges of input voltage and temperature. A small value of input capacitance is often required, and the variation of input capacitance with input voltage and temperature should be small.

A large load capacitance C_L, having a low reactance at the signal frequency, is always used in high-impedance detectors to maximize the voltage efficiency for a given load resistance and minimize the input capacitance. A large load resistance R_L is normally used to produce high voltage efficiency and input resistance. The voltage efficiency and input resistance increase with load resistance until the limiting value determined by the diode characteristics and the voltage measuring instrument is reached. Maximum load resistance results in maximum voltage efficiency and input resistance for any given diode, input voltage and temperature. A lower load resistance may result in lower voltage efficiency and in a smaller input resistance that varies less with input voltage, temperature, and diode characteristics. In most practical high-impedance detectors the diode current is very small (due to the large load resistance), and the diffusion capacitance is therefore small compared with the barrier capacitance. The resulting detector input capacitance is approximately equal to the diode barrier capacitance, and does not vary appreciably with input voltage and temperature.

The performance of a high-impedance detector circuit (particularly one having maximum load resistance) is largely dependent on the characteristics of the diode. Factors that affect the selection of diode type are as follows:

1. Low forward voltage in the range of operating forward diode currents (usually of the order of microamps.) results in high voltage efficiency.
2. Low diode reverse current results in high input resistance and high voltage efficiency.
3. Fast switching (i.e., low charge storage) results in high input resistance at high frequencies.
4. Low diode barrier capacitance results in low detector input capacitance.
5. The maximum reverse voltage rating must be larger than twice the largest peak input voltage.

Further discussion of the choice of diode type is given in Section V-4.

The measured voltage efficiency, input resistance and input capacitance of high-impedance detectors with maximum load resistance and S570G germanium and FD100 silicon diodes are plotted in Figs. 25 through 30 as functions of input voltage. The voltage efficiency is greater than 90 percent for input voltages greater than 0.7 volt peak for the S570G diode, and 2.0 volts peak for the FD100 diode. For smaller input voltages the voltage efficiency is lower. The variation of the voltage efficiency with frequency is negligible. The input resistance varies directly with input voltage and inversely with signal frequency. (See also Figs. 22 and 23.) The lowest input resistance is obtained at low input voltages where the input resistance approaches the diode small-signal resistance, plotted in Figs. 22 and 23 as a function of signal frequency for the S570G and FD100 diodes respectively. At 100 Mcps the small-signal resistances of the S570G and FD100 diodes are approximately 10 K ohms and 25 Kohms respectively.

The input capacitance of the high-impedance detector with the S570G diode (Fig. 29) is nearly constant at 0.75 μμf with varying signal level. The input capacitance of the detector with the FD100 diode (Fig. 30) increases from 0.7 μμf to 1.2 μμf as the peak input voltage increases from 0.1 volt to 5 volts.

The variations of the detector-circuit parameters with temperature can be calculated using the results given in Section III-6. Sample calculations and measurements reported in Section IV-6 show that the change in voltage efficiency of a high-impedance detector using either diode is negligible. The calculated and measured changes of input resistance with temperature, for an input voltage of 3.2 volts peak, are plotted in Fig. 50. The input resistance at $50^{o}C$ is approximately 70 percent of the value at $20^{o}C$. The theoretical calculation predicts a decrease of approximately 50 percent under the same conditions. At low input voltages, where the detector input resistance approaches the diode small-signal resistance, the expression for the variation of input resistance with temperature derived in Section III-6 is approximately

$$\frac{1}{R_{in}} \cdot \frac{d R_{in}}{dT} = - \frac{\alpha k T}{cq} \quad , \text{ (small signal).}$$

Using the parameters of Section IV-6, the decrease of input resistance with increasing temperature should be approximately four percent per degree C for both diodes. No measurements were made to verify this result because of the limitations of admittance-bridge accuracy for measurements of this type. (See Section IV-1.)

The input capacitance of the high-impedance detectors plotted in Fig. 51 increases less than 0.1 μμf as the temperature increases from 20 to 50 degrees C. This variation is discussed in Section IV-6.

3. Pulse Detectors

Some considerations that affect the selection of pulse-detector circuit components are as follows:

1. A large load resistance R_L gives high voltage efficiency with good linearity at low signal levels, high input resistance and current efficiency, and low input capacitance. A small load resistance produces short rise- and fall-times and facilitates output coupling from the detector.
2. A large value of load capacitance C_L gives high voltage efficiency and low input capacitance. A small load capacitance gives short rise- and fall-times.
3. A large driving-circuit resistance R_A gives high

current efficiency and a current efficiency that is more nearly constant with signal level. A small value of driving-circuit resistance produces more nearly constant loading on the (transistor) current source.

4. A small driving-circuit capacitance C_A produces short rise- and fall-times and may produce higher current efficiency. A large value of C_A results in little flattening of the detector input voltage waveform, and hence in a current efficiency that is more nearly constant with signal level.

Desirable qualities for a diode that is used in a pulse detector and their influence on detector performance are as follows:

1. High forward current at the diode operating voltage results in high voltage efficiency.
2. Low diode capacitance results in low detector input capacitance.
3. A diode with low charge storage gives high detector input resistance at high frequency, and hence high current efficiency at high frequency.
4. The maximum reverse-voltage rating must be larger than approximately twice the maximum peak detector input voltage.

The design of a diode requires some compromises among these qualities. A particular diode may be superior in some qualities at the expense of others. The selection of a diode type for a detector is therefore also a compromise.

The procedure for the design of pulse-detector circuits will be illustrated by the design of four sample pulse detectors. The specifications for the sample detectors are given in Table 3 The center frequency, minimum input voltage and rise-time are normally dictated by the system requirements. The bias current is determined by the transistor circuit to which the detector output is connected. (It may be desirable, under certain circumstances, to buck out the bias current, in which case the uncertainty in bias current would have to be considered.) The minimum possible value of C_L and C_A, and the maximum possible values of R_A and R_L are determined by the residual circuit capacitances and losses. The sample detectors and their driving circuits are designed to provide maximum current efficiency over the range of input currents from 0.1 to 1.0 ma peak.

Table 3

Specifications for Sample Pulse Detectors

Detector Number	Center Freq. (Mcps)	Rise-Time (μsec)	Min Input Voltage (volts peak)	Bias Current I_E (ma)	Min. C_L (μμf)	Max. R_A (K ohms)	Min. C_A (μμf)
1	15	0.5	0.1	-0.05	[illegible]	20	6
2	30	0.5	0.1	-0.05	5	20	6
3	30	0.1	0.1	-0.05	5	20	6
4	100	0.1	0.1	-0.05	5	10	6

The detectors are designed as follows

1. The maximum value of load resistance R_L that produces a detector output for an input voltage of 0.1 volt with a bias current if -0.05 ma is (see Section III-7).

$$R_{L\,max} = \frac{0.1}{0.05\ m} = 2\ \text{K ohms}$$

This maximum value is used in all the detectors in order to produce the highest possible voltage efficiency, input resistance, and current efficiency, and to minimize the detector input capacitance. (Additional specifications on detector linearity could lead to a requirement for a smaller value of R_L, as discussed in Section III-7.)

2. The maximum value of driving-circuit resistance R_A is used to obtain the highest possible current efficiency.

3. The largest value of load capacitance C_L that will give the desired rise-time is used in order to maximize the voltage efficiency and minimize the detector input capacitance. (The discussion of Section III-4 shows that there is no advantage in increasing C_L beyond the point where $\omega R_L C_L$ is much larger than unity.)

4. The minimum value of driving circuit capacitance C_A is used to permit the use of as large a value of C_L as possible.

When R_A is much larger than R_{in}, the rise-time derived in Section III-8 is approximately

$$\tau_r = 2.2\, R_L\, (C_L + C_A/h) \quad .$$

Since the parameter $h = R_L/2R_{in}$ varies with signal level, the rise-time is more nearly constant with signal level when C_L is larg and C_A is small. (The converse is also true. If R_{in} is much larger than R_A, then the rise-time is more nearly constant with level when C_A is large and C_L is small.)

Table 4

Design Values for Sample Pulse Detectors

Detector Number	R_L (Kohms)	C_L (μμf)	R_A (K ohms)	C_A (μμf)	Diode Type
1	2	100	20	6	S570G
2	2	100	20	6	S570G
3	2	15	20	6	S570G
4	2	15	10	6	S570G

Design values of C_L are obtained from the expression for the rise-time given above, assuming a nominal value for the parameter h of unity. For detectors Number 1 and 2 C_L 108 μμf, and for detectors Number 3 and 4, C_L 17 μμf. To be on the safe side, values of 100 μμf and 15 μμf were used. The inequality of Equation 15 in Section III-8 is satisfied in both cases, so the fall-times and rise times should be equal.

Table 5

Calculated Performance for Sample Pulse Detectors
(for an output voltage of 1.0 volt)

Detector Number	e_v (percent)	R_{in} (K ohms)	C_{in} (μμf)	e_i (percent)	τ_r (μsec)
1	66.9	1.50	1.15	66.5	0.446
2	67.3	1.36	0.80	55.1	0.446
3	60.8	1.60	1.38	55.8	0.101
4	63.9	1.06	0.85	35.8	0.089

The design values for the sample pulse detectors are given in Table 4. Type S570G germanium diodes were used because they combine fast switching and low capacitance with moderately high forward current and adequate back voltage ratings. Further comparison of diode types is made in Section V-4.

The performance of the sample pulse detectors was calculated using the methods of Section III, and the diode parameters from Table 2 in Section IV-4. (A value of unity is assumed for $G(\omega)$ at 15 Mcps.) The values of C_{in} measured with the detector having a large load capacitance were used in the calculations. A load bias current $I_E = 0$ was assumed. The detector parameters calculated for an output voltage V_L of 1.0 volt are given in Table 5. The values of voltage efficiency, input resistance and input capacitance are for the detector alone, assuming a sinusoidal input voltage. The current efficiency is calculated using the approximate parameter values from Fig's. 46 and 47. The rise-time is calculated using Equation 12 in Section III-8. The fall-time should be the same.

The sample pulse detectors were built and tested using the transistor driving circuit described in Section IV-1. The tuned-circuit inductances were adjusted for resonance with an input current that produced a detector output voltage of 0.7 volt. The measured current efficiencies for the four detectors are plotted as functions of peak input current in Fig. 54. The calculated current efficiencies for a detector output of 1.0 volt are shown as solid points on the plot. In all cases the agreement between the calculated and measured values is better than 10 percent. The current efficiency is constant to within ±7 percent for input currents between 0.2 and 1.25 ma peak. Below 0.2 ma. the current efficiency decreases. At low signal levels the input capacitance decreases and the resonant frequency of the tuned circuit rises. This detuning results in somewhat lower values of current efficiency for small input currents than would be obtained if the circuit were tuned at low level. The reduction of current efficiency at low levels is particularly pronounced in detector Number 1

The CW passbands of the detectors were measured at three signal levels, as follows: The detector output voltage is held constant, as the signal frequency is varied by adjusting the input current. The bandwidth is taken as the difference between the frequencies at which the required input current is 3 db above the minimum input current. The center frequency is defined as the average of the 3 db frequencies. The percentage change in the measured center frequency is plotted as a function of input current for the four sample detectors in Fig. 55, with the center frequency for 1 ma peak input current taken as the reference. The changes in center frequency are due to the changes in input capacitance of the detectors.

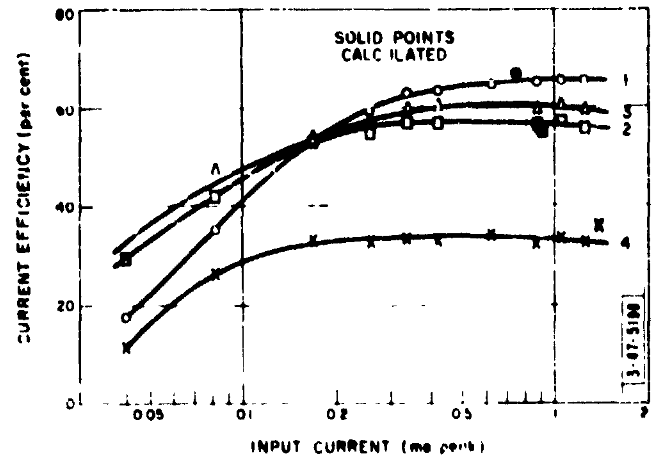

Fig. 54. Measured current efficiency as a function of input current for the sample pulse detectors. Calculated values are shown as solid points.

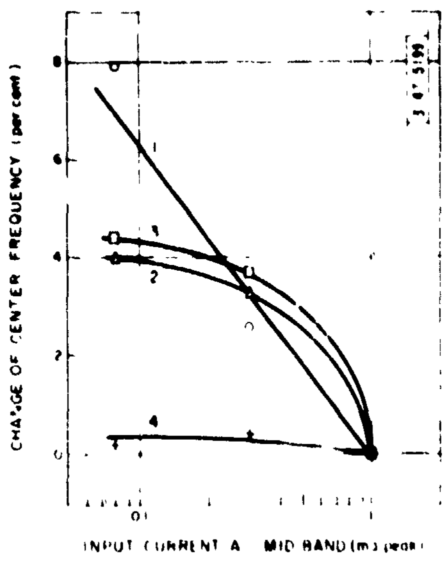

Fig. 55. Change of center frequency as a function of signal level for the sample pulse detector.

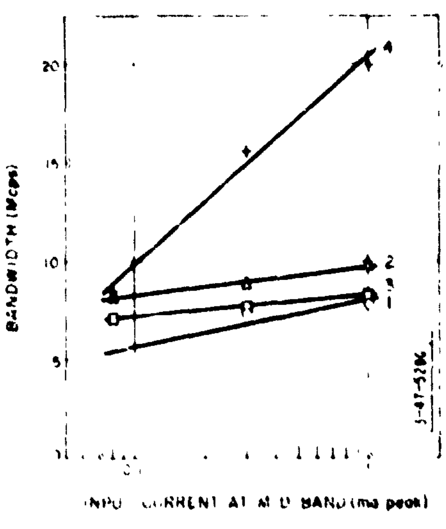

Fig. 56. Bandwidth as a function of signal level for the sample pulse detectors.

The CW bandwidths of the sample detector circuits are plotted as functions of peak input current in Fig. 56. The bandwidths increase with increasing input current due to the decreases in detector input resistance. (The increase of input capacitance with input current tends to reduce the bandwidth, but this effect is small compared with the effect of the decreasing input resistance.) The change of bandwidth for detectors Number 1, 2 and 3 is small in the range of input currents from 0.08 ma to 1 ma peak because the change in input resistance is small. In the 100 Mcps detector (Number 4) the input resistance is lower than in the lower frequency detectors, and input currents from 0.08 ma to 1 ma peak produce smaller detector input voltages than in the other detectors. At lower input voltage the variation of input resistance with input voltage is greater, as shown in Fig. 55 resulting in a larger variation of the CW bandwidth.

It should be noted that the CW bandwidth can not be used to calculate the detector rise-time, since the rise-time is a function of both the detector driving circuit and the detector load circuit. RF rise-times of of 0.1 μsec and 0.5 μsec require RF bandwidths of 7 Mcps and 1.4 Mcps respectively. Detuning of the resonant circuit may, however, result in the passband not covering the required frequency range around the signal frequency. This effect is minimized if the circuit is tuned when the input signal level is near the lowest to be used, since changes in center frequency with increasing signal level are compensated for by the increasing bandwidth. (This problem can not be alleviated by increasing the tuned-circuit capacitance C_A since the CW bandwidth is reduced by the same proportion as is the variation in center frequency.)

The rise- and fall-times of the sample detector circuits were measured using an RF pulse generator as a signal source. The detector output signal was observed with a Tektronix 545 oscilloscope and 53/54 C preamplifier. The RF filter was removed from the detector output, (see Fig. 17b) and the detector load capacitance C_L reduced to compensate for the capacitance presented by the oscilloscope probe. The measured rise time of the input pulse was 0.06 μsec. The combined rise-time of the oscilloscope and preamplifier were 0.015 μsec. The detector rise-time was calculated by assuming that the overall rise-time is the square root of the sum of the square of the pulse generator, detector, oscilloscope and preamplifier rise-times. The accuracy of the measurements is estimated to be ±0.02 μsec. The rise- and fall-times measured with a detector output voltage of 1.0 volt are given in Table 6. In all cases the agreement with the calculated values is within 15 percent. The variation of the rise- and fall-times with signal level is less than ±10 percent for detector output voltages from 0.05 volt to 1.0 volt.

Table 6

Sample Detector Rise- and Fall-Times
(Measured with an output voltage of 1.0 volt)

Detector Number	Rise-Time (μsec)	Fall-Time (μsec)
1	0.52	0.52
2	0.50	0.50
3	0.10	0.10
4	0.08	0.10

Oscilloscope photographs of the input to the transistor circuit and the output from the sample pulse detector are shown in Fig. 57. The phase of the RF pulse is synchronized with the video pulse and the oscilloscope trace. Figures 57a and b show the input RF pulse and the detector output of detectors Number 1 and 2 respectively. The sweep speed is 0.2 μsec per cm and the vertical sensitivity is 0.5 volt per cm for the upper trace and 0.2 volt per cm for the lower trace in each photograph. The RF ripple on the 15 Mcps detector output is more than twice that on the 30 Mcps detector output, as expected. (The oscilloscope response is approximately 3 db down at 30 Mcps and therefore the indicated 30 Mcps ripple is smaller than that actually present.) The RF input pulse and the output of detector Number 3 are shown in Fig. 57c. The sweep speed is 0.1 μsec per cm, and the vertical sensitivities are the same as in Figs 57a and b. The shorter rise- and fall-times and more pronounced RF ripple as compared with detector Number 2 are evident. Figure 57d shows the output of the 100 Mcps detector (Number 4). The sweep speed is 0.1 μsec per cm and the vertical sensitivity is 0.5 volt per cm. Figures 57e and f show the output of detector Number 3 with output voltages of 1.0 volt and 0.1 volt respectively. The sweep speed is 0.1 μsec per cm and the vertical sensitivities are 0.5 volt per cm and 0.05 volt per cm respectively. The constancy of the rise- and fall-times with signal level is evident.

Measurements were made of the performance of the sample detector circuits as a function of temperature from 10 to 50°C. The variations in gain, center frequency and output resistance of the transistor circuit loaded with a fixed resistor were measured over this temperature range and found to be negligible compared with the variations resulting from the pulse detectors. The variation of current efficiency with

(a)

(d)

1-07-5201(a-f)

(b)

(e)

(c)

(f)

Fig. 57. Oscilloscope photographs of sample pulse detector waveforms. The detector output pulses and input RF pulses for detectors Number 1, 2, and 3 are shown in (a), (b), and (c) respectively. The detector output pulse of detector Number 4 is shown in (d). Sweep speeds are 0.2 μsec per cm in (a) and (b), and 0.1 μsec per cm in (c) and (d). Output pu'ses from detector Number 3 having amplitude of 1.0 volt and 0.1 volt are shown in (e) and (f) respectively, with a sweep speed of 0.1 μsec per cm.

temperature was measured for input current levels of 0.1 ma and 1.0 ma peak. Figure 58 shows the results obtained with detector Number 3. The current efficiency is constant to within 4 percent for 1.0 ma input and 6 percent for 0.1 ma input. The variations in current efficiency calculated using the approximate method described in Section III-6 are shown as broken lines in Fig. 58. The agreement is within 5 percent for 1.0 ma input and 30 percent for 0.1 ma input. The large discrepancy between the calculated and measured current efficiency for 0.1 ma input is attributed to the detuning of the resonant circuit due to changes of the detector input capacitance. At low input current the detector input capacitance decreases, causing detuning of the resonant circuit and a reduction of the measured current efficiency. As the temperature increases, the input capacitance increases, bringing the resonant circuit into tune again. Similar results were obtained for the other detectors.

The CW passbands of the sample detectors were measured as functions of temperature with mid-band input current levels of 1.0 and 0.1 ma peak. The percentage change of center frequency for a mid-band input current of 1.0 ma is plotted as a function of temperature in Fig. 59 with the center frequency at 20°C taken as a reference. The center frequency decreases approximately 0.1 percent per degree C increase in temperature for all the detectors. This decrease is in good agreement with the increase of input capacitance with temperature shown in Fig. 51. Similar results are obtained with an input current of 0.1 ma peak. The CW bandwidths of the sample detector circuits increase somewhat with increasing temperature due to the decrease of detector input resistance. In all cases, the measured change is less than 20 percent over the range of temperature variations. The decrease in detector input re-

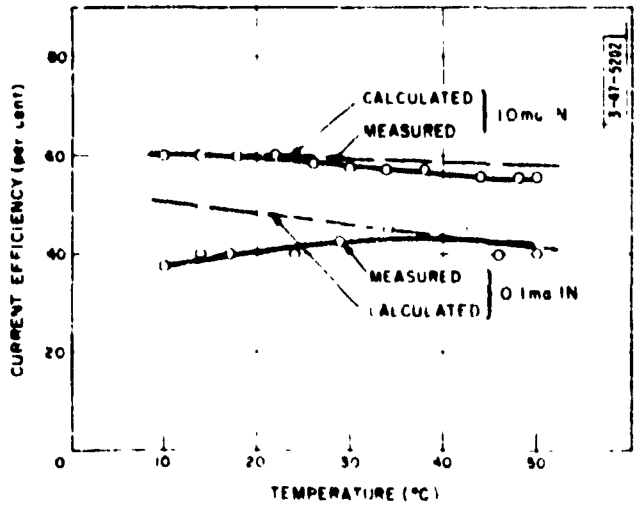

Fig. 58. Measured and calculated current efficiency as a function of temperature for sample pulse detector Number 3 at two signal levels.

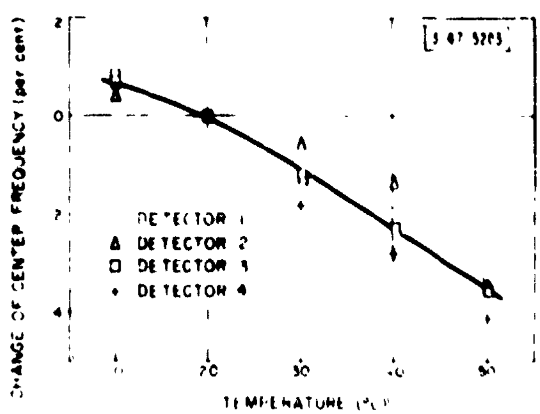

Fig. 59. Measured change of center frequency as a function of temperature for the sample pulse detectors with 1.0 ma input current.

sistance over this temperature range is of the order of 30 percent, and the increase in tuned circuit capacitance due to the increasing detector input capacitance is approximately 10 percent. The change in bandwidth resulting from these changes is in good agreement with the measured bandwidth variations.

The rise- and fall-times of the sample detectors were measured as functions of temperature. No measurable variation was observed in any of the sample detectors over the temperature range from 10 to 50° C.

4. Diode Types

Measurements were made to compare the performance of several diode types in both high-impedance and pulse detectors. At least three samples of each diode type were measured in order to obtain estimates of variations of the measured parameters from diode to diode. The diode types used in the measurements are listed in Table 7, along with the diode material, manufacturer, maximum-reverse-voltage rating, and specified reverse-recovery time. Since the reverse-recovery time depends on the charge stored in the diode, diodes having short reverse-recovery times (fast switching)should also have small charge-storage factors and therefore give high detector input resistance. Diode types having short reverse-recovery time were therefore selected for the measurements. (The IN64 is a comparatively slow-switching diode that is included for comparison.) Since the reverse-recovery times for the various diode types are not specified under the same conditions, direct comparisons of the values are not, in general, valid.

The input resistance and input capacitance of high-impedance

Table 7

Manufacturers' Specifications

Diode Type	Material	Manufacturer	Maximum Reverse Voltage (volts)	Reverse Recovery* Time (m μsec)	Forward Current (ma)	Reverse Voltage (volts)	Load Resistance (ohms)	Recovery Current (ma)
1N64	Germanium	Sylvania Electric Prod.	25	---	---	---	---	--
S347G	"	Transitron Electronic Corp.	40	300	5	10	2000	0.2
S570G*	"	" " "	8	2	10	6	120	3
CTP635	"	Clevite Transistor Prod.	8	30†	3.5	6.8	120	0.425
D1820	"	Sylvania Electric Prod.	20	4	10	6	120	3
HD2963††	"	Hughes Semiconductor Div.	7	6	10	6	100	3
HD2964††	"	" " "	20	3	10	6	100	3
FD100	Silicon	Fairchild Semiconductor Corp.	50	2	10	6	100	1
1N916	"	Texas Instruments, Inc.	75	4	10	6	75	1
HD5001††	"	Hughes Semiconductor Div.	10	0.5	10	5	100	--

*Time to recover to the specified reverse-recovery current when switched from the specified forward current to the specified reverse voltage, with the specified load-circuit resistance.

*The designation of this diode has recently been changed to 1N994.

† Measured using a mercury switch having a 12 m μsec rise time.

†† Specifications from advance data.

detectors using several samples of the various diodes, maximum load resistance, and an input voltage of 2.5 volts peak were measured at a signal frequency of 100 Mcps with the Q meter. The results are plotted in Figs. 60 and 61. At this input voltage the voltage efficiency of the high-impedance detector circuit approaches unit, for all the diodes.

Among the germanium diodes measured in high-impedance detectors, the S570G and the HD2964 gives high input resistance and low input capacitance. The S570G diode was selected for use in high impedance detectors on the basis of availability. The HD5001 silicon diode gives the highest input resistance and lowest input capacitance among the silicon diode measured. It was not, however, available in quantity at the time. The FD100 diode was selected for the high impedance detector measurements since it was also used in the pulse detectors. Its performance is comparable to that of the 1N916 diode. Both diodes are inferior to the S570G for use in high impedance detectors.

The voltage efficiency, input resistance and input capacitance of pulse detectors with the various diodes, a load resistance of 2 K ohms and a load capacitance of 47 μμf were measured with the Q meter at a signal frequency of 100 Mcps. The detectors using germanium diodes were measured with an input voltage of 0.35 volt peak. Those using silicon diodes were measured with 0.55 volt peak. The results of the measurements are plotted in Figs. 62 through 64. The current efficiency that would be obtained with a driving-circuit resistance R_A much larger than the detector input resistance R_{in} is given by

$$e_i = \frac{e_v R_{in}}{R_L} , \qquad (R_A \gg R_{in})$$

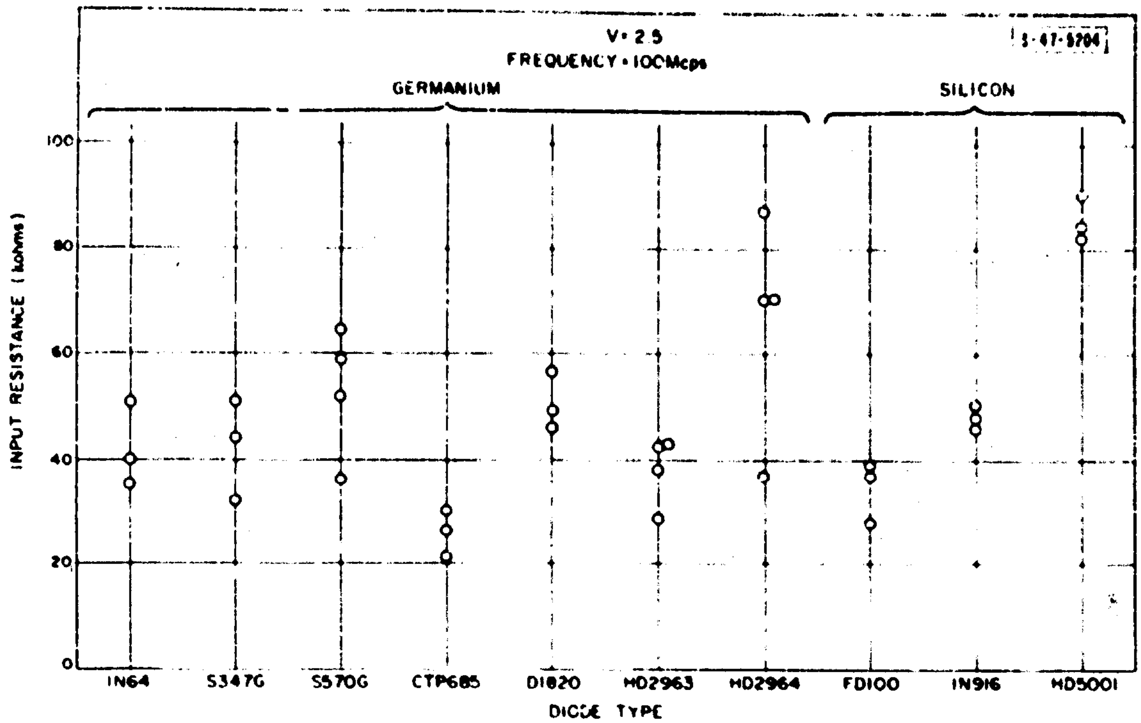

Fig. 60. Input resistance of high-impedance detectors using various diode types.

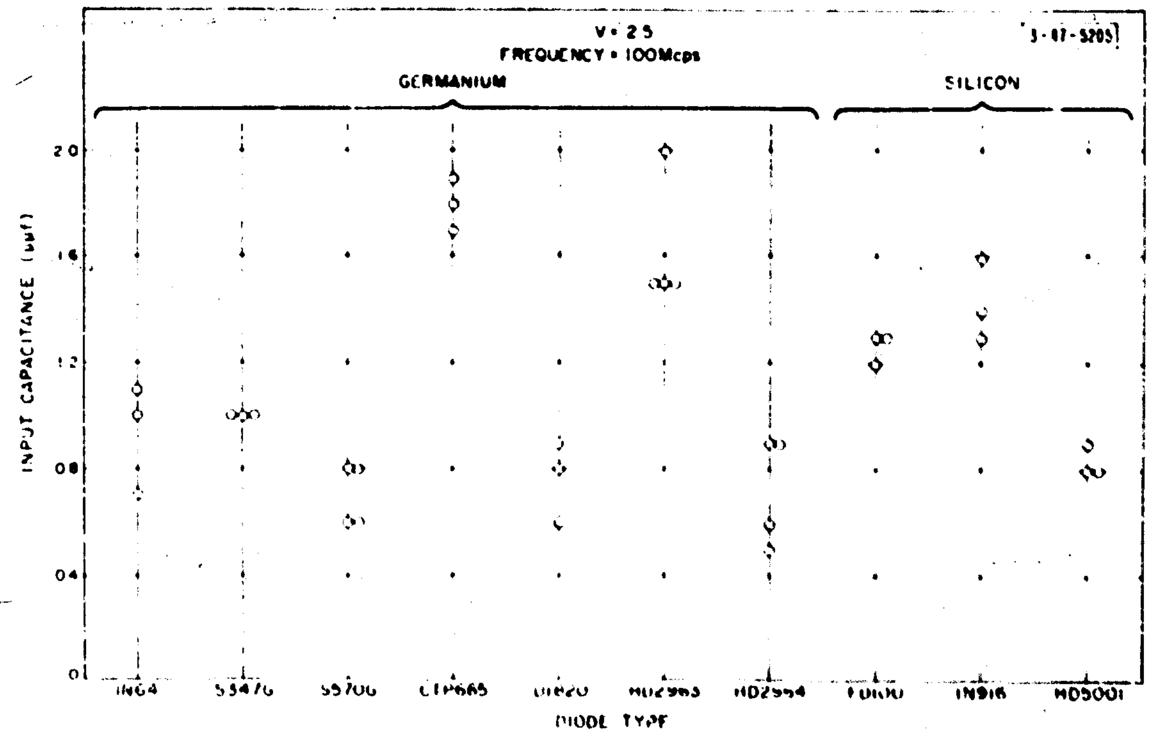

Fig. 61. Input capacitance of high-impedance detectors using various diode types.

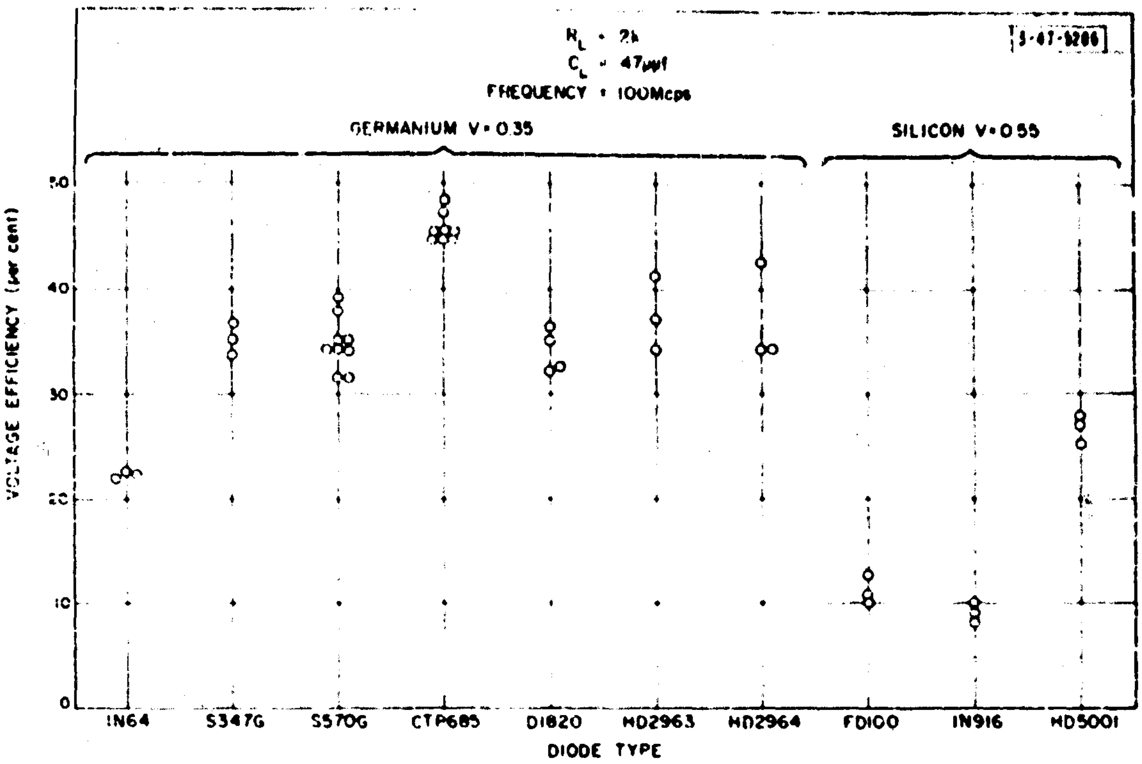

Fig. 62. Voltage efficiency of pulse detectors using various diode types.

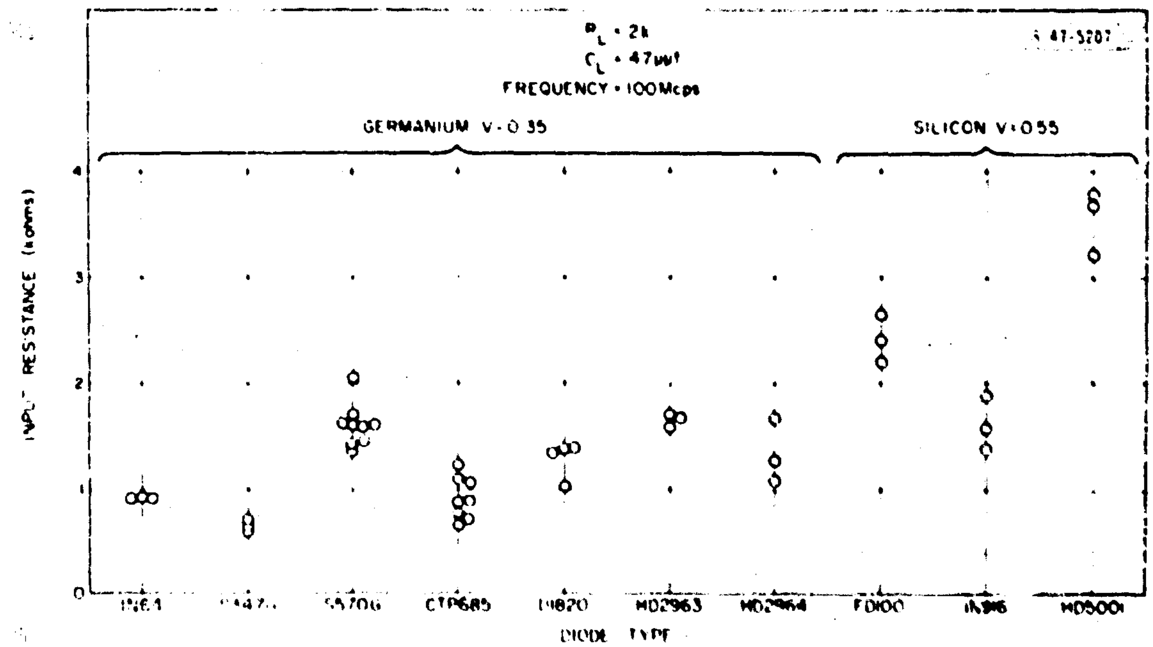

Fig. 63. Input resistance of pulse detectors using various diode types.

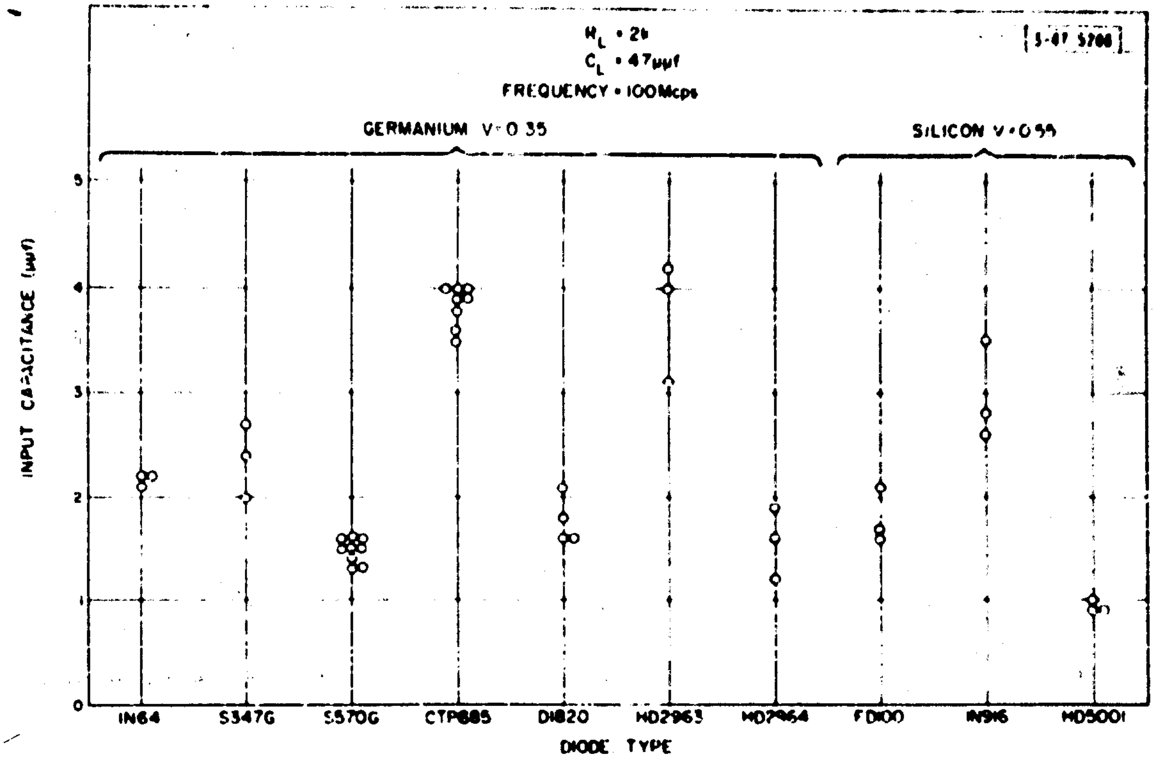

Fig. 64. Input capacitance of pulse detectors using various diode types.

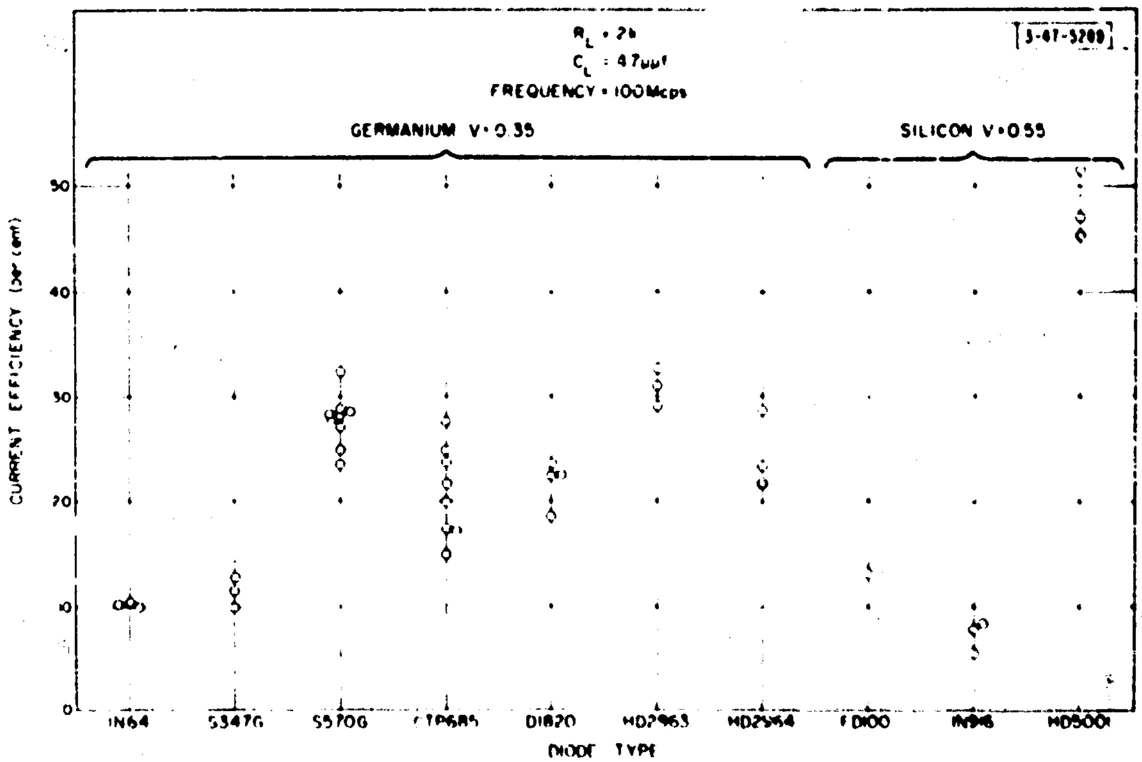

Fig. 65. Current efficiency of pulse detectors using various diode types.

This current efficiency was calculated for each diode measured. The results are plotted in Fig. 65.

The S570G diode was selected for the pulse detector circuits because it gives the lowest input capacitance and close to the highest current efficiency among the germanium diodes tested. The HD2963 diode gives slightly higher current efficiency at the expense of a much larger input capacitance. The HD5001 diode is outstanding among the silicon diodes tested for pulse detectors since it gives a current efficiency approximately three times that given by the next best diode, and has the lowest input capacitance. However the HD5001 diode was not readily available at the time. Of the remaining silicon diodes, the FD100 gives a higher current efficiency and a lower input capacitance and was therefore used in the pulse detectors.

VI. Summary and Conclusions

The design of semiconductor-diode detectors intended for use with low-level transistor circuits in the 10-100 Mcps frequency range has been investigated. A study of the literature on detector-circuit design and semiconductor-diode theory has been made. A survey of the applicable literature appears in Section II. As a result of the complex nature of the semiconductor diode, detector-circuit analyses using simple diode equivalent circuits do not yield accurate results. On the other hand, the results of theoretical studies of diode operation are too complex to be used for practical circuit design.

The detector-design theory that is presented in Section III makes use of semiconductor-diode theory, with simplifying approximations. The theory permits calculation of detector-circuit performance in the basis of measurements of diode parameters. The measured performance of high-impedance and pulse detectors using both germanium and silicon diodes is compared in Section IV with the performance calculated using the design theory. The agreement between measured and calculated performance is good over moderate ranges of signal level.

The voltage efficiency of high-impedance detectors is accurately predictable for input voltages greater than one or two tenths of a volt peak. The usefulness of the design theory for predicting the input resistance of a high-impedance detector is limited by the difficulty of accurately measuring the charge-storage factor in some diodes, and by an apparent increase in the charge-storage factor with signal level. Since high-impedance detectors are normally designed for negligible loading, this limitation is not serious

The range of signal level over which the calculations yield good agreement with measured pulse detector performance is governed by the range over which the assumed diode static characteristic closely approximates to the actual characteristic. In the examples of Section IV, the agreement is good over a range of input voltages of approximately a decade for the germanium diode and approximately a half decade for the silicon diode. It should be possible to obtain good agreement over other ranges of input level by using different assumed characteristics.

The input capacitance of a pulse detector is not predicted accurately by the detector-design theory as a result of bulk inductance in the diode. The input capacitance of detectors using diodes such as those measured is of the order of 1.0 μμf and varies only slightly with signal level and temperature. These variations are explained by the design theory. The change in detector input capacitance resulting from a change of detector load capacitance can be calculated on the basis of the theory.

At very high signal frequencies the bulk impedance of the semiconductor diode becomes appreciable compared with the barrier impedance, and some of the approximations used in the design theory are not valid. The voltage efficiency is no longer constant with frequency and the input resistance is higher than the theory predicts. These effects have been observed in pulse detectors using comparatively slow-switching diodes (e.g., 1N64) in the 10-100 Mcps frequency range. The theory appears to be valid to frequencies at least as high as 100 Mcps for the other diodes that were measured (see

Section V-4), all of which (with the exception of the S347G and CTP685) have specified reverse-recovery times below ten millimicroseconds.

The effect of low-Q driving circuits on detector performance can be estimated using the results of Section III-5 and the parameter values shown in Figs. 46 and 47. Although the resulting change in current efficiency is small in most practical cases, substantial errors in voltage measurements may occur if the flattening of the input voltage waveform is not taken into account.

Theory is presented in Section III-6 that describes the changes of detector-circuit performance with moderate variations of temperature. The agreement with experiment is good over a range of temperature considerably larger than normal room-temperature variations. The variations in performance are approximately the same for detectors using germanium and silicon diodes.

The application of the theory to the practical design of high-impedance and pulse detectors is given in Sections V-2 and V-3 respectively. Sample designs have been carried out for both types of detectors. Measurements of the performance of the sample detectors are reported. Additional measurements that compare the performance of a variety of diode types in both high-impedance and pulse detector circuits are presented in Section V-4

ACKNOWLEDGEMENT

The assistance of J. L. Gibbons in performing the measurements and many of the calculations for this report is gratefully acknowledged.

APPENDIX A

Solution of the Simplified Diffusion Equation for Large AC Signals

The simplified diffusion equation, boundary conditions and current equation given by Shockley[8,9] for a planar diode having wide diffusion regions are as follows:

$$\frac{\partial p}{\partial t} = -\frac{p - p_n}{\tau_p} + D_p \frac{\partial^2 p}{\partial x^2} ,$$

$$p(0) = p_n e^{V_D q/kT} ,$$

$$p(\infty) = p_n ,$$

$$J_{p_x} = -q D_p \frac{\partial p}{\partial x} .$$

The symbols used here are defined in Section II-3. Figure 7a shows the diode configuration that is assumed.

Taking $(p - p_n)$ as the independent variable, the diffusion equation is solved by separation of variables:

$$p - p_n = \sum_n \left[A_n e^{\gamma_n t - \frac{x}{L_p}\sqrt{1+\gamma_n \tau_p}} + B_n e^{\gamma_n t + \frac{x}{L_p}\sqrt{1+\gamma_n \tau_p}} \right] ,$$

where γ_n is a parameter and $L_p = \sqrt{D_p \tau_p}$. Applying the boundary conditions,

$$B_n = 0 .$$

$$p - p_n = p_n \left(e^{V_D q/kT} - 1\right) = \sum_n A_n e^{\gamma_n t} \quad .$$

Assuming an applied junction voltage of the form

$$V_D = V \cos \omega t - V_L \quad ,$$

and letting the parameter γ_n take on values,

$$\gamma_n = nj\omega \;, \quad \text{for} \quad n = 0, \pm 1, \pm 2, \text{ etc.} \quad ,$$

the solution takes the form of a Fourier series:

$$p - p_n = p_n \left[e^{\frac{(V \cos \omega t - V_L)q}{kT}} - 1 \right] = \sum_{n=-\infty}^{\infty} A_n e^{jn\omega t}$$

The coefficients A_n are found by Fourier analysis:

$$A_o = p_n \left[e^{-\frac{V_L q}{kT}} I_o \left(\frac{Vq}{kT} \right) - 1 \right] \quad .$$

$$A_n = p_n \, e^{-\frac{V_L q}{kT}} I_n \left(\frac{Vq}{kT} \right) , \quad \text{for} \quad n \neq 0$$

The hole density p is given by

$$p = p_n \left\{ 1 + \left[e^{-\frac{V_L q}{kT}} I_o\left(\frac{Vq}{kT}\right) - 1 \right] e^{-\frac{x}{L_p}} \right.$$

$$+ e^{-\frac{V_L q}{kT}} \sum_{n=1}^{\infty} I_n\left(\frac{Vq}{kT}\right) \left[e^{jn\omega t - \frac{x}{L_p}\sqrt{1 + jn\omega\tau_p}} \right.$$

$$\left.\left. + e^{-jn\omega t - \frac{x}{L_p}\sqrt{1 + jn\omega\tau_p}} \right] \right\} .$$

The hole current density J_{p_x} at the junction is

$$J_{p_x} = \frac{qD_p p_n}{L_p} \left[e^{-\frac{V_L q}{kT}} I_o\left(\frac{Vq}{kT}\right) - 1 + 2e^{-\frac{V_L q}{kT}} \sum_{n=1}^{\infty} I_n\left(\frac{Vq}{kT}\right) \sqrt{1 + jn\omega\tau_p} \right].$$

The components of the diode hole current are given by

$$I_{p_o} = \frac{qAp_n D_p}{L_p} \left[e^{-\frac{V_L q}{kT}} I_o\left(\frac{Vq}{kT}\right) - 1 \right] .$$

$$I_{p_1} = 2 \frac{qAp_n D_p}{L_p} e^{-\frac{V_L q}{kT}} I_1\left(\frac{Vq}{kT}\right) \sqrt{1 + j\omega\tau_p} .$$

$$I_{p_2} = 2 \frac{qAp_n D_p}{L_p} e^{-\frac{V_L q}{kT}} I_2\left(\frac{Vq}{kT}\right) \sqrt{1 + j2\omega\tau_p} .$$

etc.

When the small-signal approximations.

$$
\left.
\begin{aligned}
&I_o\left(\frac{Vq}{kT}\right) \approx 1 , \\
&I_1\left(\frac{Vq}{kT}\right) \approx \frac{Vq}{2kT} , \\
&I_n\left(\frac{Vq}{kT}\right) \approx 0 \quad \text{for} \quad n \neq 0, 1,
\end{aligned}
\right\} \quad V \ll \frac{kT}{q} ,
$$

are used, these results agree with those of Shockley.[8,9]

Corresponding expressions can be derived for electron current. The components of the total diode current are

$$
I_o = I_S \left[e^{-\frac{V_L q}{kT}} \, I_o\left(\frac{Vq}{kT}\right) - 1 \right] ,
$$

$$
I_1 = 2qA \, e^{-\frac{V_L q}{kT}} \, I_1\left(\frac{Vq}{kT}\right) \left[\frac{D_p p_n \sqrt{1 + j\omega\tau_p}}{L_p} + \frac{D_n n_n \sqrt{1 + j\omega\tau_n}}{L_n} \right] ,
$$

(wide planar diode),

$$
= 2I_S \, e^{-\frac{V_L q}{kT}} \, I_1\left(\frac{Vq}{kT}\right) \left[\frac{\dfrac{D_p p_n}{L_{p_\omega}(\omega)} + \dfrac{D_n n_n}{L_{n_\omega}(\omega)}}{\dfrac{D_p p_n}{L_{p_\omega}(\omega)} + \dfrac{D_n n_n}{L_{n_\omega}(\omega)}} \right] ,
$$

$$
I_2 = 2qA \, e^{-\frac{V_L q}{kT}} \, I_2\left(\frac{Vq}{kT}\right) \left[\frac{D_p p_n \sqrt{1 + j2\omega\tau_p}}{L_p} + \frac{D_n n_n \sqrt{1 + j2\omega\tau_n}}{L_n} \right] ,
$$

(wide planar diode),

$$= 2I_S\, e^{-\frac{V_L q}{kT}}\, I_2\left(\frac{Vq}{kT}\right) \left[\frac{\dfrac{D_p p_n}{L_{p_\omega}(2\omega)} + \dfrac{D_n n_n}{L_{n_\omega}(2\omega)}}{\dfrac{D_p p_n}{L_{p_\omega}(o)} + \dfrac{D_n n_n}{L_{n_\omega}(o)}} \right]$$

etc.

The quantities I_S, L_{p_ω} and L_{n_ω} used here are those defined in Section II-3 that apply to the wide planar diode. It can be shown that the same solutions for the total diode current are obtained for a narrow planar diode and a hemispheric diode if the corresponding expressions for I_S, L_{p_ω} and L_{n_ω} from Sections II-3 are used. The solutions for these cases follow that presented above.

APPENDIX B

Calculation of the Derivatives of Detector Parameters with Respect to Reverse-Saturation Current

The detector voltage efficiency e_v is calculated from the expression given in Section III-2:

$$\left[\frac{V_L}{I_R R_L} + 1\right] e^{V_L/c} = I_o (V/c) ,$$

where the reverse resistance R_R is included in the load resistance R_L. The detector input voltage V is held constant and the derivative of V_L with respect to I_R is calculated:

$$I_R = \frac{V_L}{R_L \left[I_o (V/c)\, e^{-V_L/c} - 1\right]} ,$$

$$dI_R = \frac{R_L \left[I_o (V/c)\, e^{-V_L/c} - 1\right] + \frac{V_L}{c} R_L I_o (V/c)\, e^{-V_L/c}}{R_L^2 \left[I_o (V/c)\, e^{-V_L/c} - 1\right]^2}\, dV_L ,$$

$$= \frac{\frac{V_L}{I_R} + \frac{V_L^2}{I_R c} + \frac{R_L V_L}{c}}{\left(\frac{V_L}{I_R}\right)^2}\, d V_L .$$

Rearranging terms,

$$\frac{dV_L}{dI_R} = \frac{V_L c}{I_R \left[V_L + c + R_L I_R\right]} .$$

The normalized derivative of voltage efficiency e_v with respect to I_R is then given by

$$\frac{1}{e} \frac{de_v}{dI_R} = \frac{V}{V_L} \cdot \frac{de_v}{dV_L} \cdot \frac{dV_L}{dI_R}$$

$$= \frac{c}{I_R \left[V_L + c + R_L I_R\right]}$$

The detector input resistance R_{in} and input capacitance C_{in} are calculated using the diode AC current I_1. The portion of the diode AC current due to diffusion flow I_{1_D} is given by (see Section III-3).

$$I_{1_D} = 2I_R e^{V_L/c} I_1 (V/c) \left[G(\omega) + j B(\omega)\right]$$

The derivative is calculated as follows

$$\frac{dI_{1_D}}{dI_R} = 2 I_R I_1 (V/c) \left[G(\omega) + j B(\omega)\right] \left[\frac{e^{V_L/c}}{c} \cdot \frac{V_L c}{I_R (V_L + c + R_L I_R)} \right]$$

$$+ 2 e^{V_L/c} I_1 (V/c) \left[G(\omega) + j B(\omega)\right]$$

$$= 2\, e^{-V_L/c}\, I_1(V/c)\, \left[G(\omega) + j\,B(\omega)\right] \frac{c + R_L I_R}{V_L + c + R_L I_R} .$$

$$= \frac{I_{1_D}(c + R_L I_R)}{I_R(V_L + c + R_L I_R)} .$$

The portion of the detector input resistance due to diffusion current is given by

$$R_D = \frac{V}{I_{1_D}} \quad \frac{G(\omega) + j\,B(\omega)}{G(\omega)} .$$

The normalised derivative of R_D with respect to I_R is

$$\frac{1}{R_D} \cdot \frac{dR_D}{dI_R} = - \frac{I_{1_D}\, G(\omega)}{V\left[G(\omega) + j\,B(\omega)\right]} \cdot \frac{V\left[G(\omega) + j\,B(\omega)\right]}{I_{1_D}^{\,2}\, G(\omega)} \cdot \frac{dI_{1_D}}{dI_R} .$$

$$= - \frac{c + R_L I_R}{I_R(V_L + c + R_L I_R)} .$$

The portion of the detector input capacitance due to diffusion current is given by

$$C_D = \frac{I_{1_D}}{\omega V} \quad \frac{B(\omega)}{G(\omega) + j\,B(\omega)}$$

The normalized derivative of C_D with respect to I_R is

$$\frac{1}{C_D} \cdot \frac{dC_D}{dI_R} = \frac{\omega V \left[G(\omega) + j\,B(\omega)\right]}{I_{1_D}\, B(\omega)} \cdot \frac{B(\omega)}{\omega V \left[G(\omega) + j\,B(\omega)\right]} \cdot \frac{dI_{1_D}}{dI_R}$$

$$= \frac{\phi + R_L I_R}{I_R (V_L + \phi + R_L I_R)} \; .$$

BIBLIOGRAPHY

Papers that utilise linear approximations to diode characteristics and neglect reactive effects:

1. J. Marique. "Notes on the Theory of Diode Rectification," Wireless Eng., Vol. 12, pp. 17-22, January, 1935. An analysis of a diode detector is made assuming constant diode forward resistance and infinite back resistance. The results, obtained graphically, show the variation of voltage efficiency as a function of load resistance and load capacitance.

2. H. A. Wheeler, "Design Formulas for Diode Detectors," Proc. IRE, Vol. 26, pp. 745-780, June, 1938. Detector circuits having various source impedances, load impedances and signal inputs are analyzed. Narrow bandwidth and low diode forward resistance are usually assumed and the practical limitations of these assumptions are discussed.

3. K. R. Sturley, "Radio Receiver Design, Part I," John Wiley and Sons, Inc., New York, N. Y., Chapt. 8, 1949. A summary of early work on detectors employing vacuum diodes is given. Marique's results (Reference 1) are given in detail.

4. W. B. Whalley, C. Masucci, and N. P. Salz, "The Germanium Diode as a Video Detector," Proc. IRE, Vol. 41, pp. 638-644, May, 1953. A detector circuit is analyzed through the use of an equivalent circuit, assuming a diode with constant forward and back resistances. Exact solutions for voltage efficiency and input resistance are given for the case when the load capacitor is large. Approximate solutions are given for the case when the load capacitor is not large. Methods of measuring diode characteristics are discussed.

Analyses using diode equivalent circuits

5. P. Lapostolle, "Theoretical and Experimental Study of Detection by Silicon Crystals," Ondé Elect., Vol. 29, pp. 429-448, December, 1949. The performance of a detector circuit is calculated by assuming a simple equivalent circuit for the semiconductor diode and performing a transient analysis on the circuit. Experimental verification is given only at 3000 Mcps.

6. W. Heinlein, "Inertia in Germanium Diodes and its Effect in Simple Rectifier and Limiter Circuits," Frequenz, Vol. 12, pp. 159-163 and 191-197, May and June, 1958. Translation available from Morris D. Friedman, Inc., West Newton, Mass., No. H-103. The operation of limiter and detector circuits employing semiconductor diodes is described using an equivalent circuit for the diode. Qualitative agreement of the theory with measurements is shown.

General papers on the theory of semiconductor diodes:

7. H. C. Torrey and C. A. Whitmer, "Crystal Rectifiers," McGraw-Hill Book Co., Inc., New York, N. Y., 1948. This MIT Radiation Laboratory Series book summarizes work on crystal diodes prior to 1948.

8. W. Shockley, "The Theory of p-n Junctions in Semiconductors and p-n Junction Transistors," Bell System Tech. Jour. Vol. 28, pp. 435-489; July, 1949. The basic theory of semiconductor junctions is developed and applied to a planar diode. The analysis is restricted to small signals.

9. W. Shockley "Electrons and Holes in Semiconductors," D. Van Nostrand Co., Inc., Princeton N. J., 1950. The work in Reference 8 is included in Chapter 12.

10. A. Uhlir, "Two-Terminal P-N Junction Devices for Frequency Conversion and Computation," Proc. IRE, Vol. 44, pp. 1183-1191, September, 1956.

11. H. L. Armstrong, E. D. Metz, and I. Weiman, "Design Theory and Experiment for Abrupt Hemispherical P-N Junction Diodes" IRE Trans., Vol. ED-3, pp. 86-92, April, 1956. A theoretical analysis of gold-bonded germanium diodes is given. Experimental data are included for comparison.

12. W. E. Newell, L. Depian, and A. G. Milnes "Frequency Characteristics of a Semiconductor Rectifier at Voltages Greater Than kT/q," IRE Trans., Vol. ED-6, pp. 125-132, April, 1959. An analysis is made of a semiconductor diode assuming a junction that follows the small signal equations in series with a resistance.

13. R. E. Nelson, "Model for a Point Contact Diode," S. M. Thesis, MIT; June, 1957. A simplified model for a point contact diode is given and analyzed. Theoretical results are given for back-bias characteristics, forward characteristic, and low-level AC characteristic. Experimental verification is given.

14. R. E. Nelson, "Point-Contact Diodes in Terms of p-n Junction Theory," IRE Trans., Vol. ED-6, pp. 270-277, July, 1959. This paper is based on Reference 13 and includes most of the important results.

Analyses of semiconductor diode static characteristics:

15. R. N. Hall "Power Rectifiers and Transistors" Proc. IRE, Vol. 40, pp. 1512-1518 November 1952.

16. J . Swanson, "Diod Theory in the Light of Hole Injection," J nal Appl. Phys., Vol. 25 pp 314-325 March, 1954.

17. [illegible] nanium Point Contact Rectifiers," Journ. Appl. Phys , Vol. 26, pp. 949-954; August, 1955.

18. K. Lehovec, A. Marcus, and K. Schoeni, "Current-Voltage Characteristics and Hole Injection Factor of Point Contact Rectifiers in the Forward Direction," IRE Trans., Vol. ED-3, pp. 1-6; January, 1956.

19. M. Cutler, "Point Contact Rectifier Theory," IRE Trans., Vol. ED-4, pp. 201-206, July, 1957.

20. J. L. Moll, "The Evolution of the Theory for the Voltage-Current Characteristic of P-N Junctions," Proc. IRE, Vol. 46, pp. 1076-1082, June, 1958.

21. C. T. Sah, R. N. Noyce, and W. Shockley, "Carrier Generation and Recombination in P-N Junctions and P-N Junction Characteristics," Proc. IRE, Vol. 45, pp. 1228-1243, September, 1957.

Analyses of semiconductor diode operation at high levels:

22. E. S. Rittner, "Extension of the Theory of the Junction Transistor," Phys. Rev., Vol. 94, pp. 1161-1171; June 1, 1954.

23. T. Misawa, "Emitter Efficiency of Junction Transistor," Journal Phys. Soc. Japan, Vol. 10, pp. 362-367, May, 1955.

24. T. Misawa, "A Note on the Extented Theory of the Junction Transistor," Journal Phys. Soc. Japan, Vol. 11, pp. 728-739; July, 1956.

25. T Misawa, "Impedance of Bulk Semiconductor in Junction Diode," Journal Phys. Soc. Japan, Vol. 12, pp. 882-890 August, 1957.

26. T. E. Firle and O. E. Hayes, "Some Reactive Effects In Forward Biased Junctions," IRE Trans., Vol. ED-6, pp. 330-334, July, 1959.

27. I. Ladany, "An Anlysis of Inertial Inductance in a Junction Diode," IRE Trans., Vol ED-7, pp. 303-310, October, 1960.

Transient response of semiconductor diodes:

28. B. Lax and S. F. Neustadter, "Transient Response of a p-n Junction," Journal Appl. Phys., Vol. 25, pp. 1148-1154, September, 1954.

29. R. H. Kingston, "Switching Time in Junction D... Transistors," Proc. IRE, Vol. 42, pp. 829-83...

30. T. E. Firle, M. E. McMahon, and J. F. ... Measurements on Point-Contact Germanium Diodes, ... Vol. 43, pp. 603-607; May, 1955.

Effect of temperature on semiconductor diodes

31. J. S. Schaffner and R. F. Shea, "The Variation ... Characteristics of Junction Diodes with Temperature ... Vol. 43, p. 101; January, 1955

Transient response of diode detectors.

32. M. V. Callendar, "Pulse Response of ... Eng., Vol. 32, pp. 3-14, January, 1955. A ... current source and loaded ... detector ... is given for the response time of the combined ... a constant forward diode resistance. Experim... given.

33. L. S. Gutkin and O. ... Chentsova, "Analysis of ... Detection by Means of Low-Frequency ... Radio ... No. 6, pp. 40-60; 1957 translation ... a detector following an amplifier stage is analy... level is assumed to be varying slowly, and app... to take into account the diode character... applied to complex amplifier and detector load

34. L. S. Gutkin and O. S. Chentsova, "Transient ... 'High Frequency Amplifier-Detector' System ... Vol. 12, No. 11, pp. ... 61; 1957 translation ... analysis of Reference 33 is applied to a several ...

35. A. van Weel, "Design of Detector Stages ... S... and Assymmetrical Sidebands ... September, 1958. The response of ... detector to modulated signals is d...

Tables and handbooks:

36. British Association for the Advancement of Science ... Tables, Vol. 10, Bessel Functions Part ... Cambridge, England, 1952

37. F. E. Terman, "Radio Engineers Handbook," ... Inc., New York, N. Y., 1943